

AN INVESTIGATION INTO THE MECHANICS OF ABRASIVE JET MACHINING

A Thesis

Submitted to

THE UNIVERSITY OF CALICUT

in fulfillment of the requirements for the award of the degree of

DOCTOR OF PHILOSOPHY
in
MECHANICAL ENGINEERING

by


R.VIJAYAKUMAR



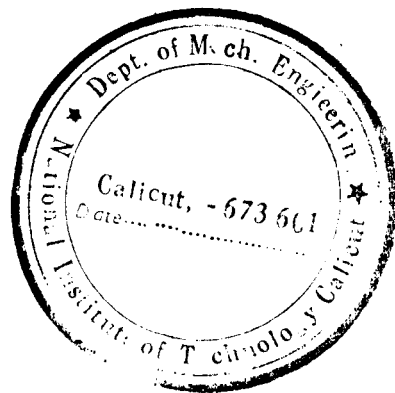
**DEPARTMENT OF MECHANICAL ENGINEERING
NATIONAL INSTITUTE OF TECHNOLOGY CALICUT
CALICUT 673601, KERALA
November 2002**

CERTIFICATE

This is to certify that the thesis entitled 'An Investigation into the Mechanics of Abrasive Jet Machining' is the bonafide work done by R. Vijayakumar under my supervision and guidance. The thesis is submitted to the University of Calicut in fulfillment of the requirements for the award of the degree of Doctor of Philosophy in Mechanical Engineering. The work contained herein has not been submitted to any other university for the award of any degree.


19.11.2002

Dr. R. RAVINDRAN NAIR
(Professor of Mechanical Engineering and Dean (Academic)
National Institute of Technology Calicut)
THESIS SUPERVISOR AND GUIDE



DEDICATED TO
The Memory of My Friend, Colleague and Teacher
Late Dr. E. VIJAYAN NAIR

ACKNOWLEDGEMENT

It is with profound sorrow and the feeling of the loss of a very good friend and teacher that I prepare to submit this thesis. **Dr. Vijayan Nair** said good-bye to this world at the time when I had completed the skeleton of the write up of the thesis. He had guided me for the major part of my work. His death was so sudden and without warning that it left me paralyzed for a month. I hope his soul is granted "Nirvana".

No amount of thanks to my guide **Dr. R. Ravindran Nair** is too much, without whose help and guidance, I would not be submitting the thesis now. In spite of his busy schedule as the Dean (Academic) of the Institution, he agreed to help me and has guided me with keen interest and understanding. I thank him.

Thanks are due to the Professors, who had been the Head of the Department of Mechanical Engineering from time to time. The present Head **Dr. N.M. Nagarajan**, took special interest in my work and put an encouraging word now and then. Thank you **Dr. Nagarajan**.

Many of my colleagues in the Department of Mechanical Engineering also must be thanked, for their help and suggestions during the research work and compilation of the thesis. **Dr. C. Muraleedharan, Dr. Ghulam Jilani, Dr. Jose Mathew, Dr. C. B. Sobhan, Dr. N. Ramachandran, Mr. M. A. Joseph and Mr. Sibi Chacko** are specially remembered. I thank them too.

My graduate students, Gibi and Lakshman Kishore, helped me a lot in compiling the data and in the preparation of the charts. I am grateful to them. Mr. Anoop has already

completed his M.Tech. He was of great help at the time when I was solving the flow equations. I also acknowledge the help rendered by Ganesh, Vishnu, Aparna, Ebin and Geomy in the preparation of specimen for surface studies. These students have already graduated.

This work was begun as part of a **DST sponsored project “Mechanics of Abrasive Jet Machining and the effect of Electrostatic field on it”**. (No. III-6(2)/86-ET dated 26-10-1987). The entire experimental set up was also fabricated under that project. The financial assistance of DST is acknowledged.

My wife **Laila Vijayan** and son **Jyothish Vijay** helped my cause by making my home a ‘happy home’ all the time. I am thankful to them also.

Finally, I give my ‘**pranams**’ to the goddess of knowledge “**Saraswathi**”, without whose blessings no academic activity is possible.

R.VIJAYAKUMAR

ABSTRACT

Abrasive Jet Machining is an unconventional machining method in which, a jet of high velocity air-abrasive particles is directed onto a work piece to remove material from it. The AJM process is especially useful in machining brittle materials and is seldom employed for machining ductile materials. Early researches in the field had mostly been experimental investigations. The few attempts to theorize the mechanics of material removal used very crude models. The present research work is aimed mainly at proposing a suitable theory, which explains the mechanics of AJM. To do this, the established theories of elasticity and fluid flow have been employed.

It is widely recognized that the impact of abrasive particles and the consequent transfer of energy to the work medium is the cause for material removal. The impact is modeled as an impulse resulting in transient stress and strain field in the medium. The standard equations of elasticity theory (Navier's formulation) are solved to determine the stress and strain field. For ascertaining fracture, a criterion based on strain energy density is employed and a material property (SED_{cr}) is introduced. The process parameters are introduced at this stage, through the analysis of the air-abrasive flow. The governing equations for the flow are the adaptations of the Navier - Stokes equations for the fluid and equations of motion for the particles. The solutions of the above equations in conjunction with the boundary conditions give a theoretical basis for predicting the material removal rate in AJM.

The theoretical prediction of the material removal rate (mrr) is found to be in very good agreement with experimental results. The comparison is done with experiments

conducted for the purpose. An empirical correlation for mrr has been obtained from the results of experiments. This is presented in the form of plots also. Another set of experiments has been done to investigate the surface roughness of the parts machined by the process. The surface is characterized by its CLA (Ra) and RMS (Rq) values. The variation of the surface roughness parameter with the process parameters of pressure, stand off distance, grit size and feed are studied.

It is seen that, the proposed theory can predict to a reasonable accuracy the material removal rate in an AJM process in the context of machining brittle materials. Further, the optimum stand off distance with respect to material removal rate as predicted by other investigators is obtained in this study also. The optimum stand off distance is found to be between 20 mm and 30 mm for the range of parameters considered. Better machining rates than those claimed by early researchers have been observed in the present experiments and are also predicted by the theory. It is also concluded that the hardness of the impacting particles is not an influencing criterion for material removal. It turns out to be that the surface roughness is practically unaffected by the stand off distance and the abrasive grit size. It has been found that over the range investigated the roughness parameter increases with pressure, but shows a decreasing trend with feed. The threshold velocity and the threshold pressure as reported by earlier investigators have also been evaluated in this study.

CONTENTS

	Page
Acknowledgement	i
Abstract	iii
Contents	v
Nomenclature	vii
List of figures	xi
List of tables	xvi
Chapter 1 Introduction	
1.0 General	1
1.1 The abrasive jet machining process	2
1.2 Importance of the present work	4
1.3 The parameters of AJM process	5
1.4 Organization of the thesis	6
Chapter 2 Literature review	
2.1 Studies on general aspects of AJM	7
2.2 The impact problem and erosion analysis for ductile materials	12
2.3 Material removal from brittle materials	16
2.4 Review of literature on gas-particle flows	23
2.5 Conclusion	27
Chapter 3 Theory of material removal in AJM	
3.1 Outline of the theory	28
3.2 Theory for the material removal from the impact of one abrasive grain	30
3.3 The boundary conditions	32
3.4 The method of solution	34
3.5 Technique of solving for A_1, A_2, B_1, B_2 and T_c	37
3.6 Algorithm for the iterative procedure	38
3.7 Prediction of material removal rate	39
3.8 Conclusion	45

Chapter 4	Determination of particle velocity	
4.1	Introduction	46
4.2	Flow through the nozzle	46
4.3	Particle velocity in the jet	51
4.4	Conclusion	54
Chapter 5	Results of Analytical and Experimental Investigations and discussions	
5.1	Introduction	55
5.2	Results and discussions on analytical investigations	56
5.3	Experimental investigations	82
	5.3.1 Validation of the theoretical predictions	85
	5.3.2 Empirical relation for material removal rate	91
	5.3.3 Surface studies	119
Chapter 6	Conclusions	
6.0	General	133
6.1	Specific conclusions	134
6.2	Suggestions for further research	136
	References	138
Appendix A	Solution of the wave equation	145
Appendix B	Flow-charts	148
Appendix C	The critical strain energy density	162

NOMENCLATURE

a	constant
a_1, a_2	constants
A	area
b_1, b_2	constants
B_1, B_2	constants
c	constant
C_1	velocity of longitudinal wave
C_2	velocity of shear wave
C_D	coefficient of drag
C_p	specific heat of air at constant pressure
C_{pp}	specific heat of the abrasive particles
d	constant
d_n	diameter of nozzle at exit
d_p	diameter of particles
d_{pipe}	diameter of pipe
e	constant
E	Young's modulus of work material
f	constant
G	modulus of rigidity of work material
h	heat transfer coefficient between gas and particles
H	matrix used in Davidon Fletcher Powell method
I	the identity matrix
j	the imaginary number $\sqrt{-1}$
K, k	constant
\dot{m}	mass flow rate
\dot{m}_{ab}	mass flow rate of abrasives
\dot{m}_a	mass flow rate of air
\dot{m}_p	mass flow rate of particles

m_r	mixing ratio ($= \frac{\dot{m}_{ab}}{\dot{m}_a + \dot{m}_{ab}}$)
mrr	material removal rate
N	matrix used in Davidon Fletcher Powell method
\dot{N}	number of particles striking the work surface per unit time
Nu	Nusselt Number
O	matrix used in Davidon Fletcher Powell method
p	pressure
P	average surface pressure
Pr	Prandtl number
p_s	supply pressure
p_{at}	atmospheric pressure
Q	matrix used in Davidon Fletcher Powell method
r	r -coordinate
r^*	non-dimensional r-coordinate
r_c	r -coordinate of the fracture profile
r_{cmax}	the r coordinate of the fracture profile at $z = 0$
R	function of r
\mathcal{R}	characteristic gas constant
R_j	the residue of the j^{th} boundary condition
R_p	radius of particles
R_c	radius of contact
Re	Reynolds Number
R_{max}	the radius of the jet at the work surface
s_d	stand off distance
S	matrix used in Davidon Fletcher Powell method
SED	strain energy density function
SED_{cr}	critical strain energy density
t	time
T	function of time
T_c	period of contact

T_p	the temperature of the particles
T_a	temperature of air
u	the axial component of the velocity of the jet
U_{amb}	velocity of the ambient fluid
U_{jet}	velocity of the jet (air) at the exit of the nozzle
U_r	r- component of displacement
U_θ	θ -component of displacement
U_z	z component of displacement
∇_0	volume of material removed in a single impact
V_{max}	the velocity of the particles at the time of impact with the work surface
V_a	velocity of air
V_e	velocity for elastic impact
V_{ini}	initial velocity of air
V_{pini}	initial velocity of particles
V_{pjet}	velocity of the particles at the exit of the nozzle
x_c	length of the potential core
X	solution vector
Y	yield strength of medium
z	z- coordinate
z^*	non-dimensional z coordinate ($= \frac{z}{R_p}$)
Z	function of z
z_c	z coordinate of the fracture profile
β	$\sqrt{(1+z^*)^2 + r^{*2}}$
χ	Constant
δ_R	depth of penetration
ε	a small number
ε_T	the trace of the strain matrix
ϕ	wave function, volume fraction of particles
γ	shear strain

λ	Lame's constant
λ^*	optimum step length
μ	absolute viscosity of the fluid
ν	Poisson's ratio
θ	θ - coordinate
θ_{crack}	θ at which crack propagates
ρ_a	density of air
ρ_p	density of particles
ρ_w	density of work material
σ	normal stress
σ_m	rupture strength
τ	shear stress
ψ	wave function
ζ_1, ζ_2	damping factors for ϕ and ψ

Other notations used are explained in the text itself.

LIST OF FIGURES

Fig. No.	Title of the Figure	Page
1.1	Schematic arrangement of an AJM set up	3
2.1	Variation of material removal rate with pressure (Pandey and Shan)	8
2.2	Variation of material removal rate with pressure (Pandey and Shan)	8
2.3	Variation of material removal with stand off distance (Pandey and Shan)	8
2.4	Variation of penetration rate and material removal rate with stand off distance (Verma and Lal)	9
2.5	Variation of material removal rate with some of the parameters of AJM (Venkatesh)	10
2.6	Hertz's solution of the impact problem	12
2.7	Model for material removal used by Finnie	13
2.8	Conical cracks on brittle work material (Evans et.al.)	17
2.9	Shaw's model for material removal	18
2.10	Elastic-plastic model used by Jain et.al.	21
3.1	Impact of a spherical particle on a semi infinite elastic medium	31
3.2	Typical fracture profile for different values of particle radius	41
4.1	Differential element of the nozzle for flow analysis	47
4.2	The potential core and similarity zone in a turbulent jet	52
5.1	Theoretical prediction of the variation of material removal rate with stand off distance	57

5.2	Theoretical prediction of the variation of material removal rate with stand off distance (mixing ratio as parameter)	59
5.3	Theoretical prediction of the variation of material removal rate with stand off distance (pressure as parameter)	60
5.4	Theoretical prediction of the variation of material removal rate with stand off distance (diameter of nozzle as parameter)	61
5.5	Theoretical prediction of the variation of material removal rate with stand off distance (grit size as parameter)	62
5.6	Theoretical prediction of the variation of material removal rate with mixing ratio (stand off distance as parameter)	65
5.7	Theoretical prediction of the variation of material removal rate with mixing ratio (pressure as parameter)	66
5.8	Theoretical prediction of the variation of material removal rate with mixing ratio (diameter of nozzle as parameter)	67
5.9	Theoretical prediction of the variation of material removal rate with mixing ratio (grit size as parameter)	68
5.10	Theoretical prediction of the variation of material removal rate with pressure (stand off distance as parameter)	71
5.11	Theoretical prediction of the variation of material removal rate with pressure (mixing ratio as parameter)	72
5.12	Theoretical prediction of the variation of material removal rate with pressure (diameter of nozzle as parameter)	73
5.13	Theoretical prediction of the variation of material removal rate with	74

	pressure (grit size as parameter)	
5.14	Theoretical prediction of the variation of material removal rate with diameter of nozzle (stand off distance as parameter)	76
5.15	Theoretical prediction of the variation of material removal rate with diameter of nozzle (mixing ratio as parameter)	77
5.16	Theoretical prediction of the variation of material removal rate with diameter of nozzle (pressure as parameter)	78
5.17	Theoretical prediction of the variation of material removal rate with diameter of nozzle (grit size as parameter)	79
5.18	Theoretical prediction of the variation of material removal rate with grit size (stand off distance as parameter)	81
5.19	Photograph of the experimental set up	85
5.20	Experimental data and best fit curves	88
5.21	Experimental points and best fit curve for the variation of material removal rate with stand off distance	89
5.22	Experimental validation of the theory	90
5.23	Variation of material removal rate with stand off distance (from experiments) (mixing ratio as parameter)	94
5.24	Variation of material removal rate with stand off distance (from experiments) (pressure as parameter)	95
5.25	Variation of material removal rate with stand off distance (from experiments) (diameter of nozzle as parameter)	96
5.26	Variation of material removal rate with stand off distance (from	97

	experiments) (grit size as parameter)	
5.27	Variation of material removal rate with mixing ratio (from experiments) (stand off distance as parameter)	99
5.28	Variation of material removal rate with mixing ratio (from experiments) (pressure as parameter)	100
5.29	Variation of material removal rate with mixing ratio (from experiments) (diameter of nozzle as parameter)	101
5.30	Variation of material removal rate with mixing ratio (from experiments) (grit size as parameter)	102
5.31	Variation of material removal rate with pressure (from experiments) (stand off distance as parameter)	104
5.32	Variation of material removal rate with pressure (from experiments) (mixing ratio as parameter)	105
5.33	Variation of material removal rate with pressure (from experiments) (diameter of nozzle as parameter)	106
5.34	Variation of material removal rate with pressure (from experiments) (grit size as parameter)	107
5.35	Variation of material removal rate with diameter of nozzle (from experiments) (stand off distance as parameter)	109
5.36	Variation of material removal rate with diameter of nozzle (from experiments) (mixing ratio as parameter)	110
5.37	Variation of material removal rate with diameter of nozzle (from experiments) (mixing ratio as parameter)	111

5.38	Variation of material removal rate with diameter of nozzle (from experiments) (grit size as parameter)	112
5.39	Variation of material removal rate with grit size (from experiments) (stand off distance as parameter)	113
5.40	Variation of material removal rate with grit size (from experiments) (mixing ratio as parameter)	114
5.41	Variation of material removal rate with grit size (from experiments) (pressure as parameter)	115
5.42	Variation of material removal rate with grit size (from experiments) (diameter of nozzle as parameter)	116
5.43	Variation of material removal rate with stand off distance (Rani and Seshan)	118
5.44	Variation of material removal rate with pressure and mixture ratio (Rani and Seshan)	118
5.45	Close up views of nozzle and some glass slides after machining	122
5.46	Typical numerical output of SURFTEST SJ301	123
5.47	Typical graphical output of SURFTEST SJ301	124
5.48	Variation of surface roughness with pressure	125
5.49	Variation of surface roughness with stand off distance	126
5.50	Variation of surface roughness with grit size	127
5.51	Scatter of CLA and RMS (Ra and Rq) values	130
5.52	Trend of variation of average roughness with feed	131

LIST OF TABLES

Table No.	Title of the table	Page
3.1	Values of the constants for different values of the parameters	40
3.2	The results of computation of fracture volume	43
3.3	Volume of material removed in a single impact as a function of the parameters of the process	44
5.1	Material properties used for calculation	55
5.2	Experimental conditions	84
5.3	Data obtained on the AJM set up for comparison with theory	86
5.4	Experimental data for empirical correlation for material removal rate	93
5.5	Data obtained from measurements on SURFTEST SJ301	121
5.6	Roughness data obtained for different feeds	129

Chapter 1

INTRODUCTION

1.0 General

The concept of removing material from a work piece with an edged cutting tool is ages old. The cutting tool is moved relative to the work piece for the purpose. The mechanism of material removal is related to plastic deformation and the consequent chip formation. The cutting tool is traditionally harder than the work material. Use of such tools and processes of machining are satisfactory in most cases.

However, there are hard and brittle work materials for which the conventional cutting processes for material removal can not fulfill the requirements. For example, the production of fine holes of intricate shapes on thin brittle jobs is very difficult by conventional methods. The techniques of piercing, stamping and extrusion do not work satisfactorily on brittle materials because of their limited plasticity. These materials may develop cracks or may even crumble under such processes. Even the drilling of circular holes on brittle materials is a difficult task, if conventional drills are employed. Techniques like **electro-discharge machining (EDM)**, **laser beam machining (LBM)**, **electron beam machining (EBM)**, **ultrasonic machining (USM)** and **abrasive jet machining (AJM)** are some of the methods which are suggested for such situations. These processes are called unconventional machining processes.

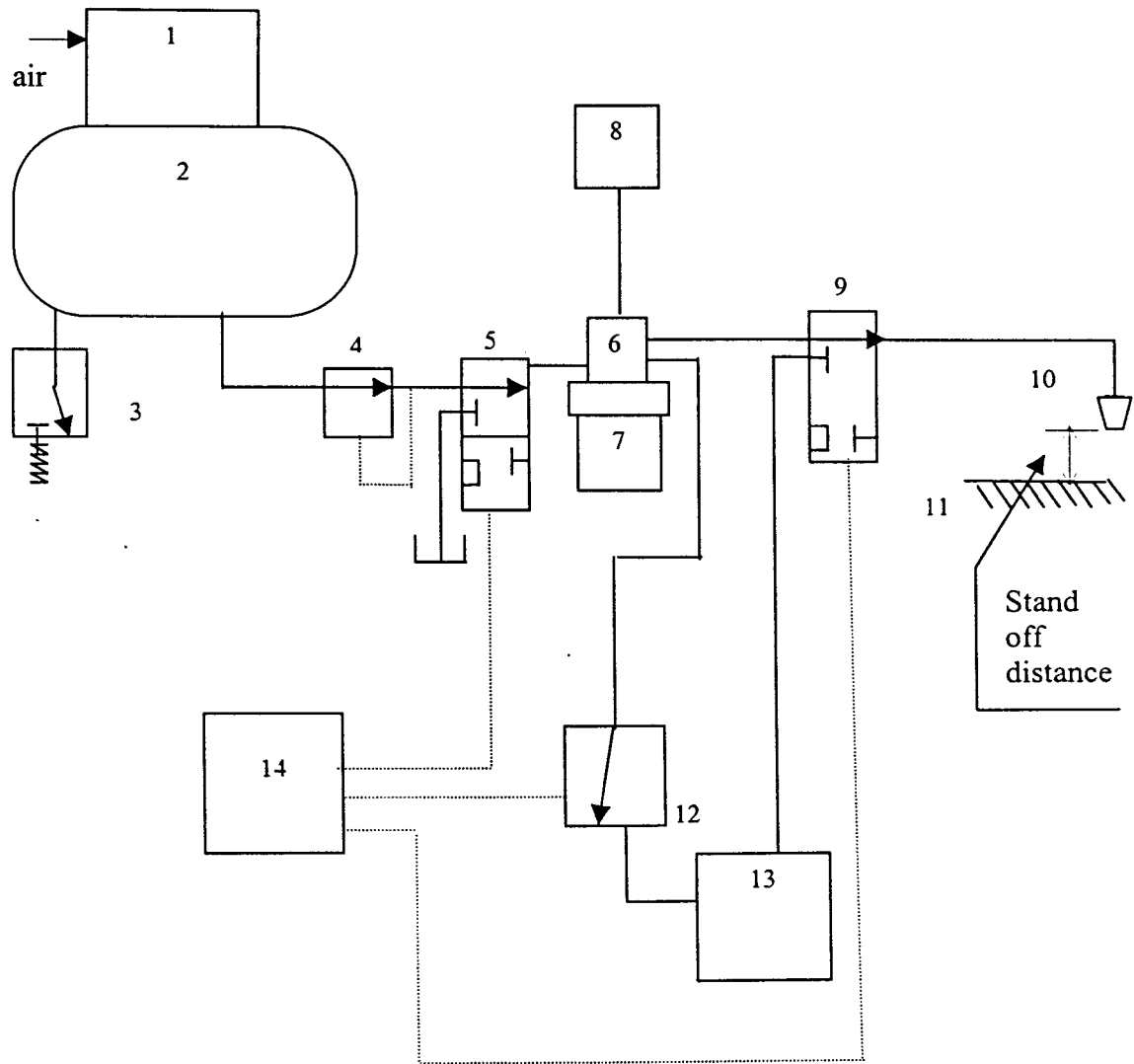
The abrasive Jet Machining (AJM) is one of the unconventional machining processes. Even though, the possibility of machining with powdered form of abrasives had been in use, the use of abrasive powder in the form of abrasive-jet is relatively new.

Conventional grinding, honing, lapping and super finishing are some of the other processes in which powdered abrasive is used.

1.1 The Abrasive Jet Machining Process.

In AJM process, material removal from a work material is achieved, by directing a jet of high velocity air with abrasive powder, on to its surface. A carrier-gas (usually compressed air) is used for the purpose of transporting the abrasive powder. The compressed carrier-gas will transfer a part of the energy it possesses to the abrasive powder so that it will get the required velocity for material removal. The abrasive powder is introduced to the compressed gas in a device called the mixing chamber.

The schematic diagram of an abrasive jet machining set up is shown Figure 1.1. Air is compressed in the compressor and is stored in the reservoir. The tank removes the fluctuations in the flow. The air stored in the tank is fed into the system through a pressure regulator. The pressure regulator maintains a constant pressure in the line leading to the jet. This is the system pressure, which can be selected by the pressure regulator. The mixing of the abrasive powder with the air stream takes place in the mixing chamber. The abrasive is fed into the mixing chamber from an abrasive chute. The mixing chamber is vibrated at random frequencies in order using an electromagnetic vibrator to ensure thorough mixing of the powder with the air stream. Air-abrasive mixture is directed through the nozzle to achieve the required velocity for the removal of material from the work piece.



- | | |
|------------------------------|------------------------------|
| 1. Compressor | 8. Abrasive tank |
| 2. Reservoir | 9. Three way valve |
| 3. Relief valve | 10. Nozzle |
| 4. Pressure regulating valve | 11. Work piece |
| 5. Three way valve | 12. Two way valve |
| 6. Mixing chamber | 13. Abrasive sump |
| 7. Electromagnetic vibrator | 14. Stepper motor controller |

Figure 1.1 Schematic arrangement of AJM set up

The valves 5, 9 and 12 shown in the figure do not operate during the normal functioning of the machine. They come into operation only when the machining is stopped. Valve 5 bypasses the compressed air into the atmosphere while 9 and 12 bypasses the abrasive air mixture into a sump 13 in which the unused abrasive powder gets collected. These valves are operated in the desired sequence by stepper motors, which in turn are controlled by the stepper motor controller 14. The signals for the stepper motor controller are generated by a microprocessor. The sequence of operation is valve 12 first, followed by 9 and 5. Before a new machining operation starts, the valves are put back to their normal operating position either manually or with the help of the microprocessor. The entire set up was fabricated under a DST sponsored project "The Mechanics of Abrasive Jet Machining and the effect of Electrostatic field on it". (No. III-6(2)/86-ET dated 26-10-1987).

1.2 Importance of the Present Work

The principle of this process and its applicability were known for many decades [1, 2, 3][§]. Unfortunately there is no scientific theory available so far, which explains the mechanics of material removal of the process. Because of the inadequacies in the theories many of the theoretical predictions of the material removal rate are inaccurate. Further, most of the research in this field is semi empirical in nature and requires modification of the estimates of material removal to suit real machining situations. This makes the design of an abrasive jet machine and the prediction of the material removal rate (mrr),

[§] The numbers within the square brackets indicate the references given at the end of the thesis.

(which is acknowledged to be one of the important parameters of AJM), a very difficult task. It is improbable, if not impossible, that the diameter of nozzle, the stand off distance and other parameters of the process can be chosen accurately for the purpose of drilling a hole of a given diameter on a work piece. Published research work in the field also is very few. The present investigation is aimed at addressing some of the inadequacies in understanding the mechanics of abrasive jet machining.

The major objectives of the present work are:

- (i) to develop an analytical theory for the mechanics of material removal, using the fundamental concepts of continuum mechanics,
- (ii) to predict from the theory, the effect of the various identified parameters of the process,
- (iii) to verify the theoretical predictions from the results of experiments and
- (iv) to examine critically the surface roughness of the flat surfaces produced by the process.

1.3 The Parameters of AJM Process

The material removal rate (mrr) in the AJM process is considered to depend on the following important independent parameters.

- (i) The mixing ratio (m_r): This is the mass flow rate of abrasive powder \dot{m}_{ab} per unit

mass flow rate of the mixture. ie., $m_r = \frac{\dot{m}_{ab}}{\dot{m}_{ab} + \dot{m}_{air}}$

- (ii) The stand off distance (S_d) : The distance of the nozzle tip from the work surface

- (iii) Nozzle diameter (d_n)
- (iv) System pressure (p_s)

In addition to the above process parameters, the following material properties are also considered in the analysis. They are:

- (i) the density of the abrasive ρ_{ab}
- (ii) mean diameter of the abrasive particles d_p , obtained from their size distributions
- (iii) elastic constants of the work medium. (Young's modulus E and Poisson's ratio ν)
and
- (iv) the mean ultimate strength of the material (The critical strain energy density).

1.4 Organization of the Thesis

The thesis is organized in six chapters. Chapter 1 is an introduction. Chapter 2 gives a survey of the literature on the experimental and theoretical aspects of Abrasive Jet Machining process. The theoretical study is carried out in two stages. With the help of the established theory of elasticity, the volume of material removed is attempted to be estimated by modeling the impact of a single particle as a boundary value problem. This is outlined in Chapter 3. The method of analysis of flow and the determination of particle velocity are discussed in Chapter 4. The results of the analytical theory and discussions on them along with the details of the experimental work carried are presented in chapter 5. The experimental results showing the influence of process parameters on the material removal rate, together with the results of surface studies are also presented in that chapter. Chapter 6 summarizes the conclusions and gives some suggestions for further research in this area.

Chapter 2

LITERATURE REVIEW

2.1 Studies on General Aspects of AJM

Feasibility of machining with a jet of a carrier fluid laden with particles was known for many decades. Most of the literature on AJM describes the mechanics of material removal in a qualitative manner while some others report the experimental findings [4-11]. The dependence of the material removal rate on the process parameters is ascertained experimentally [8]. The variation of material removal rate with some of the parameters is given in Figures 2.1, 2.2 and 2.3. Abrasive Jet Machining process is credited with the possibility of closely controlling the material removed [12]. Hence, polishing of surfaces, deburring and finishing operations can be effectively done by this process. Ordinary, optical and other types of glass are easily machined by AJM. It is likely that machining of composite materials also is possible. Most of the early research in the field of AJM is experimental in nature.

Ramachandran and Ramakrishnan [13] review the available literature on the theoretical and applied research in the field. They conclude that AJM is highly suitable for deburring, finishing and cutting operations. In experimentally investigating the nozzle wear during AJM process, Kumar, Verma and Lal [10] used a set up similar in details to the one shown in Figure 1.1. The results of the experiments are not relevant for the present study. Verma and Lal [9] studied the erosion rate, the diameter of the eroded cavity and the depth of penetration experimentally. The important findings are given in Figure 2.4. The results indicate the existence of an optimum stand off distance at which

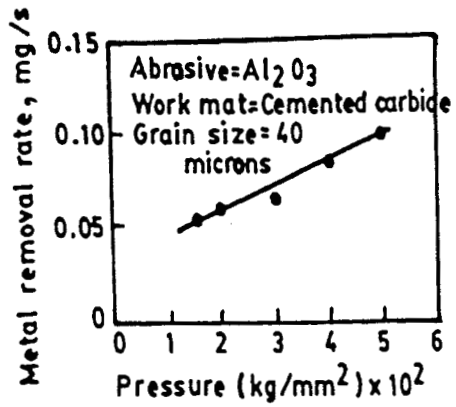


Figure 2.1 Variation of Material removal rate with pressure (Pandey and Shan [8])

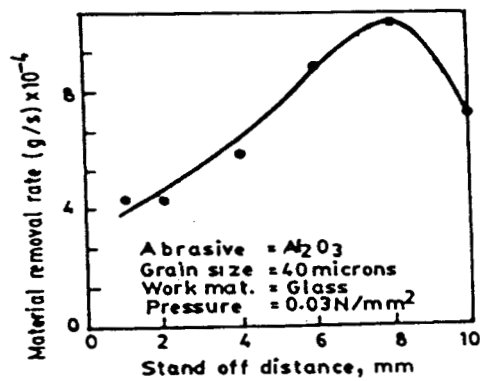


Figure 2.2 Variation of Material removal rate with Pressure (Pandey and Shan [8])

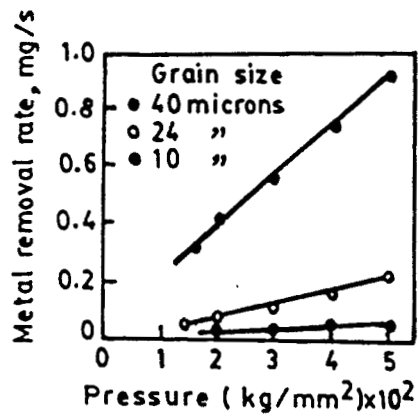
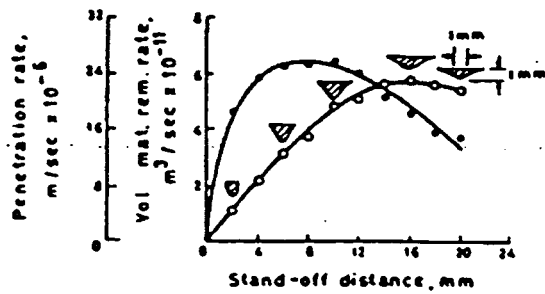
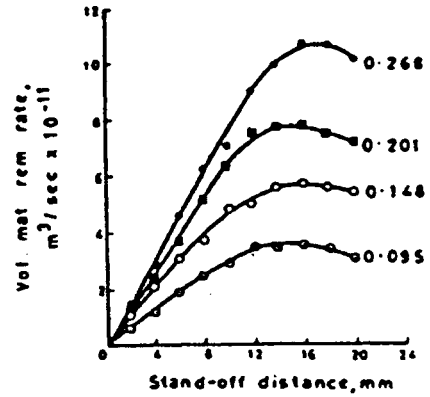


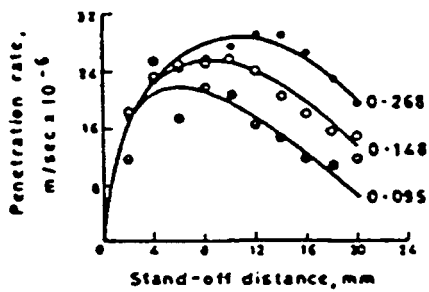
Figure 2.3 Variation of Material removal rate with Stand off distance (Pandey and Shan[8])



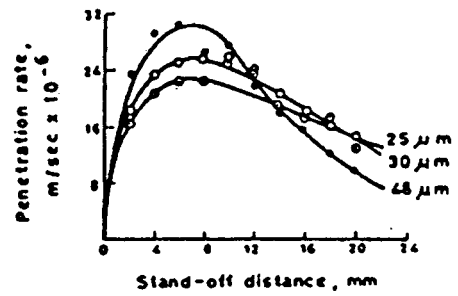
a, $30 \mu\text{m}$, $P_r: 14.715 \times 10^4 \text{ N/m}^2$ (gauge),
mixture ratio = 0.148,
cutting time = 60 sec.



b, m.r.r. for various mixture ratio
($30 \mu\text{m}$, $14.715 \times 10^4 \text{ N/m}^2$)

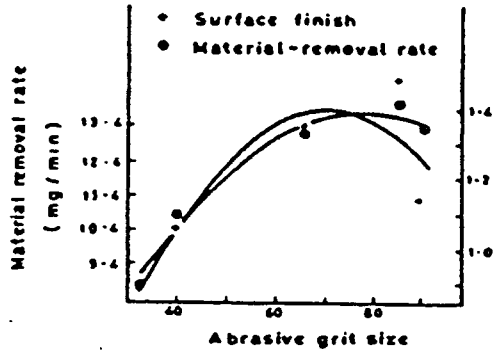


c, penetration rate for various
mixture rates
($30 \mu\text{m}$, $14.715 \times 10^4 \text{ N/m}^2$)

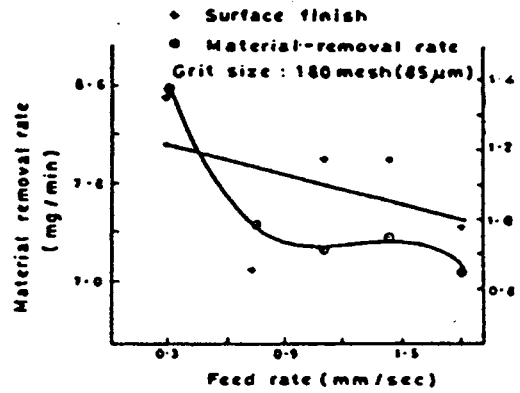


d, p.r. for various particle sizes
($14.715 \times 10^4 \text{ N/m}^2$, mixture
ratio = 0.148)

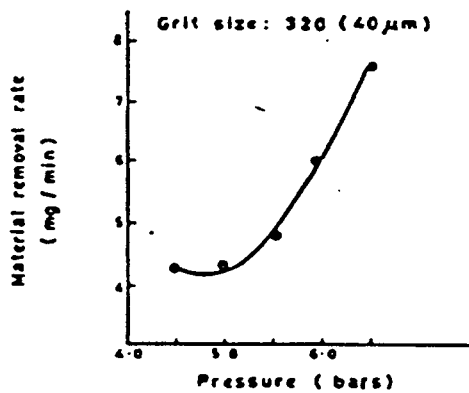
Figure 2.4 Variation of penetration rate and material removal rate with stand off distance (Verma and Lal [9])



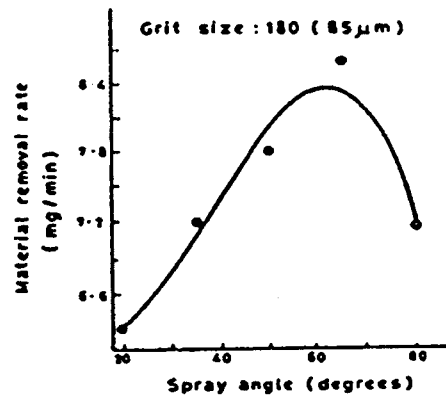
a. Effect of abrasive grit size



b. Effect of feed rate



c. Effect of changing the nozzle pressure on the material-removal rate.



d. Effect of the spray angle on the material-removal rate

Figure 2.5 Variation of material removal rate with some of the parameters of the

AJM process (Venkatesh[14])

the machining rate is a maximum. The penetration rate reaches a maximum at a different stand off distance when other parameters are changed. Venkatesh [14] included the impingement angle and feed rate as parameters in his study. The results are as shown in Figure 2.5.

The above experimental studies do not explain the effect of all the parameters of the process on the machining rate. The findings are not sufficient to predict the material removal rate either. Theoretical analysis of the mechanics of material removal is not attempted. The cause of material removal in AJM is the impact of abrasive particles on the work piece. Abrasive powder of a given grit size will contain grains of different sizes. The impacts of these grains are of two types: (i) simultaneous impact of different abrasive particles on different locations and (ii) successive impact of particles at the same location. Both these impacts take place in a machining situation. Recognizing this, the starting point for developing a theory for the mechanics of AJM is the impact of solid particles on the work piece medium.

Although the impact problem has not been studied theoretically in the context of AJM, the nature of the stress fields and brittle fracture due to the contact had been studied extensively. Hertz [15] analyzed the indentation of a semi-infinite linearly elastic medium by an indenter loaded by a constant normal force. The indenter also is assumed to be linearly elastic. The stress in the entire half space is compressive except in two narrow regions, one near the surface and the other near the axis of symmetry as shown in Figure 2.6. The magnitudes of these stresses depend on the normal force on the indenter. The first cracks, which are circular in nature, appear as soon as the tensile stress near the

surface exceeds the tensile strength of the material. Subsequently, these cracks grow as a conical crack and a conical volume under the contact zone is dislodged [16].

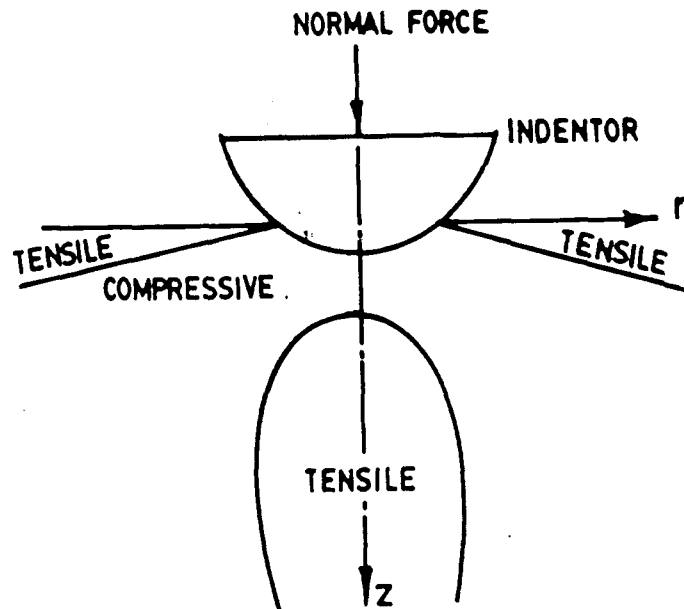


Figure 2.6 Hertz's solution of the impact problem

2.2 The Impact Problem and Erosion Analysis for Ductile Materials.

The first study of particle impact was done in Germany, in 1931, in connection with the collection of dust and smoke particles [17]. Finnie also reports that literature of work up to 1946 could not reveal much about the mechanics of material removal by erosion. Erosion tests carried out by Wellinger and colleagues (as reported by Finnie) are considered as the first to attempt to collect data on erosion. They attributed the erosion to

two processes called “rub” and “shock” erosions. It is generally acknowledged that these are some of the factors of the wear process.

Finnie obtained the following equation for Q , the volume of material removed from a medium, when a single spherical particle impacts it. The equation is:

$$Q = \frac{m_p V_p}{\sigma_f \lambda k_f} S_f \quad (2.1)$$

In equation (1), m_p is the particle mass, V_p is the particle velocity, σ_f is the plastic flow stress induced immediately after the impact, $\lambda = \frac{l}{y_t}$ where l is the depth of contact and y_t is the depth of cut (see Figure 2.7).

$$k_f = \frac{3 C_d \rho_0}{8 R_p \rho_p} \quad (2.2)$$

$$S_f = \sin 2\alpha - \frac{6}{k_r} \sin^2 \alpha \text{ for } \tan \alpha \leq \frac{k_r}{6} \text{ and } S_f = k_r \cos^2 \alpha / 6 \text{ for } \tan \alpha \geq \frac{k_r}{6} \quad (2.3)$$

Here, k_r is the ratio of vertical force to horizontal force on the particle.

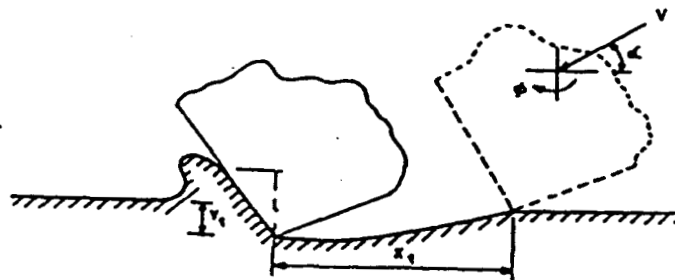


Figure 2.7 Model for material removal used by Finnie [17]

Finnie [19] modified this equation later. The factors influencing the erosion, as listed by Finnie are: (i) The angle of impingement, (ii) The particle size, (iii) Particle shape and strength, (iv) particle concentration in the fluid, (v) particle rotation at impingement, (vi) particle velocity, (vii) the shape of the surface, (viii) Properties of the work material, (ix) stress level of the surface and (x) the nature of the carrier gas. After making suitable assumptions, Finnie arrived at the following equation for the volume of material removal:

$$Q = \frac{2}{P} (\sin 2\alpha - \sin \frac{2}{P} \sin^2 \alpha) \text{ for } \alpha \leq \hat{\alpha} \text{ and}$$

$$Q = \cos^2 \alpha \text{ for } \alpha \geq \hat{\alpha} \quad (2.4)$$

In the above equation, P is a factor, which depends on the m_p , R_p , k_r and the moment of inertia I of the particle about its center of mass. This relationship is given by

$$P = \frac{Ik_r}{I + m_p R_p^2} \quad (2.5)$$

$\hat{\alpha}$ is the angle at which maximum erosion takes place. The above equations were further modified by Finnie and others [18, 20, 21].

It can be seen that, the theory cannot predict the erosion rate at normal incidence ($\alpha=90^\circ$). This is because; the theory assumes that the material removal is by an action similar to ploughing of the abrasive particles on the work surface. However, in AJM process the material is removed when the jet axis is normal to the work surface. This apparent contradiction is explained by suggesting that, at first the abrasive particles simply indent the surface without removing material from it. Particles impinging this roughened surface encounter a favorable angle of impingement due to the roughness.

Through photographic and metallographic studies, Tilly [22] found that the erosion of ductile materials takes place in two stages. They are: (1) on impact, the particles cause an indentation and sometimes remove a chip and (2) these impinging particles disintegrate. The fragments are projected radially from the site of impact, causing secondary damage. Tilly obtained analytical expressions for these two stages and experimental validation for the theory. The influence of the parameters like velocity, particle size and angle of impingement is also explained by the theory. According to this theory, the energy responsible for primary erosion is, $E_p = (E^{0.5} - E_e^{0.5})^2$ where E is the initial kinetic energy and E_e is the energy of the particle to cause elastic deformation.

Then,

$$E_p = 0.5m_p(V-V_0)^2 \quad (2.6)$$

where V is the velocity of the particles at impact, and V_0 is the velocity of the particles at and below which the work surface experiences only elastic deformations, without causing damage. Similar to this threshold velocity, a threshold diameter is defined, which is the minimum diameter required for erosion to take place. Denoting this threshold diameter as d_0 ,

$$E_p = \frac{1}{12} \rho_p \pi (d_p^{1.5} V - d_0^{1.5} V_0)^2 \quad (2.7)$$

The primary erosion ε_1 , which is the material removed by unit mass of impacting particle

$$\text{is given by } \varepsilon_1 = \frac{V_r^2}{\phi} \left(1 - \left(\frac{d_0}{d_p} \right)^{1.5} \left(\frac{V_0}{V_r} \right) \right)^2 \quad (2.8)$$

ϕ is related to the energy required to remove unit mass of material by the primary erosion process. The secondary erosion ε_2 is calculated from the impact velocity, by introducing a

secondary erosion factor γ and a factor F that measures the degree of fragmentation.

$$\text{i.e. } \varepsilon_2 = \left(\frac{V^2}{\gamma} \right) F \quad (2.9)$$

Tilly, Goodwin and Sage [23] calculated the fragmentation considering all particle sizes within a distribution. The final expression for erosion is written in the form

$$\varepsilon = \hat{\varepsilon}_1 \left[\frac{V}{V_r} \right]^2 \left[1 - \left(\frac{d_0}{d_p} \right)^{0.5} \left(\frac{V_0}{V_r} \right) \right]^2 + \hat{\varepsilon}_2 \left(\frac{V}{V_r} \right)^2 F \quad (2.10)$$

$\hat{\varepsilon}_1$ and $\hat{\varepsilon}_2$ are to be determined experimentally for test conditions at velocity V_r .

The idea of using energy in the criterion for material removal notwithstanding, the aforementioned theory requires two empirical coefficients. The stress analysis of the work medium is not attempted and probably because of this, the material properties do not appear in the equations.

2.3 Material Removal from Brittle Materials

Being one of the unconventional machining techniques, AJM is put to good use for machining materials like glass and ceramics, which are brittle and difficult to machine by conventional methods. For such materials the theory of material removal by erosion does not look suitable. This is because of the reason, that, during the fracture of brittle materials little or no plastic deformation is observed. The cracks appear without warning of the impending failure. The theory for material removal for such materials must then take into account this aspect and also cater to the situation where the particles impact normally with the work surface.

Assuming that the particles impact at 90° to the target surface, Sheldon and Finnie [24] investigated the erosion of brittle materials. Lee et.al. [25] studied the indentation of a semi infinite medium by a spherical ball and obtained results, which are comparable with experimental observations . Evans and others [26] reported that during a single particle impact, the surface of the work material showed radial and lateral cracks. The sections of the work medium also revealed that the cracks consist of a series of radial and conical cracks, which penetrate into the target as shown in Figure 2.8. These authors forget an important aspect, that the impact of a particle on a medium gives rise to an impulse, rather than a steady normal force. The stress and strain fields set up by the impact is transient in nature. The indentation problem is solved without considering the inertia of the medium, treating the problem as quasi-static. In the impact problem the inertia of the material is to be taken into account.

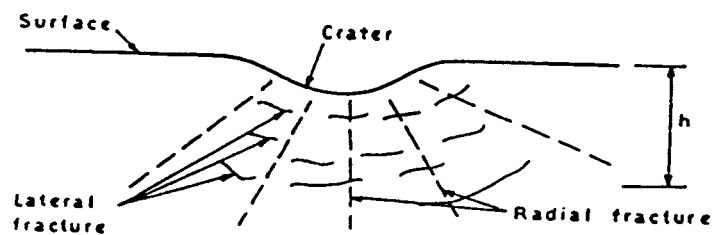


Figure 2.8 Conical cracks on brittle materials (Evans and others [26])

In studying the mechanics of ultrasonic machining (USM), Shaw [27] analyzed the problem of a spherical particle impinging on an elastic half space. According to him, the material removed by the impact of one particle on the medium is given by

$$w = Kd_p^3 V_{\max}^{1.5} \left(\frac{\rho_{ab}}{Y} \right)^{0.75} \quad (2.11)$$

where d_p is the diameter of the particle, V_{\max} is the velocity of the particle at impact, ρ_{ab} is the density of the particle, Y is the yield strength of the medium in uni-axial tension test and K is a constant. Shaw arrived at the above result after postulating that, the volume of material removed is proportional to R_c^3 where R_c is the radius of the contact

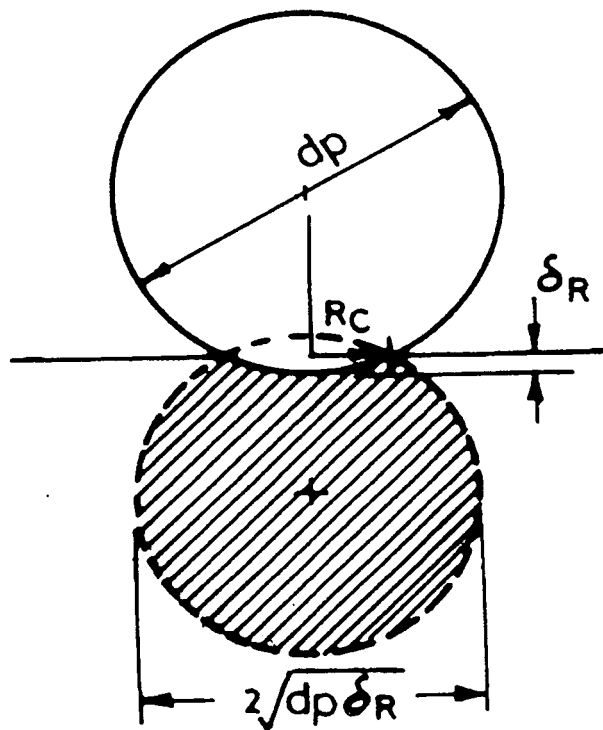


Figure 2.9 Shaw's model for material removal

zone after full indentation is over. The material removed in a single impact is spherical. (Figure 2.9). The penetration depth δ_R is calculated by equating the work done by the abrasive during penetration and the kinetic energy of the particle. The resistance to the penetration is the average contact-pressure $\bar{\sigma}$ where $\bar{\sigma}$ is the rupture strength of the work piece material.

It is seen that the penetration depth is not calculated with the aid of a stress analysis of the work medium. Further, material is assumed to be dislodged from the work piece, when the abrasive particles penetrate to a depth δ_R and the fragmentation profile is taken to be spherical. These are not based on any theory. However, this mode of material removal accounts for about 3% of the total material removal in USM and is insignificant. These shortcomings can therefore be overlooked. In AJM, on the other hand, this is the major mechanism of material removal and Shaw's theory is thus inadequate in the present context.

Assuming that each grain of the abrasive removes a hemisphere of material and that the theory of indentation is applicable to impact also, Murthy, Roy and Mishra [28] developed relationship for the material removal rate for brittle materials. The depth of penetration is calculated as

$$\delta_p = \left\{ \frac{9}{16} \pi^2 P_1^2 \left[\frac{1 - \nu_p^2}{\pi E_p} + \frac{1 - \nu_t^2}{\pi E_t} \right] \left(\frac{1}{R_p} + \frac{1}{R_t} \right) \right\}^{0.33} \quad (2.12)$$

In this relation P_1 is the indentation load, ν_p, ν_t , E_p and E_t are the Poisson's ratio and Young's modulus of the particles and target material respectively and R_p and R_t are the radii of curvature of the abrasive particle and target surface respectively. For plane work

pieces R_t is infinite. Making other assumptions and utilizing the depth of penetration, the following equation for material removal rate (mrr) is arrived at.

$$\text{mrr} = 0.5 \left(\frac{5\pi}{4} \right)^{0.6} \left[\frac{1 - v_p^2}{E_p} + \frac{1 - v_t^2}{E_t} \right]^{0.6} \frac{\dot{m}_{ab} V_1^2}{\rho_p^{0.4}} \quad (2.13)$$

where \dot{m}_{ab} is the flow rate of the abrasives and V_1 is the velocity of the particles at impact. However, this analytical formula is not experimentally corroborated. Ramachandran [29] pointed out the following deficiencies for the analysis. (1) All particles may not be contributing equally to mrr and the assumption that material removed is hemispherical in shape is not correct. (2) Detailed analysis for velocity is not done. (3) The effect of angle of impingement is not investigated. Ramachandran's work is based on the assumption that material is removed by erosive cutting. He also has overlooked the real nature of the problem, that an impact is not Hertzian contact.

Sarkar and Pandey [6] borrowed Shaw's theory for material removal (Equation 2.12) and adapted it to AJM. After incorporating N , the number of particles striking the surface, the material removal rate in AJM is obtained as:

$$\text{mrr} = KNd_p^3 V_{\max}^{1.5} \left(\frac{\rho_{ab}}{Y} \right)^{0.75} \quad (2.14)$$

While Shaw's work is mainly concerned about elastic impact, Jain, Chitale and Nagar [30], studied the material removal rate in AJM process by considering the impact to be elastic-plastic in nature. This also follows the Hertz's solution of elastic impact. The extents of elastically and plastically loaded region are determined by comparing the average pressure at the surface of contact to the yield strength Y , as shown in Figure 2.10.

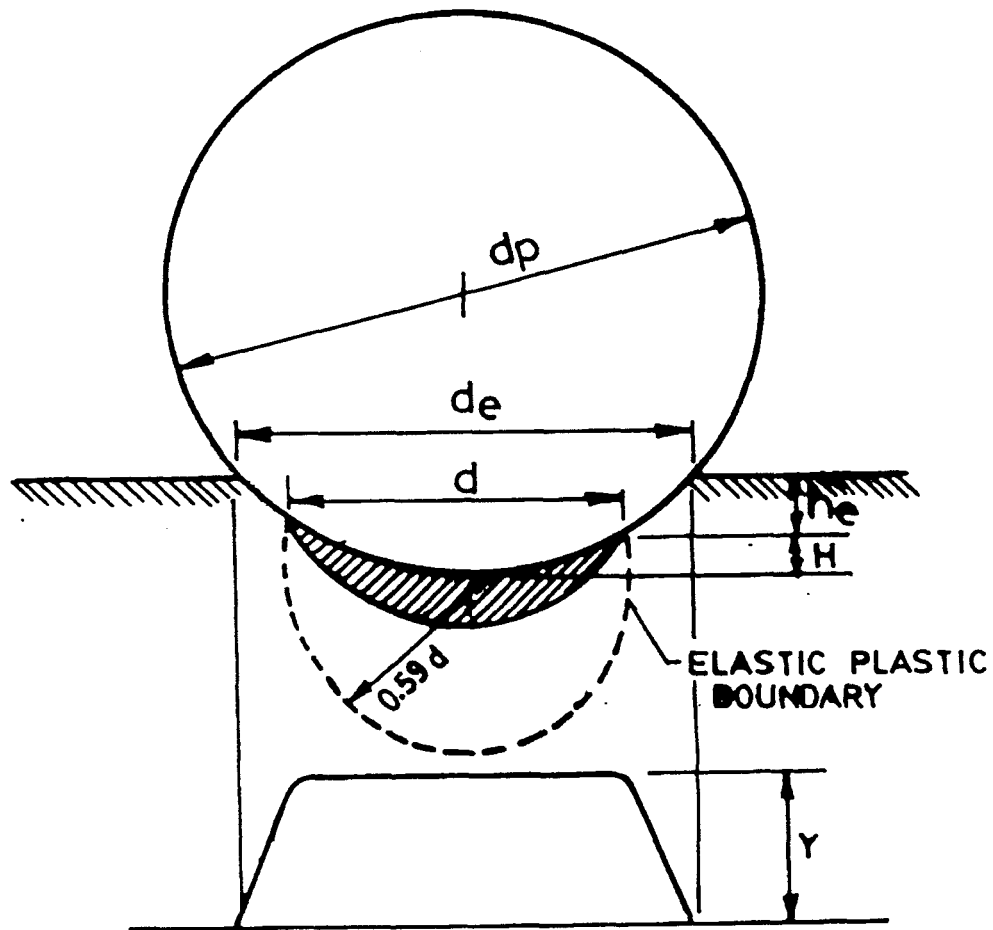


Figure 2.10 Elastic-Plastic model used by Jain et.al. [30]

The volume chipped out is then assumed to be proportional to the plastically deformed volume. The material removal rate mrr is found as

$$mrr = Kd_p^3 N \left\{ \left[V_{\max}^2 - V_e^2 \right] \frac{P}{12Y} \right\}^{0.75} \quad (2.15)$$

In this equation V_e is the velocity of particles for elastic impact and P is the average surface pressure. The threshold velocity V_e is found from the equation

$$V_e = \frac{\pi^2}{2\sqrt{10}} \frac{Y^{2.5}}{P} \left[\frac{1-\nu_p^2}{E_p} + \frac{1-\nu_t^2}{E_t} \right]^2 \quad (2.16)$$

The notations have the same meanings as in Equations (2.13), (2.14) and (2.15). In the above analysis, the impact problem is modeled as an elastic problem. But, the plastic zone is not identified by a stress analysis. The criterion is based on the average surface pressure as calculated by Hertz. Further, the fracture volume is assumed to be proportional to the volume of a sphere of diameter d_p . This idea is in line with Shaw's intuition. A redeeming feature of the study is that the elastic nature of the particles also is taken into account.

In discussing problems associated with USM, Bhoi and Mishra [31] use Shaw's model for material removal. Many researchers [16, 32] used Hertz's theory for discussing brittle fracture and wear.

Nair [33] modeled the impact problem as a boundary value problem of elasticity. Theory of wave propagation in elastic media is used for the purpose. The impulse given to the medium is assumed to generate a longitudinal wave and a shear wave. This is in the context of USM where the main mechanism of material removal is the hammering action of the abrasives on the work piece. The main assumptions made are:

1. the work piece material is linearly elastic
2. the abrasive particles are rigid and spherical in shape
3. during the impact the abrasive particles penetrate into the tool and work piece
4. the tool tip motion is simple harmonic
5. the abrasive grit receives only a single impact
6. during each cycle, abrasive particles will be available under the tool and

7. Sih's [34] hypothesis regarding crack initiation and propagation are valid for the three-dimensional case also.

Working from fundamentals, Nair developed a model, which predicts the machining rate. These theoretical predictions are in good agreement with experimental findings. Many of the above assumptions are not relevant in the present situation. He simulated the impact problem by a series of symmetrically placed point disturbances. This is probably to take into account the fact that a point impact is physically impossible if the particles are not truly spherical in shape.

2.4 Review of Literature on Gas-Particle Flows.

Some of the early research in the field was centered on defining an equivalent fluid with properties different from that of its constituents [35, 36]. The realization of the equivalent fluid assumes that the gas and particles are in thermal and mechanical equilibrium. Nelson and Gilchrist [37] studied the gas-particle flow inside a nozzle analytically and experimentally. The effects of the parameters like particle size, particle density and initial velocity are incorporated in the study. In this, it is suggested that the aerodynamic drag is the cause for particle motion. Since the coupling between particle motion and fluid flow is very difficult to treat analytically, the more popular approach is to use numerical methods for solutions. Sharma and Crowe [38] developed a computational model to meet with this requirement. In this model, the basic conservation equations themselves are solved over a computational cell, taking the coupling nature of the problem along with the computation, in the form of source terms. (**Particle-source-in**

cell (PSI) method). The suggested model does not include the source terms due to particle-particle collisions, which can be neglected, for low particle loading (mixing ratio in the context of AJM) [39].

For the flow of gas particle mixtures through short nozzles, the effects of friction and heat transfer are so small that, they can be neglected. Further, the effects of the boundary layer also can be neglected, enabling the flow to be modeled as a one-dimensional flow. Zuckrow and Hoffman [40] give a set of equations governing the steady flow of a gas particle mixture through a nozzle. The equations pertain to particle samples having a single average diameter. The collisions between the particles are neglected. Arastoopour et.al. [41] extended the above analysis to gas particle flows in which the particles are classified to belong to two classes. The model used is an isothermal model, which is inadequate when the velocity and pressure changes are large, as would be the case in a nozzle flow. In a later work reported by the same authors [42], the effect of particle-to-particle collisions is also taken into account. Adopting the isothermal model for analysis, Doss [43] modified the above by incorporating the particle size distribution and inter-particle collisions. The analytical findings are compared with Farber's [35] experimental results. The effects of the mixing ratio, the supply pressure and the nozzle geometry were investigated by Hatta and others [44]. The same authors studied supersonic internal flows [45]. In these, the space occupied by the particles is neglected, primarily because the specific volume of the particles is very small. Zuckrow and Hoffman took care of this by defining 'volume fraction', which is a measure of the volume occupied by the particles. At reasonable velocities, the effects of gravity and wall heat transfer are also negligible.

The characteristics of the flow of a jet of fluid, (with or without particles in it) are different from that of the flow through a nozzle. The major difference is the exchange of momentum between the jet and the surrounding fluid. As a result of this, the velocity distribution in the jet changes as it moves downstream and the mass flow rate across a plane normal to the jet axis increases continuously (entrainment). The component of the velocity normal to the jet axis is very small and therefore the flow in a jet is described by the corresponding boundary layer equations [46, 47]. In most of the practical situations, the jets are turbulent. In addition, the behavior of the jet in the vicinity of a wall is even more difficult to analyze.

While analyzing the heat transfer characteristics of a laminar jet impinging on a flat plate of uniform temperature, Al- Sanea [48] observed that the cross flow effects degraded the heat transfer rate. The velocity field is not explicitly calculated in this. Moreover, the analysis is on a laminar jet. In general, turbulent flows are formulated after making hypotheses regarding the turbulent fluctuations, which must be supplemented by experimental observations. Most of such studies, experimental and analytical are summarized by Abramovich [49]. Restricting the analysis to the similarity zone, Abramovich observed that, the presence of particles or droplets made the jets narrower [50]. However, Goldschmidt and Eskinazi [51] found that the dispersed phase has very little effect on the main flow. This is attributable mainly to the low mixing ratios at which the calculations are done. Hetzroni and Sokolov [52] obtained relationships between the fluctuations in the longitudinal velocity and its time average. The study of Danon et.al. [53] is on an axi-symmetric jet. The focus is on turbulence and the effect of particles on turbulence energy. The investigations of Laats and Frishman [54] and Elshorbaggy et.al.

[55] revealed that the spreading rate of a particle laden jet is slower than the spreading rate of a single-phase jet. The above analyses are with droplets in a gas phase. In solid-gas streams, evaporation and condensation do not take place, as would be the situation in droplet gas jets.

As a sequel to earlier papers, Hatta and others [56] report the results of numerical calculations of two-phase jets. In their study, the flow is assumed to be non-dissipative (non viscous). This means that the modification to the inviscid flow is only through the particle drag terms. This is a big deficiency, because the entrainment of the surrounding fluid and subsequent spreading of the jet is through the viscous effects. In AJM this effect is important because, it is known that with the same nozzle diameter, the diameter of holes drilled are larger at larger stand off distances. This effect is due to the spreading of the jet. The works of Kim and Aihara [57] and Ozdemir and Whitclaw [58] are on single-phase gas jets impinging on a flat plate. Two-phase jets are not considered. Ramachandran [29] employs Sharma and Crowe's [38] PSI cell method and has formulated the flow in the free jet region. This method is a finite volume formulation. However, the results of his numerical calculations are not presented.

The above survey reveals that researchers do not agree upon a unique method of solving the solid-gas flow. However, for solving internal flows, the equations suggested by Zuckrow are almost invariably employed. In the analysis that follows, a simple method of calculating the particle velocity at impact is presented. The Gas flow field is determined from the Eulerian equations while the particle velocities are found from the Lagrangian equations. The method is similar to the one adopted by Verma and Lal [59].

2.5 Conclusion

Studies on abrasive jet machining process, the method of estimating the material removal rate by erosion analysis for ductile and brittle materials and the analysis of the flow of gas-abrasive mixtures are reviewed in the preceding sections. In the present work, the problem of impingement by a single particle is simulated by a point disturbance at the origin of the coordinates. This utilizes the theory of wave propagation in elastic medium. For analyzing the nozzle flow, the equations suggested by Zuckrow are adopted. In the free jet region, the gas flow is solved from the relevant boundary layer equations and their standard solutions. The particle flow is studied in both the regimes by the Lagrangian method.

Chapter 3

THEORY OF MATERIAL REMOVAL IN AJM

3.1 Outline of the theory

A survey of the literature points to the fact that analysis of the mechanics of material removal in AJM, are mostly dependent on erosion models pioneered by Hertz and Finnie. Brittle materials undergo very little or no plastic deformation before fracture. Keeping these in mind, a theory for the mechanics of material removal in AJM is proposed. In developing the theory, the work material is considered to be a conservative, linearly elastic continuum. The impacting abrasive particles are assumed to be rigid and spherical in shape. Further, the impact of the particles on the medium is considered to be normal to the surface. These assumptions enable one to formulate the problem as a boundary value problem in elasticity.

The fracture profile and fracture volume are determined by the failure hypothesis proposed by Sih [34]. This hypothesis is based on the strain energy density function SED.¹ The hypothesis is: “the onset of cracking occurs when SED reaches a critical value SED_{cr} ”. This hypothesis is proposed with respect to two-dimensional case. It is extended to the present three-dimensional axi-symmetric problem also.

¹ Strain energy density is an abstract function. This function is such that for linearly elastic media $\sigma_{ij} = \frac{\partial(SED)}{\partial \varepsilon_{ij}}$ and $\varepsilon_{ij} = \frac{\partial(SED)}{\partial \sigma_{ij}}$. No experimental methodology is developed so far to characterize the critical value for fracture of a medium.

During the AJM process, the impact of the abrasive particles is of two modes. They are: (i) the impact of the particles on the same location and one after the other and (ii) simultaneous impact of particles at different locations of the work piece. In the analysis no differentiation is made between these two types of impacts. Each impact is assumed to remove the same quantity of material, provided that the other conditions are the same. The dispersion of the particles in the jet and the diameter distribution of the particles in the jet are not taken into account.

The parameters of the process which are considered in the analysis are:

1. The supply pressure of air p_s
2. The mixing ratio m_r
3. The diameter of the nozzle d_n and
4. The stand off distance S_d

In addition to these the material properties of the work piece and the abrasives are also considered.

The proposed theory has several novelties. They are

1. The material properties of the medium (The Young's modulus, the Poisson's ratio and the critical strain energy density) need only be prescribed, to theoretically evaluate the material removal rate
2. the method is scientific as it makes use of the established theories of elasticity
3. no experimental corrections need be done for the estimate of the material removal rate and
4. a complete model for the AJM process is made.

3.2 Theory of Material Removal from the Impact of one Abrasive Grain

To make a mathematical model for the impact of an abrasive particle on the work piece the following simplifying assumptions are made.

1. The impacting particles are perfectly rigid and spherical in shape. All the particles are of the same average diameter. In general, the particles are of some irregular shape. Being abrasive particles, they are likely to exhibit sharp edges. However, in the proposed theory, the presence of sharp edges is not a requisite for the removal of material. Similarly, the diameter distribution of particles is not considered and the abrasive is assumed to compose of just one class of particles having the diameter corresponding to the grit size.
2. In this analysis, the AJM process is assumed to be used only in the situation where brittle materials like glass and ceramics are machined. This makes it possible to assume that the work material is linearly elastic.
3. The impact is non dissipative in nature. This will mean that the energy possessed by the abrasive particles during impact is transferred to the work medium completely. A requisite for this condition is that, there is no or negligible friction between the work piece and the particle.
4. Sih's hypothesis is valid for the three-dimensional case also. Thus the region where $SED \geq (SED)_{cr}$ corresponds to material dislodged from it.
5. At any time during the impact, the kinetic energy lost by the particle is transferred to the medium.

6. Waves reflected from the bounding surface into the medium do not contribute to material removal and are not considered for the stress analysis.

Figure 3.1 represents a rigid spherical particle impacting a semi-infinite elastic medium. The velocity of impact is V_{\max} . As the particle penetrates into the medium, it transfers its kinetic energy to the medium. Eventually the velocity of the medium becomes zero. The time duration from the moment of impact to the time where the particle velocity becomes zero is the contact time T_c . The standard Navier's formulation of the boundary value problem of elasticity is taken as the governing equation for this physical phenomenon. The appropriate system of coordinates is the cylindrical polar coordinates. The origin of co-ordinates is at the point of contact of the particle. Z-axis is an axis of symmetry.

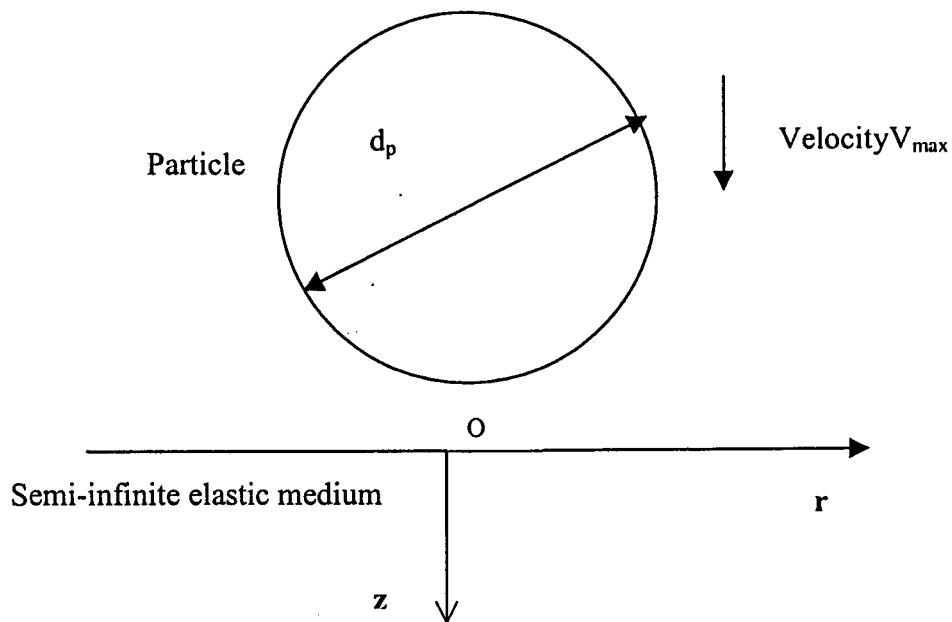


Figure 3.1 Impact of a spherical particle on a semi infinite elastic medium

Assuming that there is no rigid body rotation, the circumferential displacement U_θ does not exist. U_r and U_z are the radial and axial displacements and are functions of r and z only. With these, the equilibrium equations are:

$$(\lambda + G) \frac{\partial}{\partial r} \left(\frac{\partial U_r}{\partial r} + \frac{U_r}{r} + \frac{\partial U_z}{\partial z} \right) + G \left(\nabla^2 U_r - \frac{U_r}{r^2} \right) = \rho_w \frac{\partial^2 U_r}{\partial t^2} \quad (3.1)$$

$$\text{and } (\lambda + G) \frac{\partial}{\partial z} \left(\frac{\partial U_r}{\partial r} + \frac{U_r}{r} + \frac{\partial U_z}{\partial z} \right) + G \left(\nabla^2 U_z \right) = \rho_w \frac{\partial^2 U_z}{\partial t^2} \quad (3.2)$$

$$\text{where } \nabla^2 = \frac{\partial^2}{\partial r^2} + \frac{1}{r} \frac{\partial}{\partial r} + \frac{\partial^2}{\partial z^2} ,$$

λ is the Lamé's constant and G is the shear modulus.

3.3 The Boundary Conditions

The initial and boundary conditions are:

At time $t = 0$, $r = 0$, and $z = 0$

$$\frac{\partial U_z}{\partial t} = V_{\max} ; U_r = 0 \text{ and } U_z = 0. \quad (3.3)$$

This condition sets the work medium free of any displacement at the time when the impact begins. Similarly the initial velocity of the particle is set equal to V_{\max} .

At the end of the impact, i.e. at time $t = T_c$,

$$\frac{\partial U_z}{\partial t} = 0 \text{ at } r = 0 \text{ and } z = 0 \quad (3.4)$$

If V is the velocity of the particle at any instant and ΔE_K is the kinetic energy transferred to the medium up to the instant

$$\Delta E_K = \rho_{ab} \frac{4}{3} \pi \left(\frac{d_p}{2} \right)^3 \left(\frac{V_{max}^2 - V^2}{2} \right) \quad (3.5)$$

In this, ρ_{ab} is the density of the abrasive particle.

The strain energy density in the medium at any instant t is

$$\Delta E_s = \int_0^\infty \int_0^\infty \int_0^\infty \frac{\partial}{\partial t} (SED) 2\pi r dr dz dt \quad (3.6)$$

The rigid particle transfers all its energy to the medium during the time interval T_c . The particle velocity is zero at time T_c . This is mathematically represented by the following:

$$\text{at } t = T_c, \Delta E_K = \rho_{ab} \frac{4}{3} \pi \left(\frac{d_p}{2} \right)^3 \left(\frac{V_{max}^2}{2} \right) \text{ and} \quad (3.7)$$

$$\Delta E_s = 2\pi \int_0^\infty \int_0^\infty SED_{t=T_c} r dr dz \quad (3.8)$$

Equating the two equations (3.7) and (3.8) we get the condition

$$\int_0^\infty \int_0^\infty SED_{t=T_c} r dr dz = \frac{1}{3} \left(\frac{d_p}{2} \right)^3 \rho_{ab} V_{max}^2 \quad (3.9)$$

In the equations, SED is the strain energy density function.

T_c is determined from the boundary condition (3.4). The depth of penetration of the particle into the medium is h_{max} . This is to be determined from the deformation of the medium. That is: h_{max} is the displacement U_z of the point of contact $(0, 0)$ at the time $t = T_c$.

Apart from these, the following boundary conditions are also prescribed. They are:

$$\text{At time } t = T_c, r = R_c, z = 0, \sigma_z = 0 \text{ and } \tau_{rz} = 0. \quad (3.10)$$

$$\int_{R_c}^{\infty} 2\pi r \sigma_z dr = 0 \quad \text{and} \quad \int_{R_c}^{\infty} 2\pi r \tau_{rz} dr = 0 \quad (3.11)$$

$$\text{Here } R_c \text{ is the radius of the contact zone given by } R_c^2 = R_p^2 - (R_p - h_{\max})^2 \quad (3.12)$$

These conditions are specified to satisfy the conditions of the unloaded surface $r \geq R_c$, $z = 0$. The displacements are transient. The stress and strain are also transient. The time dependent part takes care of this.

The governing equations 3.1 and 3.2 with boundary conditions 3.3, 3.4, 3.9, 3.10 and 3.11 are to be solved.

3.4 Method of Solution.

The governing equations 3.1 and 3.2 form a set of second order coupled partial differential equations. Before they are decoupled and solved the equations and their boundary conditions are non-dimensionalised. The following set of non-dimensional variables is introduced. They are

$$r^* = \frac{r}{R_p}; \quad z^* = \frac{z}{R_p}; \quad t^* = \frac{tV_{\max}}{R_p}; \quad U_r^* = \frac{U_r}{R_p}; \quad \text{and} \quad U_z^* = \frac{U_z}{R_p} \quad (3.13)$$

With these, the governing equations are transformed into

$$\frac{\lambda + G}{\rho_w V_{\max}^2} \frac{\partial \varepsilon_T^*}{\partial z^*} + \frac{G}{\rho_w V_{\max}^2} \nabla^{*2} U_z^* = \frac{\partial^2 U_z^*}{\partial t^{*2}} \quad (3.14)$$

$$\frac{\lambda + G}{\rho_w V_{\max}^2} \frac{\partial \varepsilon_T^*}{\partial r^*} + \frac{G}{\rho_w V_{\max}^2} \left(\nabla^{*2} U_r^* - \frac{U_r^*}{r^{*2}} \right) = \frac{\partial^2 U_r^*}{\partial t^{*2}} \quad (3.15)$$

where ε_T^* is the first invariant of the strain tensor $= \varepsilon_r^* + \varepsilon_\theta^* + \varepsilon_z^*$ and

$$\epsilon_r^* = \frac{\partial U_r^*}{\partial r^*}$$

$$\epsilon_0^* = \frac{U_r^*}{r^*}$$

$$\epsilon_z^* = \frac{\partial U_z^*}{\partial z^*}$$

In a similar fashion the boundary conditions are transformed to the following:

At time $t^* = 0$, $r^* = 0$ and $z^* = 0$,

$$\frac{\partial U_z^*}{\partial t^*} = 1.0, U_r^* = 0 \text{ and } U_z^* = 0 \quad (3.16)$$

$$\text{At } t^* = T_c^* = \frac{T_c V_{\max}}{R_p}, \frac{\partial U_z^*}{\partial t^*} = 0 \quad (3.17)$$

$$\text{And } \int_0^{\infty} \int_0^{\infty} r^* (\text{SED})^*_{t^*=T_c} dr^* dz^* = \frac{\rho_{ab} V_{\max}^2}{3\lambda} \quad (3.18)$$

$$\text{Here } \text{SED}^* \text{ is calculated from } \text{SED}^* = \frac{1}{2} \epsilon_r^2 + \frac{G}{\lambda} (\epsilon_r^2 + \epsilon_0^2 + \epsilon_z^2) + \frac{G}{2\lambda} \gamma_{rz}^2 \quad (3.19)$$

$$\text{In this, } \gamma_{rz} = \frac{\partial U_r^*}{\partial z^*} + \frac{\partial U_z^*}{\partial r^*} \quad (3.20)$$

The conditions given by 3.10 and 3.11 are replaced by the following conditions:

$$\epsilon_r^* + \frac{2G}{\lambda} \frac{\partial U_z^*}{\partial z^*} = 0; \text{ and } \frac{\partial U_r^*}{\partial z^*} + \frac{\partial U_z^*}{\partial r^*} = 0 \text{ at } r^* = R_c^*, z^* = 0 \text{ and } t^* = T_c^* \quad (3.21)$$

$$\int_{R_c^*}^{\infty} \left[\left\{ \epsilon_r^* + \frac{2G}{\lambda} \frac{\partial U_z^*}{\partial z^*} \right\}_{z^*=0} \right] r^* dr^* = 0 \text{ and } \int_{R_c^*}^{\infty} \left[\frac{\partial U_r^*}{\partial z^*} + \frac{\partial U_z^*}{\partial r^*} \right]_{z^*=0} r^* dr^* = 0 \quad (3.22)$$

$$\text{In these } R_c^* = \sqrt{1 - \left(1 - \frac{h_{\max}}{R_p} \right)^2} \quad (3.23)$$

The governing equations are decoupled and expressed as wave equations by introducing the non-dimensional potentials $\phi(r^*, z^*, t^*)$ and $\psi(r^*, z^*, t^*)$. These potentials are related to the displacement field by [35]

$$U_r^* = \frac{\partial \phi}{\partial r^*} + \frac{\partial^2 \psi}{\partial r^* \partial z^*} \quad \text{and} \quad U_z^* = \frac{\partial \phi}{\partial z^*} - \frac{1}{r^*} \frac{\partial}{\partial r^*} \left(r^* \frac{\partial \psi}{\partial r^*} \right) \quad (3.24)$$

The governing equations are decoupled into the following equations:

$$C_1^2 \nabla^{*2} \phi = \frac{\partial^2 \phi}{\partial t^{*2}} \quad (3.25)$$

$$\text{and } C_2^2 \nabla^{*2} \psi = \frac{\partial^2 \psi}{\partial t^{*2}} \quad (3.26)$$

$$\text{where } C_1 = \sqrt{\frac{\lambda + 2G}{\rho_w V_{\max}^2}} \quad \text{and} \quad C_2 = \sqrt{\frac{G}{\rho_w V_{\max}^2}} \quad (3.27)$$

The equations 3.25 and 3.26 are standard wave equations. C_1 and C_2 are the corresponding wave velocities. They can be solved by the method of separation of variables. (See appendix A). The solutions are:

$$\phi = \frac{a_1}{\beta} \exp\left(-\zeta_1 \left(t^* - \frac{\beta}{C_1}\right)\right) \left\{ \frac{a_2 - j\left(t^* - \frac{\beta}{C_1}\right)}{a_2^2 + \left(t^* - \frac{\beta}{C_1}\right)^2} \right\} \quad (3.28)$$

$$\text{and } \psi = \frac{b_1}{\beta} \exp\left(-\zeta_2 \left(t^* - \frac{\beta}{C_2}\right)\right) \left\{ \frac{b_2 - j\left(t^* - \frac{\beta}{C_2}\right)}{b_2^2 + \left(t^* - \frac{\beta}{C_2}\right)^2} \right\} \quad (3.29)$$

In these equations ζ_1 and ζ_2 can be regarded as damping factors for ϕ and ψ respectively and $\beta = \sqrt{(1+z^*)^2 + r^{*2}}$. ϕ and ψ represented by equations 3.24 and 3.25 are complex.

They are made real functions by taking a_1, a_2, b_1 and b_2 to be purely imaginary numbers.

Thus $a_1 = jA_1, a_2 = jA_2, b_1 = jB_1$ and $b_2 = jB_2$. These, when put into the solutions yield

$$\phi = \frac{A_1}{\beta} \exp(-\zeta_1(t^* - \frac{\beta}{C_1})) \left\{ \frac{(t^* - \frac{\beta}{C_1}) - A_2}{(t^* - \frac{\beta}{C_1})^2 - A_2^2} \right\} \quad (3.30)$$

$$\psi = \frac{B_1}{\beta} \exp(-\zeta_2(t^* - \frac{\beta}{C_2})) \left\{ \frac{(t^* - \frac{\beta}{C_2}) - B_2}{(t^* - \frac{\beta}{C_2})^2 - B_2^2} \right\} \quad (3.31)$$

The constants A_1, A_2, B_1, B_2 and T_c in the above equations are found with the help of the boundary conditions.

3.5 Technique of Solving for A_1, A_2, B_1, B_2 and T_c

The constants A_1, A_2, B_1, B_2 and T_c in the above equations (equations 3.30 and 3.31) are found from the boundary conditions. This is done numerically in a computer. The numerical scheme is as follows [36]:

An initial guess for the solution vector $\mathbf{X} = \{A_1, A_2, B_1, B_2, T_c\}^T$ is given. With this initial guess for \mathbf{X}_i , the values of $U_r, U_z, \frac{\partial U_z}{\partial t}$ etc. are calculated as required in the boundary conditions. If \mathbf{X}_i is the solution vector, all conditions will be satisfied. Otherwise each condition will yield a residue. A function $F_i = \sum_{j=1}^n R_j^2$ is obtained. In this, n is the number of boundary conditions, and R_j is the residue of the j^{th} boundary condition. The \mathbf{X}_i that minimizes the function F_i is chosen as the solution vector. \mathbf{X}_i is

modified by an iterative procedure. The iterative procedure is the variable metric method of Davidon, Fletcher and Powell. The algorithm of the method is given below. The corresponding flow charts are given in appendix B.

3.6 Algorithm for the Iterative Procedure

- i) Start
- ii) Give initial guess for X_i and an $N \times N$ positive definite matrix H_i . H_i is the identity matrix I initially. Set iteration number = i .
- iii) Calculate the residues R_j and evaluate $F_i = \sum_{j=1}^n R_j^2$.
- iv) If $F_i < \epsilon$ a small number (which is set earlier), output X_i as the solution and stop. Else
- v) Compute the gradient of $F_i = \nabla F_i$ at X_i and set $S_i = -H_i \nabla F_i$.
- vi) Compute an optimum step length λ_i^* in the direction of S_i . (This is done by any one of the one dimensional optimization techniques).
Set $X_{i+1} = X_i + \lambda_i^* S_i$.
- vii) Test X_{i+1} for $F_{i+1} \leq \epsilon$. If this is satisfied, output X_i as the solution and stop. Else,
- viii) Update H matrix as $H_{i+1} = H_i + M_i + N_i$

$$\text{where } M_i = \frac{\lambda_i^* S_i S_i^T}{S_i^T Q_i}$$

$$N_i = -\frac{(H_i Q_i)(H_i Q_i)^T}{Q_i^T H_i Q_i} \quad \text{and}$$

$$Q_i = \nabla F(X_{i+1}) - \nabla F(X_i)$$

ix) Set iteration number $i = i+1$ and go to step (v)

3.7 Prediction of Material Removal Rate

The values of the constants A_1 , A_2 , B_1 , B_2 and T_c are determined as outlined in the previous section. Some of the values of the constants are given in the Table 3.1 below:

Parameters	$V_{\max} m^3/s$	$A_1 \times 10^3$	A_2	$B_1 \times 10^2$	B_2	T_c
$E = 0.66735 \times 10^{11} \text{ Pa}$	150	2.268	0.06314	4.20596	4.5	2.51
$v = 0.20$	175	3.1328	0.07931	5.2897	4.25	2.32
$\rho_w = 2200 \text{ kg/m}^3$	200	4.2188	0.093925	5.9706	4.00	2.12
$\rho_p = 3650 \text{ kg/m}^3$	225	5.4908	0.108375	6.7765	3.875	1.91
	250	7.06687	0.12441	7.9695	3.848	1.7
	275	8.6731	0.13822	8.7432	3.825	1.5
	300	10.56	0.15315	9.7092	3.80	1.25
Parameters	$E \times 10^{-11} \text{ Pa}$	$A_1 \times 10^3$	A_2	$B_1 \times 10^2$	B_2	T_c
$V_{\max} = 250 \text{ m/s}$	1.5	3.6295	0.057	5.11775	3.2604	1.75
$v = 0.20$	2.0	2.7806	0.08	4.4337	3.203	1.60
$\rho_w = 2200 \text{ kg/m}^3$	2.5	2.2589	0.07221	3.9531	3.152	1.50
$\rho_p = 3650 \text{ kg/m}^3$	3.0	1.9532	0.06733	3.6818	3.12	1.42
	3.6	1.6844	0.06255	3.8133	3.08	1.35

Parameters	$\rho_w \text{ kg/m}^3$	$A_1 \times 10^3$	A_2	$B_1 \times 10^2$	B_2	T_c
$E=3.0 \times 10^{11} \text{ Pa}$	2500	1.8869	0.057	0.015735	1.869	1.5
$V_{\max}=275 \text{ m/s}$	3250	3.8884	0.0954	0.04184	2.4213	1.4
$\nu=0.20$	3650	3.8925	0.095	0.040485	2.4135	1.65
$\rho_p=3650 \text{ kg/m}^3$	4250	4.16745	0.0977	0.0419	2.48	1.3
	5000	4.10357	0.094	0.03147	2.0545	1.92
Parameters	ν	$A_1 \times 10^3$	A_2	$B_1 \times 10^2$	B_2	T_c
$V_{\max}=250 \text{ m/s}$	0.225	0.9948	0.047188	2.8572	3.645	1.25
$E=3.0 \times 10^{11} \text{ Pa}$	0.25	1.043	0.0488	2.9115	3.502	1.15
$\rho_w=2200 \text{ kg/m}^3$	0.275	1.715	0.0501	3.0073	3.3535	1.05
$\rho_p=3650 \text{ kg/m}^3$	0.30	1.1943	0.0523	3.088	3.22	0.95
Parameters	ρ_p	$A_1 \times 10^3$	A_2	$B_1 \times 10^2$	B_2	T_c
$V_{\max}=250 \text{ m/s}$	2500	3.3836	0.08745	3.269	2.1965	1.75
$E=3.0 \times 10^{11} \text{ Pa}$	3000	3.57	0.0904	3.5679	2.285	1.65
$\nu=0.20$	3500	4.2164	0.0992	4.125	2.3115	1.55
$\rho_w=2200 \text{ kg/m}^3$	4000	4.3283	0.1006	4.331	2.38	1.45

Table 3.1 Values of the constants for different values of the parameters.

These are sufficient to determine the strain and stress distributions in the material during impact. Thus the strain energy density (SED) distribution is determined. To estimate the fracture profile and fracture volume, SED is used in a criterion for fracture.

According to Sih's hypothesis, the crack originates at those points where, the strain energy density reaches a critical value SED_{cr} and the direction of crack propagation is the direction in which the rate of change of SED is a minimum.

Mathematically, this condition can be expressed as, $\left[\frac{\partial}{\partial \theta} (SED) \right]_{\theta_{crack}} = 0$ and

$\frac{\partial^2 (SED)}{\partial \theta^2} > 0$. This hypothesis is used in the present problem also.

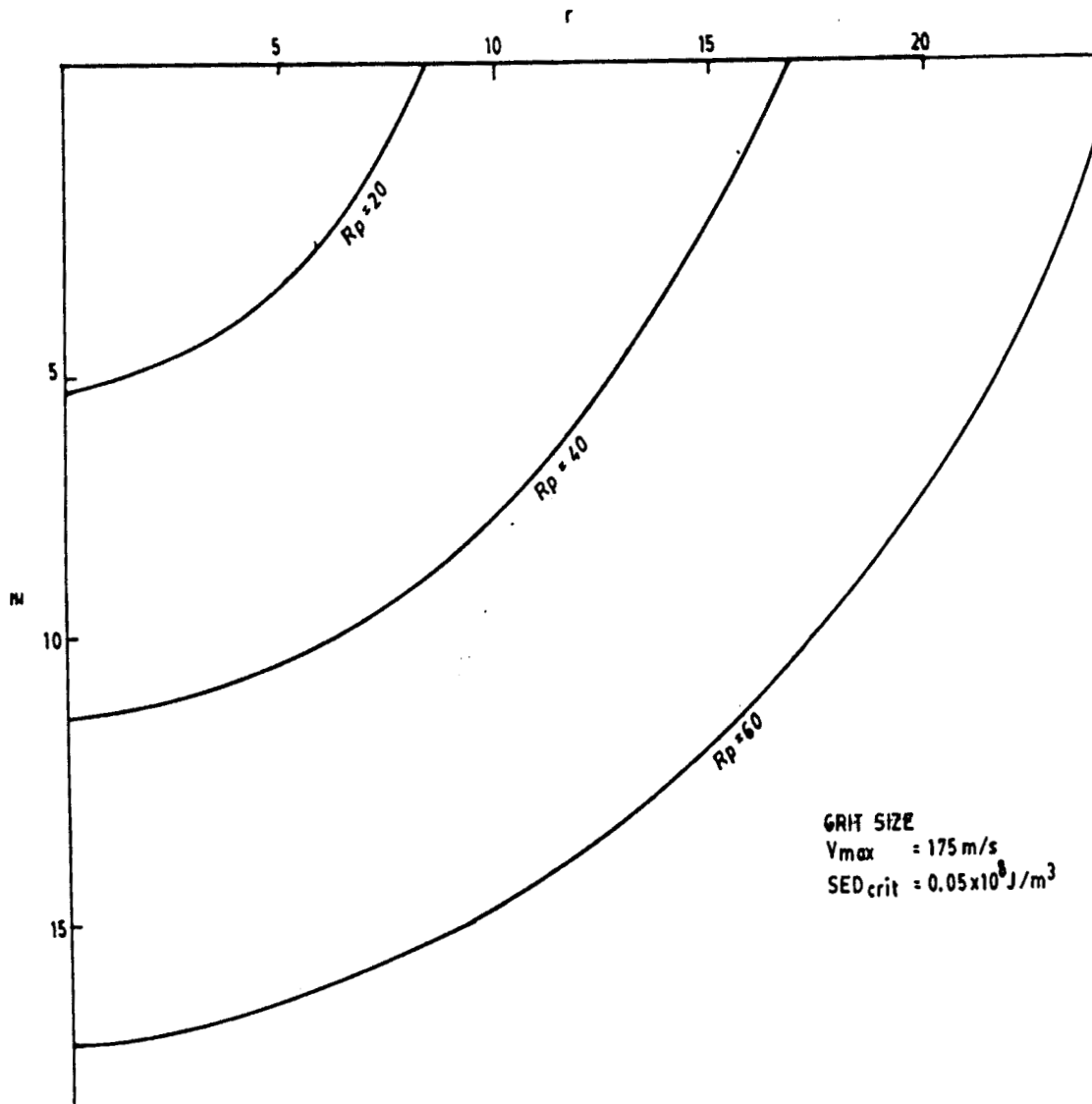


Figure 3.2 Typical fracture profiles (for different values of R_p)

The points where $SED = SED_{cr}$ is determined numerically. This is done by calculating the SED from the basic solution of the problem and comparing this with the SED_{cr} . SED_{cr} is a property of the work material. This will enable the determination of the fracture profile and fracture volume. Figure 3.2 shows a typical fracture profile. These were computed at the end of the contact period. These profiles are very nearly circular in shape corroborating Shaw's [27] intuition. The volume of material removal is found as

$$V_0 = \int_0^{R_{c\max}} 2\pi r_c z_c dr_c \quad (3.32)$$

where z_c is a function of r_c , z_c and r_c are the coordinates of the points on the fracture profile and $r_{c\max}$ is the r coordinate of the fracture profile at the surface $z = 0$. Table 3.2 gives the fracture volume as a function of the parameters.

E=0.667x10 ¹¹ Pa, v=0.2, $\rho_w=2200\text{kg/m}^3$ $\rho_p=3650\text{kg/m}^3$ SED _{cr} =0.7508x10 ⁵ J/m ³		V _{max} =250 m/s, v=0.2, $\rho_w=2200\text{kg/m}^3$ $\rho_p=3650\text{kg/m}^3$ SED _{cr} =0.7508x10 ⁵ J/m ³		E=0.667x10 ¹¹ Pa, V _{max} =250 $\rho_w=2200\text{kg/m}^3$ $\rho_p=3650\text{kg/m}^3$ SED _{cr} =0.7508x10 ⁵ J/m ³	
V _{max} m/s	Volume	E 10 ⁻¹¹ Pa	Volume	v	Volume
150	188.8	1.5	408.4	0.225	51.15
175	252.4	2.0	408.0	0.25	51.32
200	297.6	2.5	406.8	0.275	52.73
225	348	3.0	417.8	0.30	53.29
250	418.1	3.5	482.7	E=0.667x10 ¹¹ Pa, V _{max} =250 m/s, v=0.2, $\rho_w=2200\text{kg/m}^3$ $\rho_p=3650\text{kg/m}^3$	
275	473.1	V _{max} =250 m/s, v=0.2,			
300	532.7	E=0.667x10 ¹¹ Pa, $\rho_p=3650\text{kg/m}^3$ SED _{cr} =0.7508x10 ⁵ J/m ³			

$V_{\max}=250 \text{ m/s}, \nu=0.2,$ $\rho_w=2200\text{kg/m}^3$ $E=0.667\times 10^{11}\text{Pa},$ $SED_{cr}=0.7508\times 10^5\text{J/m}^3$					
		ρ_w	Volume	$SED_{cr}\times 10^{-5}$	Volume
				1.0	347.4
ρ_p	Volume	2500	14.65	5.0	113.5
2500	57.06	3250	84.12	10.0	66.85
3000	66.14	3650	80.74	50.0	15.57
3500	81.98	4250	82.35	100.0	7.108
4000	88.08	5000	52.64	500.0	0.2848

Table 3.2 The results of computation of fracture volume as a function of the parameters

The volume of material removed in the impact of a single particle is a function of several independent parameters. They are:

- (i) V_{\max} -the velocity of the abrasive particles before impact,
- (ii) R_p – the mean radius of the impacting particle,
- (iii) E – the Young’s modulus of the medium,
- (iv) ν the Poisson’s ratio of the medium,
- (v) SED_{cr} the critical strain energy density of the medium,
- (vi) ρ_{ab} the density of the abrasive particles and
- (vii) ρ_w the density of the work medium.

To relate the fracture volume as a simple function of the above parameters, fracture volume is calculated for a combination of parameters. They are given in table 3.3.

E 10^{-11} Pa	v	V _{max} m/s	ρ_w	ρ_p	SED _{cr} 10^{-7} J/m ³	R _p μ m	Vol. μ m ³
0.667	0.2	150	2200	3650	5.0	40	5701
0.667	0.2	175	2200	3650	5.0	60	11720
1.0	0.22	150	3500	4000	10.	40	590
2.0	0.24	175	4000	4500	20.	60	1196
5.0	0.25	200	2000	2750	7.5	80	21320
10.0	0.26	225	2600	2000	10	20	21.10
20.0	0.27	250	2200	2500	20	100	2137
0.250	0.20	275	3000	3500	0.5	120	0.118×10^8
0.5	0.25	300	2000	4000	1.0	60	0.1356×10^7

Table 3.3 Volume of material removed as a function of the parameters

To express the above data and the data given in table 3.2 as a simple function, a product relationship is proposed as below:

$$V_0 = k V_{\max}^a R_p^b (SED)_{cr}^c E^d v^e \left(\frac{\rho_{ab}}{\rho_w} \right)^f \quad (3.33)$$

The indices a, b, c, d, e and f in this relation are found from a least square fit for the fracture volume calculated for several values of the parameters. The result of the fit is:

$$K = 0.12316 \times 10^{-4},$$

$$a = 2.0,$$

$$b = 3.2805,$$

$$c = -1.3828,$$

$$d = -0.6735,$$

$$e = 2.3011 \text{ and}$$

$$f = -1.9625.$$

These set of values give the volume removed in a single impact in m^3 .

3.8 Conclusion

In this chapter, a theory for material removal in AJM process is proposed. The stress and strain in the elastic half space is found by solving the standard equations of equilibrium using the theory of wave propagation in elastic media. The stress and strain in the medium so calculated are used to determine the material removed during the impact of a single particle. This is estimated with the help of Sih's hypothesis for the onset of fracture. The results are presented in the form of a correlation for later use. The theory for material removal now requires the introduction of the process parameters through the flow analysis.

Chapter 4

DETERMINATION OF PARTICLE VELOCITY

4.1 Introduction

The velocity V_{\max} of the particles impinging the work surface is determined by analyzing the air-abrasive flow through the nozzle and in the free jet. The analysis of the flow of the gas is done by assuming that the gas is a continuum and the method of description is the Eulerian method. However, the flow of the particles is better studied by the Lagrangian method. Thus the analysis of the flow of the mixture becomes difficult. It is apparent that the abrasive particles gain the velocity by exchanging energy with the gas flow. Thus the method of determining the particle velocity must take into account the fluid flow aspects of the gas flow and treat the exchange of momentum and energy between gas and particles.

4.2 Flow Through the Nozzle

The flow through the nozzle is assumed to be steady, one dimensional and isentropic, except for the momentum exchange between the particles and the gas. The assumption that the flow is isentropic is valid when the nozzles are short and the temperature of the gas is nearly atmospheric. In Abrasive Jet Machining the conditions are nearly true. It is further assumed that the particles are spherical in shape and are of the same diameter (the average diameter d_p). Particle-particle interactions are neglected,

since the volume occupied by the particles is very small (due to the low mixing ratios). The exchange of momentum is through aerodynamic forces. Basset force [63] and Brownian motion are also negligible for particle sizes of practical interest [62]. In writing the field equations for the particles, a new variable called the volume fraction ϕ is introduced to take the volume occupied by the particles into account. ϕ is such that $\rho_p\phi$ may be regarded as the density of the particles at each point. With this, the mass flow rate of the particles is written as:

$$\dot{m}_p = \rho_p\phi AV_p \quad (4.1)$$

$$\text{and the mass flow rate of air is } \dot{m}_a = \rho_a(1-\phi)AV_a \quad (4.2)$$

where ρ is the density, A is the area of cross section of the nozzle and V is the velocity. Suffices p and a stand for the abrasive particles and air respectively. The equations (4.1) and (4.2) are the continuity equations for the particle phase and gas. The other equations are written by considering the flow of the mixture through a differential element of the nozzle shown in Figure 4.1 below.

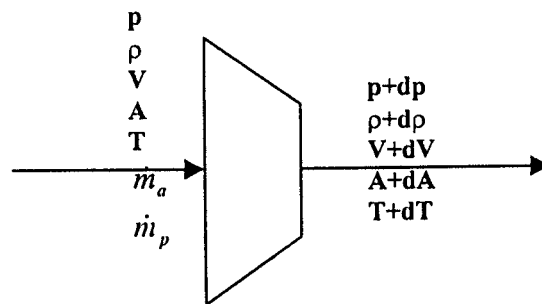


Figure 4.1 Differential element of the Nozzle for flow analysis

The momentum equation for the flow of the mixture is written by considering mixture momentum while the equation of motion of the particles is written for each particle. Thus

$$\text{the particle velocity is given by } \frac{4}{3}\pi\left(\frac{d_p}{2}\right)^3 \rho_p \frac{dV_p}{dt} = F_p \quad (4.3)$$

where F_p is the force on the particle. The derivative $\frac{dV_p}{dt} = V_p \frac{dV_p}{dx}$, where x is the distance along the nozzle axis. The aerodynamic force F_p is found from the relation

$$F_p = C_D \pi R_p^2 \frac{1}{2} \rho_a (V_a - V_p) |V_a - V_p| \quad (4.4)$$

Combining the two equations, the differential equation for the motion of the particles is

$$\text{found as } V_p \frac{dV_p}{dx} = \frac{3}{8} \frac{\rho_a}{\rho_p} \frac{C_D}{R_p} (V_a - V_p) |V_a - V_p| \quad (4.5)$$

C_D is the coefficient of drag, and is a function of the Reynolds number Re based on the diameter of the particle [42]. The relationship between C_D and Re is

$$\begin{aligned} C_D &= 24/Re \quad \text{for} \quad Re \leq 0.1 \\ &= \frac{24 + 0.379 Re^{0.66}}{Re} \quad \text{for } 0.1 \leq Re \leq 500 \\ &= \frac{2.63}{Re^{0.26}} \quad \text{for } 500 \leq Re \leq 1000 \\ &= 0.44 \quad Re > 1000 \end{aligned} \quad (4.6)$$

$$\text{The Reynolds number } Re \text{ is given by } Re = \frac{\rho_a |V_a - V_p| d_p}{\mu} \quad (4.7)$$

Here μ is the absolute viscosity of air.

When the wall friction is neglected, as is done in isentropic flows, the momentum equation for the mixture is (see fig 4.1)

$$\dot{m}_a \frac{dV_a}{dx} = \dot{m}_p \frac{dV_p}{dx} = -A \frac{dp}{dx} \quad (4.8)$$

In a similar fashion, the energy equation for the mixture is

$$\dot{m}_a C_p \frac{d}{dx} \left(T_a + V_a^2 / 2 \right) + \dot{m}_p C_{pp} \frac{d}{dx} \left(T_p + \frac{V_p^2}{2} \right) = 0 \quad (4.9)$$

The temperature of the particles is found by evaluating the heat transferred to the particles. Assuming a heat transfer coefficient h the change in temperature is found as

$$V_p \frac{dT_p}{dx} = \frac{3h}{\rho_p C_{pp}} \frac{T_a - T_p}{d_p} \quad (4.10)$$

The heat transfer coefficient h is related to the Nusselt number Nu by the correlation

$$N_u = 2 + 0.459 Re^{0.55} Pr^{0.33} \quad (4.11)$$

These equations are supplemented by the equation of the state for the gas

$$p = \rho_a \mathcal{R} T_a \quad (4.12)$$

\mathcal{R} is the characteristic gas constant.

These governing equations are expressed as a system of first order ordinary differential equations involving the variables pressure p , density ρ_a , temperature T_a , and velocity V_a of the gas phase and T_p , V_p and ϕ for the particle phase.

The initial conditions are

at $x = 0$,

$$V_p = 0, T_p = T_{amb},$$

$V_a = V_{ini}, T_a = T_{ini}, p_a = p_s$ the system pressure.

The initial condition V_{ini} is such that, this velocity is sufficient to pass the mass flow through the supply pipe. The mass flow rate $\dot{m}_a = 0.0404 \frac{p_0}{\sqrt{T_0}} \frac{\pi}{4} d_n^2$, where d_n is the diameter of the nozzle. Then $V_{ini} = \text{the mass flow rate}/(\text{density} \cdot \text{area of the supply pipe})$.

The particle flow rate is incorporated by specifying, the airflow rate along with the

mixing ratio. That is $\dot{m}_p = \frac{\dot{m}_r}{1 - \dot{m}_r} \dot{m}_a$ (4.13)

At the point of insertion, the particles are assumed to have negligible velocity. These equations can be regrouped into a set of first order ordinary differential equations.

$$V_p \frac{dV_p}{dx} = \frac{3 \rho_a C_D}{8 \rho_p R_p} (V_a - V_p) |V_a - V_p| \quad (4.14)$$

$$V_p \frac{dT_p}{dx} = \frac{3h(T_a - T_p)}{\rho_p R_p C_{pp}} \quad (4.15)$$

for a conical nozzle

$$\frac{dA}{dx} = -2\pi \left\{ \frac{d_{pipe}}{2} - \frac{d_{pipe} - d_n}{2L_{nozzle}} \right\} \frac{d_{pipe} - d_n}{2L_{nozzle}} \quad (4.16)$$

where d_{pipe} = diameter of pipe and L_{nozzle} = length of the nozzle

$$\frac{dV_a}{dx} = \frac{RT_a}{V_a \left(1 - \phi - \frac{RT_a}{V_a^2} - \frac{\gamma - 1}{\gamma} \right)} \left[\frac{dA}{Adx} + \left\{ \frac{-\phi}{1 - \phi} + \frac{\dot{m}_p}{\dot{m}_a} \left(\frac{V_p}{C_p T_a} - \frac{V_a(1 - \phi)}{RT_a} \right) \frac{1}{RT_a} \right\} \right] \quad (4.17)$$

$$\frac{dT_a}{dx} = -\frac{V_a}{C_p} \frac{dV_p}{dx} - \frac{\dot{m}_a}{\dot{m}_p} \left\{ \frac{C_p}{C_{pp}} \frac{dT_p}{dx} + \frac{V_p}{C_p} \frac{dV_p}{dx} \right\} \quad (4.18)$$

Along with these, the mass flow equations and the equation of state form a closed set of equations. The equations are supplemented by the following boundary (initial) conditions.

$V_p(0) = V_{pini}$, $T_p(0) =$ initial temperature of particles, $V_a(0) =$ initial velocity of air and $T_a =$ the initial temperature and the pressure in the pipe = the supply pressure.

These are sufficient to solve for the particle velocity and temperature and the pressure, temperature and velocity of the gas. The equations are solved by a fourth order Runge-Kutta routine from $x = 0$ to the exit of the nozzle. The field variables are the input to the solution of the particle jet.

4.3 Particle Velocity in the Jet.

The Jet, of the mixture of air and abrasive particles, coming out of the nozzle passes through the ambient to strike the work surface. The particle velocity is found after the gas field is solved. The classical solution of the laminar (and turbulent) axi-symmetric jet is a similarity solution. The governing equations are solved after the routine assumption that the viscous term in the axial direction is negligible. From experimental results as reported by Schlichting [48] and Hinze [62], the turbulent shear stress

$$\tau = \rho \varepsilon \frac{\partial u}{\partial y} = \rho \chi b U_{\max} \frac{\partial u}{\partial y}. \text{ In these, } b \text{ is the width of the jet, } U_{\max} \text{ is the centerline velocity,}$$

ρ is the fluid density, ε is the eddy viscosity, χ is a constant, u is the jet velocity in the axial direction and y is the transverse coordinate. The width b is proportional to the axial position x , and U_{\max} is inversely proportional to x . Then $\varepsilon = \varepsilon_0$ a constant. Thus, laminar and turbulent jets behave in the same manner, except that the '*viscosity*' is many folds in

turbulent flows. From experimental investigations, it is also known that, close behind the issuing orifice, the ‘mixing zone’ has zero width. The mixing zone thickens with increase in axial distance up to a distance x_c such that at $x = x_c$, the mixing zone covers the entire jet. In literature, this portion of the jet is called the *potential core*. The jet downstream of the potential core is called the similarity zone. In the entire jet the transverse component of velocity is negligibly small. Figure 4.2 illustrates these zones. The angle of flare of the jet α is usually 8 to 15 degrees.

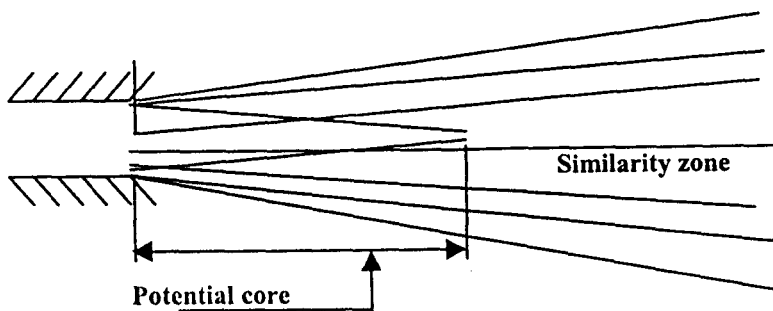


Figure 4.2 The potential core and similarity zones of a turbulent jet

The following empirical relation [63] gives the length of the potential core.

$$x_c = 4d_n + 12d_n \frac{U_{amb}}{U_{jet}} \quad (4.19)$$

However the length of the potential core is found to be greater than $4d_n$ when $U_{amb} = 0$.

Hinze suggested the value $x_c = 6.4 d_n$. (4.20)

The motion of the particles in the free jet is determined from the equations governing its motion through the flow field. The acceleration of the particles having a spherical shape and diameter d_p , through the fluid is given by:

$$\frac{4}{3}\pi\left(\frac{d_p}{2}\right)^3 \rho_p \frac{dV_p}{dt} = C_D \frac{1}{2}\rho_{jet} \frac{\pi}{4}\left(\frac{d_p}{2}\right)^3 (V_a - V_p)|V_a - V_p| \quad (4.21)$$

where ρ_{jet} is the density of the jet and C_D is the coefficient of drag discussed earlier and is related to the local Reynolds number. As is done earlier, the Lagrangian acceleration is transformed to its Eulerian equivalent $V_p \frac{dV_p}{dx}$.

The boundary condition is $V_p = V_{pjet}$ at $x=0$ where V_{pjet} is the velocity with which the particles come out of the nozzle.

The velocity V_a is found from the solution of the turbulent jet

$$\begin{aligned} V_a &= U_{jet} \text{ for } x < x_c \\ &= U_{jet} \frac{x_c}{x} \text{ for } x \geq x_c \end{aligned} \quad (4.22)$$

U_{jet} and V_{pjet} are found from the solution of the flow in the nozzle.

Equation 4.21 is nonlinear and is solved numerically. The numerical integration is continued until the particle position is on the work surface, and yields the velocity of the particles at the axis of the jet. The velocity of the particles is assumed to vary linearly from the velocity on the axis to zero at the edge of the jet. Thus the velocity of the particles V_{pr} at any radius r is given by $V_{pr} = V_{p0} \frac{R_{max} - r}{R_{max}}$ where V_{p0} is the velocity at $r = 0$ and R_{max} is the radius of the jet at the work surface. The average velocity of the particles on impact at the work surface is now obtained by equating the kinetic energy of the flowing particles to the kinetic energy based on the average velocity V_{max} .

$$\rho_p \pi R_{max}^2 \frac{V_{max}^3}{2} = \int_0^{R_{max}} \rho_p 2\pi \frac{V_{pr}^3}{2} r dr \quad (4.23)$$

The radius of the jet on impingement on the work is not explicitly required. It is calculated from the angle of flare α of the jet and the stand off distance s_d .

4.4 Conclusion

The equations governing the flow of the air-abrasive mixture in the nozzle and in the free jet region are formulated. With this the theory for material removal is complete. These equations are first order differential equations and are solved numerically using a fourth order Runge-Kutta method. The computations are done in order to obtain the material removal rate as functions of the process parameters. The results of these calculations are presented in Chapter 5.

Chapter 5

RESULTS OF ANALYTICAL AND EXPERIMENTAL INVESTGATIONS AND DISCUSSIONS

5.1 Introduction

The stress analysis and the subsequent calculation of fracture volume and the flow analysis as outlined in Chapter 3 and Chapter 4 make it possible to predict the material removal rate in Abrasive Jet Machining process. The stress analysis introduces the mechanical properties of the abrasives and the work medium as parameters. The analysis of the flow incorporates the parameters of the AJM process in the theory.

If the volume of material removed in a single impact is ∇_0 (as calculated in Chapter 3), the material removal rate is given by

$$\text{mrr} = \rho_w \frac{3\dot{m}_p}{4\rho_p \pi R_p^3} \nabla_0 \quad (5.1)$$

In this equation $\frac{3\dot{m}}{4\pi\rho_p R_p^3}$ is the number of particles striking the work surface per second with an average velocity of V_{\max} . In the calculations, the damping factors ζ_1 and ζ_2 are taken to be zero. This is consistent with the assumption that the impact is non dissipative in nature. The calculations are done with the material properties [65, 66]

shown in Table 5.1 below. (The other material properties of the abrasive are irrelevant in this theory). The diameter (and radius) of the particles is specified by the grit size.

Work medium	Glass
density ρ_w	2200 kg/m ³
modulus of elasticity E	66.7x10 ⁹ Pa
SED _{cr}	1.4x10 ⁷ J/m ³
Abrasive	Aluminium oxide
density ρ_p	3650 kg/m ³

Table 5.1 Material properties used for calculation

5.2 Results and Discussions on Analytical Investigations

The results of the theoretical calculations are presented in graphical form. In these, material removal rate ($m r r$) is plotted against the other parameters of the process (viz. the pressure, the stand off distance, the mixing ratio, the diameter of the nozzle and the grit size of the abrasives). In most of the experimental and theoretical research on AJM, the variation of material removal rate with stand off distance is considered to be the basic characteristic of the process. In Figure 5.1, the variation of material removal rate with stand off distance obtained for a set of indicated parameters is plotted. These parameters are kept constant. They are pressure = 300kPa, mixing ratio = 0.12, diameter of nozzle = 1.5mm and the grit size = 800.

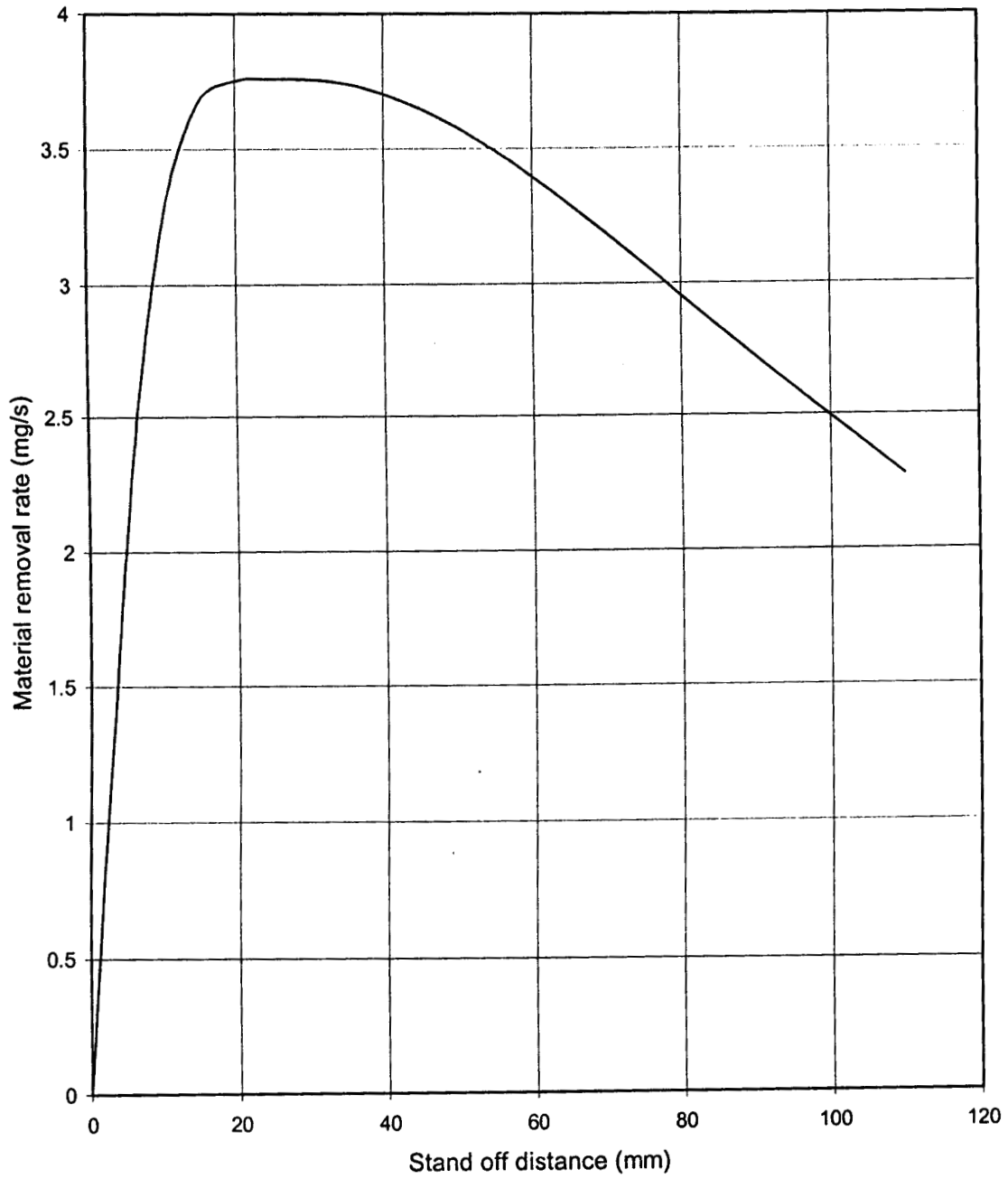


Figure 5.1 Theoretical prediction of the variation of material removal rate with stand off distance (pressure=300kPa, mixing ratio=0.12, diameter of nozzle =1.5mm, grit size=800)

The most important feature of this characteristic is the existence of an optimum stand off distance at which the material removal rate becomes a maximum. Results of experiments published (for example Figures 2.3 and 2.4 given in Chapter 2, taken from references 8 and 9) are in agreement in this aspect. For the set of parameters as above, the optimum stand off distance is about 25mm and the corresponding material removal rate is 3.76 mg/s. In figure 2.3 (ref. [8]), the optimum stand off distance is 8mm and the maximum material removal rate is 0.95mg/s at a pressure of 30 kPa, while Verma and Lal[9] reports an optimum stand off distance of 16mm and the maximum material removal rate is 0.22 mg/s at a pressure of 147.15 kPa and a mixture ratio of 0.268. In a recent paper by Verma and Lal [59], the optimum stand off distance reported is approximately 20mm.

Figures 5.2 to 5.5 illustrate how this characteristic (material removal rate vs. stand off distance) of the process, changes with variation of the other parameters. Thus in Figure 5.2 $m r r$ vs. stand off distance is plotted with mixing ratio as the variable parameter. In these, the pressure is 300kPa, the diameter of the nozzle is 1.5mm and the grit size is 800. In figure 5.3 the pressure is the variable parameter, while the mixing ratio is 0.1, the diameter of the nozzle is 1.5mm and the grit size is 800. It can be observed that the optimum stand off distance does not change appreciably with mixing ratio and supply pressure of air. The optimum stand off distance is between 20 and 30 mm. The material removal rate corresponding to the optimum value of stand off distance for the range of mixing ratios investigated varies from about 2 to 6 mg/s.

The existence of the optimum stand off distance and the independence of this optimum with pressure and mixing ratio can be explained as follows:

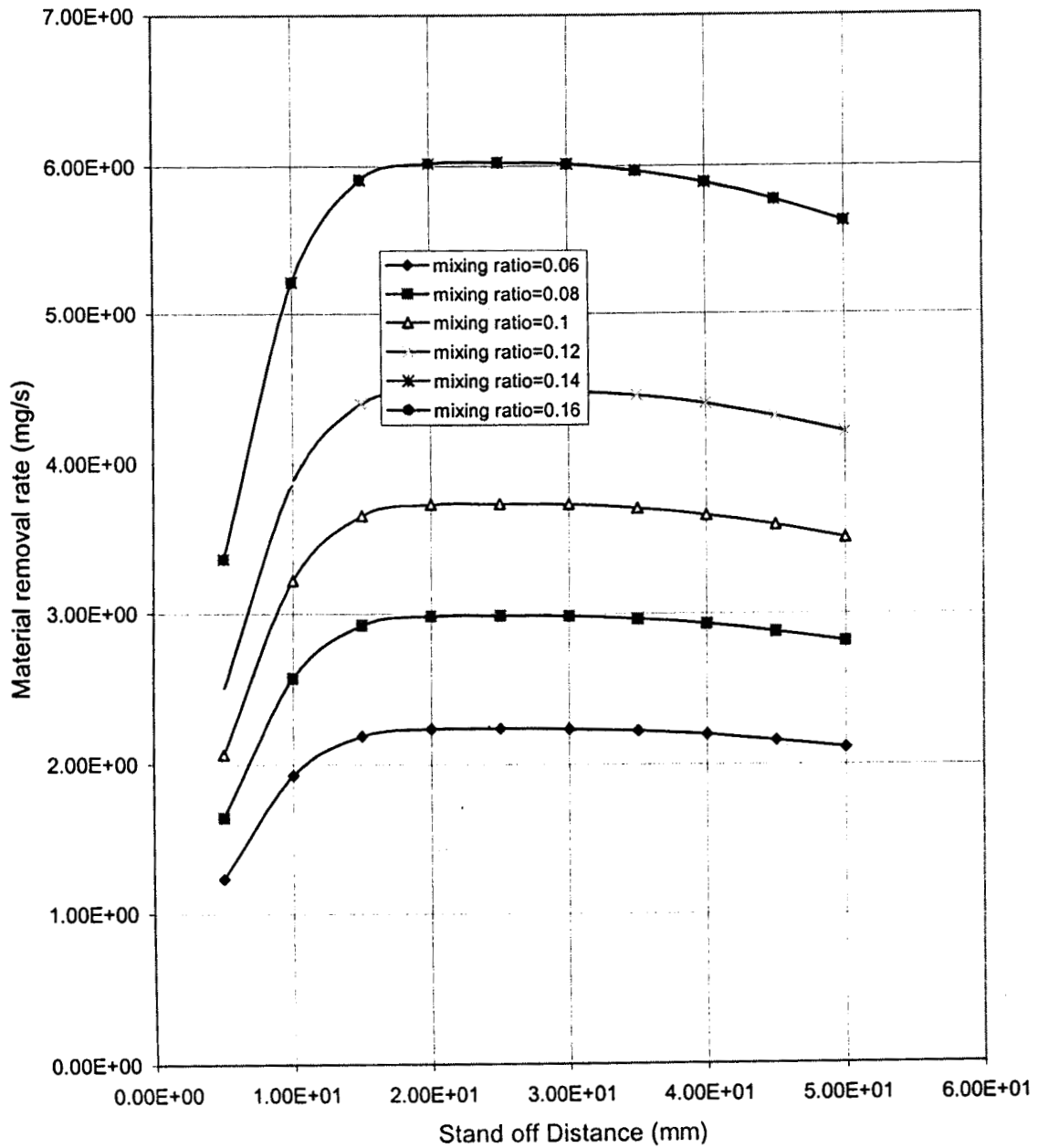


Figure 5.2 .Theoretical prediction of the variation of material removal rate with stand off distance (pressure=350 kPa, Nozzle diameter =1.5mm, grit size =800)

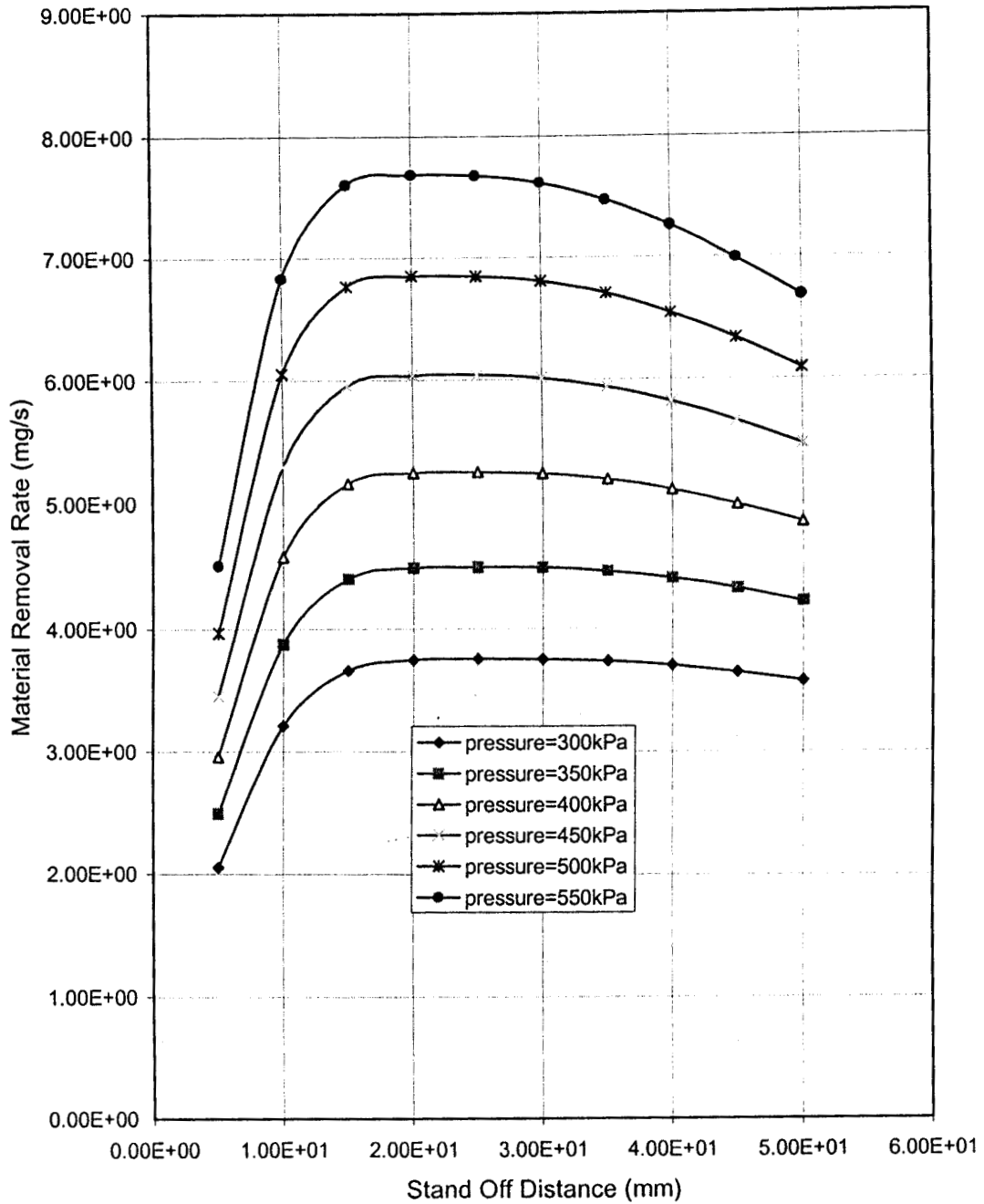


Figure 5.3 Theoretical rediction of the variation of material removal rate with stand off distance (mixing ratio=0.12, nozzle diameter=1.5mm, grit Size=800)

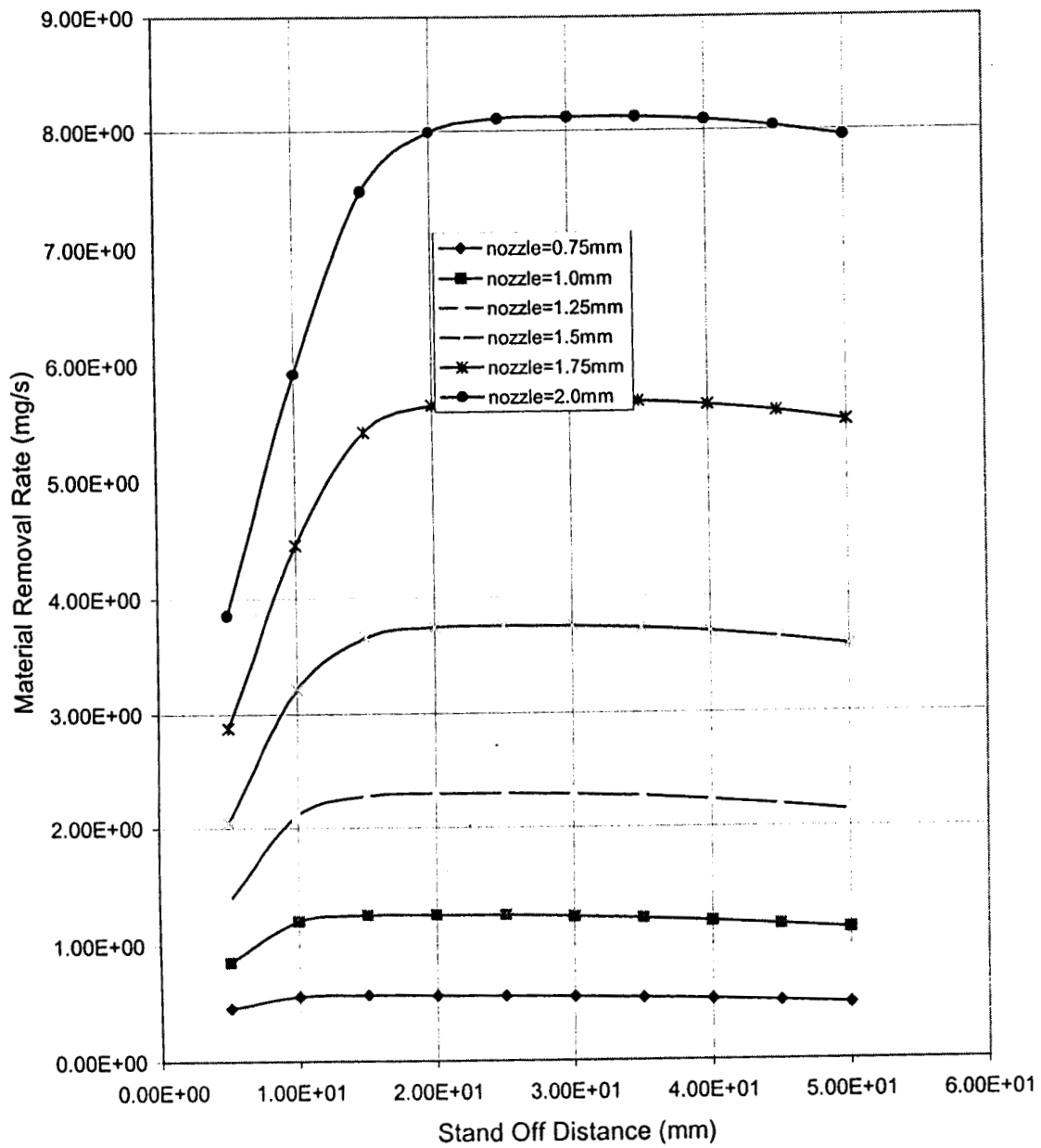


Figure 5.4. Theoretical prediction of the variation of material removal rate with stand off distance (pressue=300kPa, mixing ratio=0.12, grit size=800)

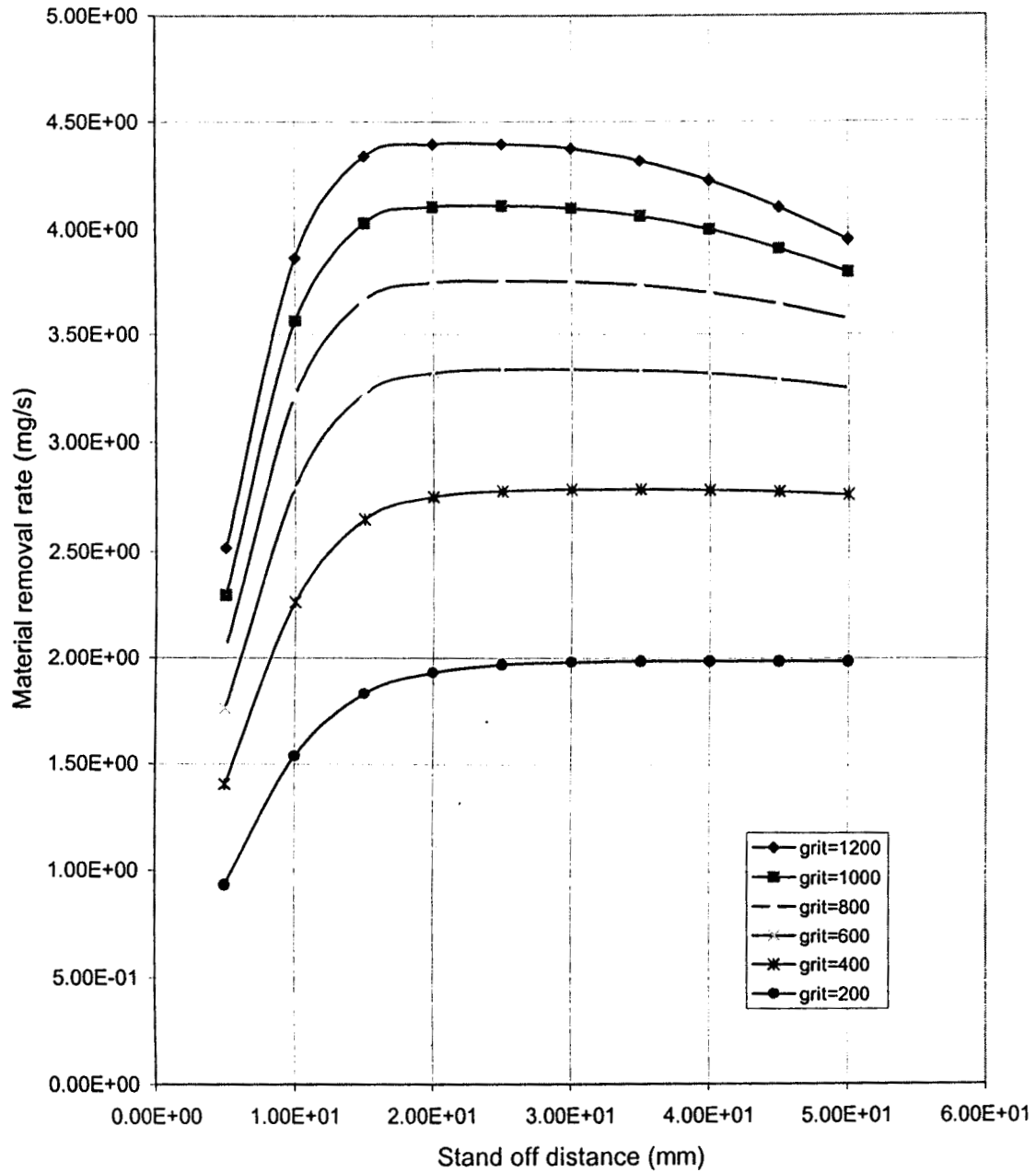


Figure 5.5 Theoretical prediction of the variation of material removal rate with stand off distance (p=300 kPa, mixing ratio=0.12, nozzle dia=1.5mm)

In the proposed theory, the kinetic energy of the impinging particles decides the volume of material removed. Therefore, the behavior of the flow field and the motion of the particles in the field decide the material removal. The velocity of the gas is a maximum at the exit of the nozzle. So long as the nozzle used is convergent in shape, the maximum velocity the gas can acquire at the exit of the nozzle is the sonic velocity. This velocity is independent of the inlet pressure and is a function of the inlet temperature. In all the calculations the inlet temperature is assumed to be the atmospheric temperature = 300 K. However in the free jet region, the gas velocity gradually decreases, because of entrainment of ambient air and exchange of energy with the ambient and the particles. The decrease in the axial velocity of the gas is very sharp near the work surface.

The particles, on the other hand, lag behind the fluid in acquiring the velocity. It has 20 to 30% of the fluid velocity as it comes out of the nozzle. At small stand off distances, the particles are not able to acquire large velocity, because the time involved is very small and therefore the material removal rate also is small. At larger stand off distances, the particles get higher velocities. Ultimately, the particles and the gas have the same velocity. This situation is the so-called 'no-slip' condition in gas-particle flows and pertains to the maximum material removal rate. At still larger stand off distances the particles tend to lose the velocity it gained because of the drag exerted by the gas. Thus it is seen that pressure and mixing ratio do not decide the nature of variation of velocity in the space between the nozzle exit and the work surface. At the same time, the particle flow rate is influenced by the mixing ratio and pressure. Thus, these factors decide the kinetic energy the particles possess and therefore the magnitude of material removal rate is influenced by these parameters.

Figure 5.4 shows the variation of material removal rate with stand off distance for different diameters of nozzle. The pressure is 300kPa, the mixing ratio is 0.1 and the grit size is 800. Figure 5.5 is drawn with grit size as varying parameter with the pressure = 300kPa, mixing ratio = 0.1 and the diameter of nozzle = 1.5mm. Both these plots show the same nature of variation of material removal rate with increasing stand off distance as in Figures 5.2 and 5.3. However these are drawn to see whether there is any change in the optimum stand off distance. It is seen that the optimum stand off distances is different for different values of the nozzle diameter and grit size.

From Figure 5.4 it can be seen that, the optimum stand off distance is 15 mm when the nozzle diameter is 0.75 mm. It is 20 mm when the diameter of nozzle is 1.0mm and increases to an optimum stand off distance between 30 and 35 mm when the diameter of nozzle is 2.0 mm. The reason for the variation of the optimum stand off distance with diameter of nozzle can be attributed to the change in the length of the potential core in the free jet. It is this part of the jet where the abrasive particles gain much of its velocity. At small nozzle diameters the length of potential core is proportionately small. Therefore the particles reach the no-slip condition even at small values of stand off distance. Hence the optimum stand off distance also is smaller.

In a similar way, large particles are sluggish in motion. Therefore they travel comparatively larger distances before catching up with the gas. Thus abrasive jets with larger particles have a larger value of optimum stand off distance than jets with smaller particles. From Figure 5.5, it is seen that, particles of grit size 1200 has an optimum stand off distance between 20 mm and 25 mm while this optimum is between 35mm and 50mm for abrasives of grit size 200. These are drawn with a nozzle diameter of 1.5 mm

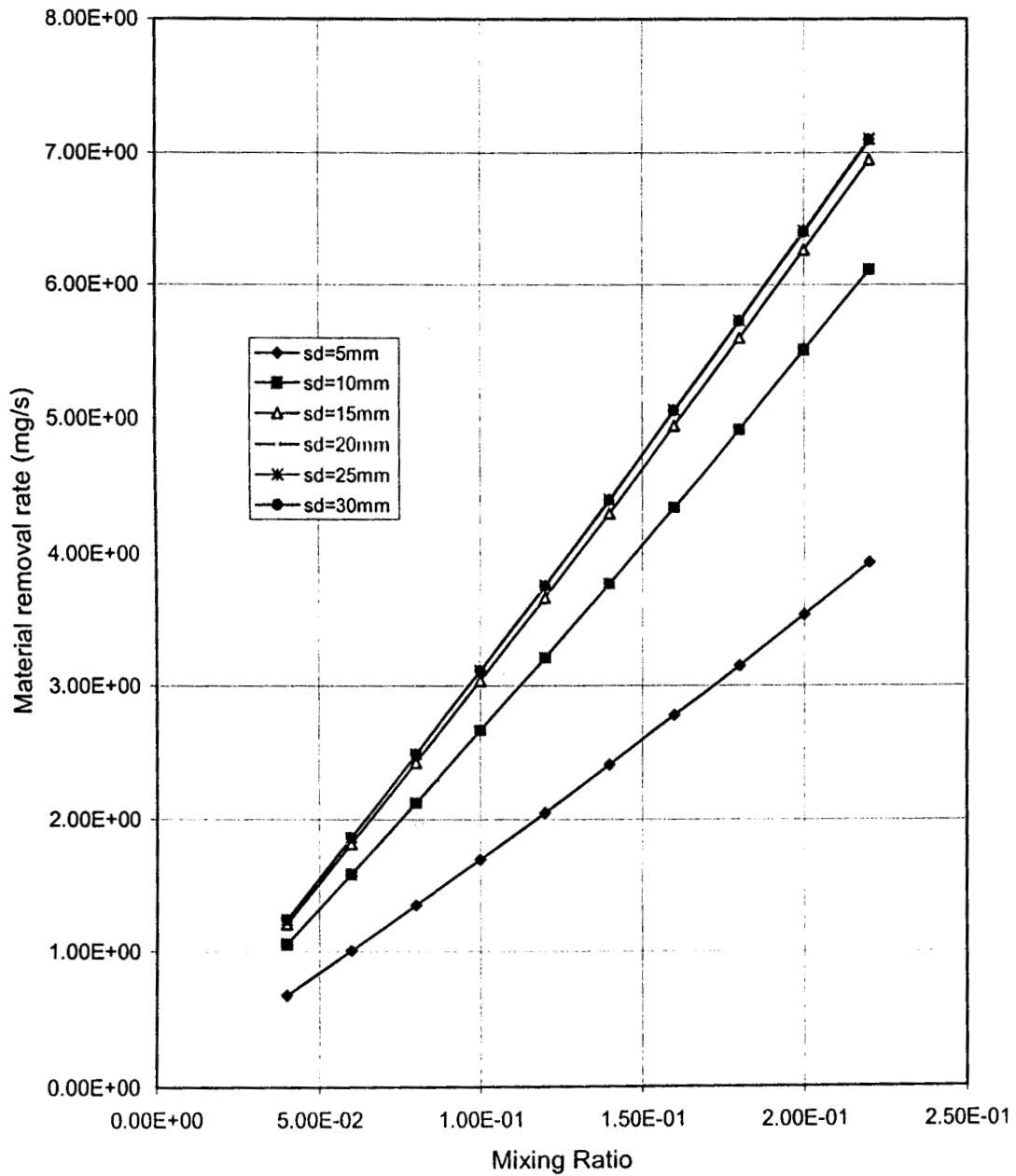


Figure 5.6 Theoretical prediction of the variation of material removal rate with mixing ratio (pressure=300kPa, nozzle diameter=1.5mm, grit size=800)

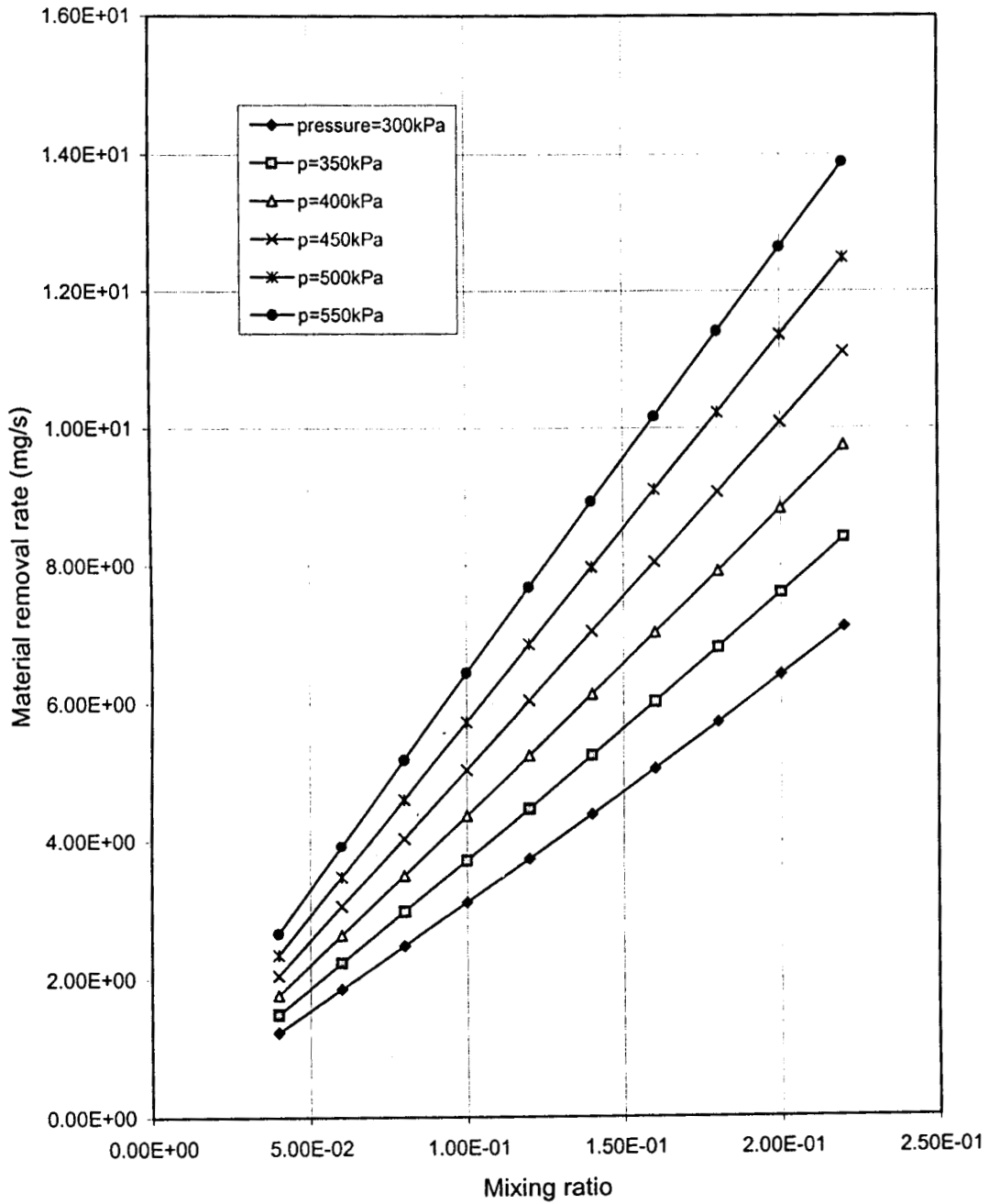


Figure 5.7 Theoretical prediction of the variation of material removal rate with mixing ratio (stand off distance=20mm, nozzle diameter=1.5mm, grit size=800)

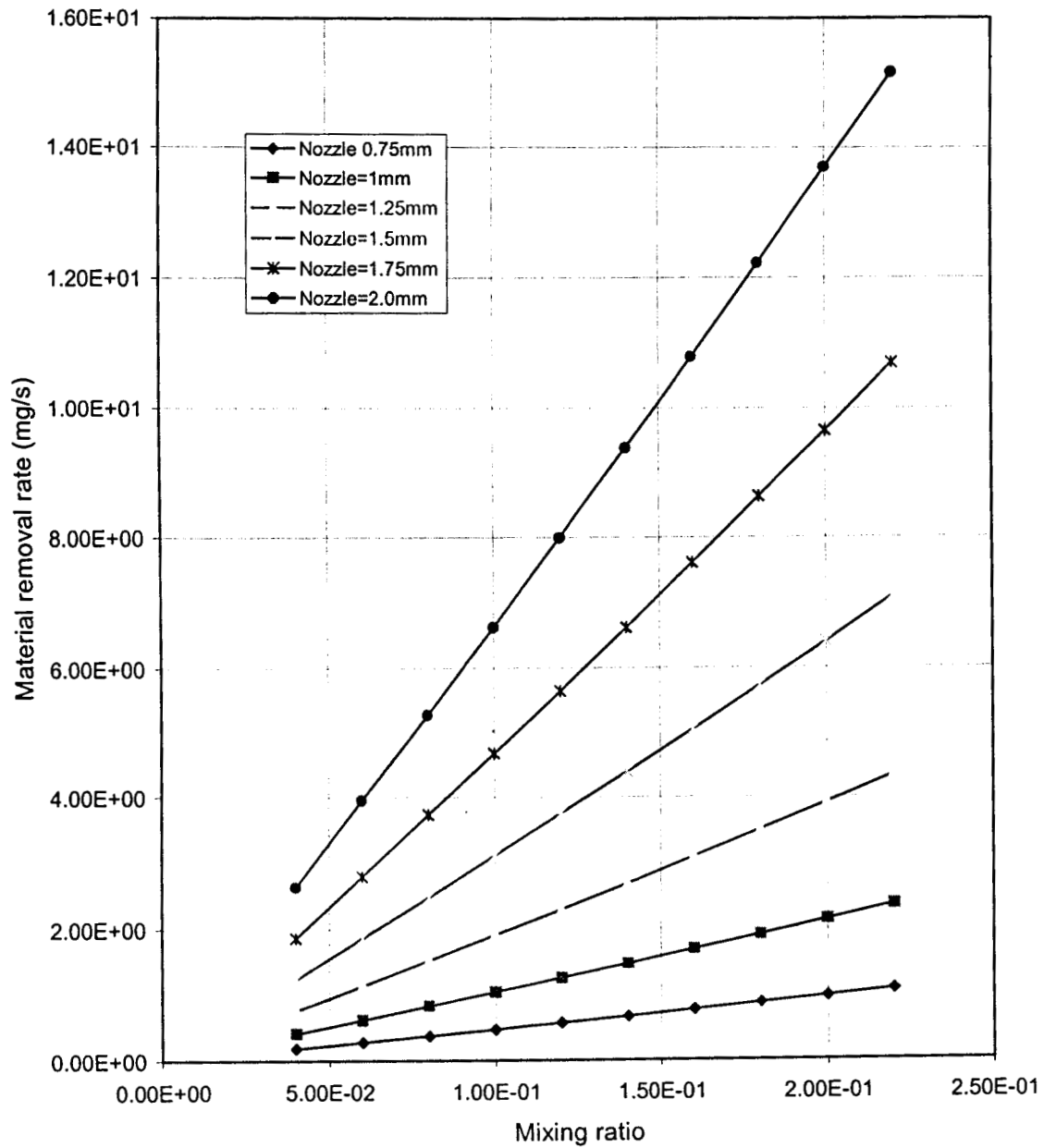


Figure 5.8 Theoretical prediction of the variation of material removal rate with mixing ratio (pressure=300kPa, stand off distance=20mm, grit Size=800)

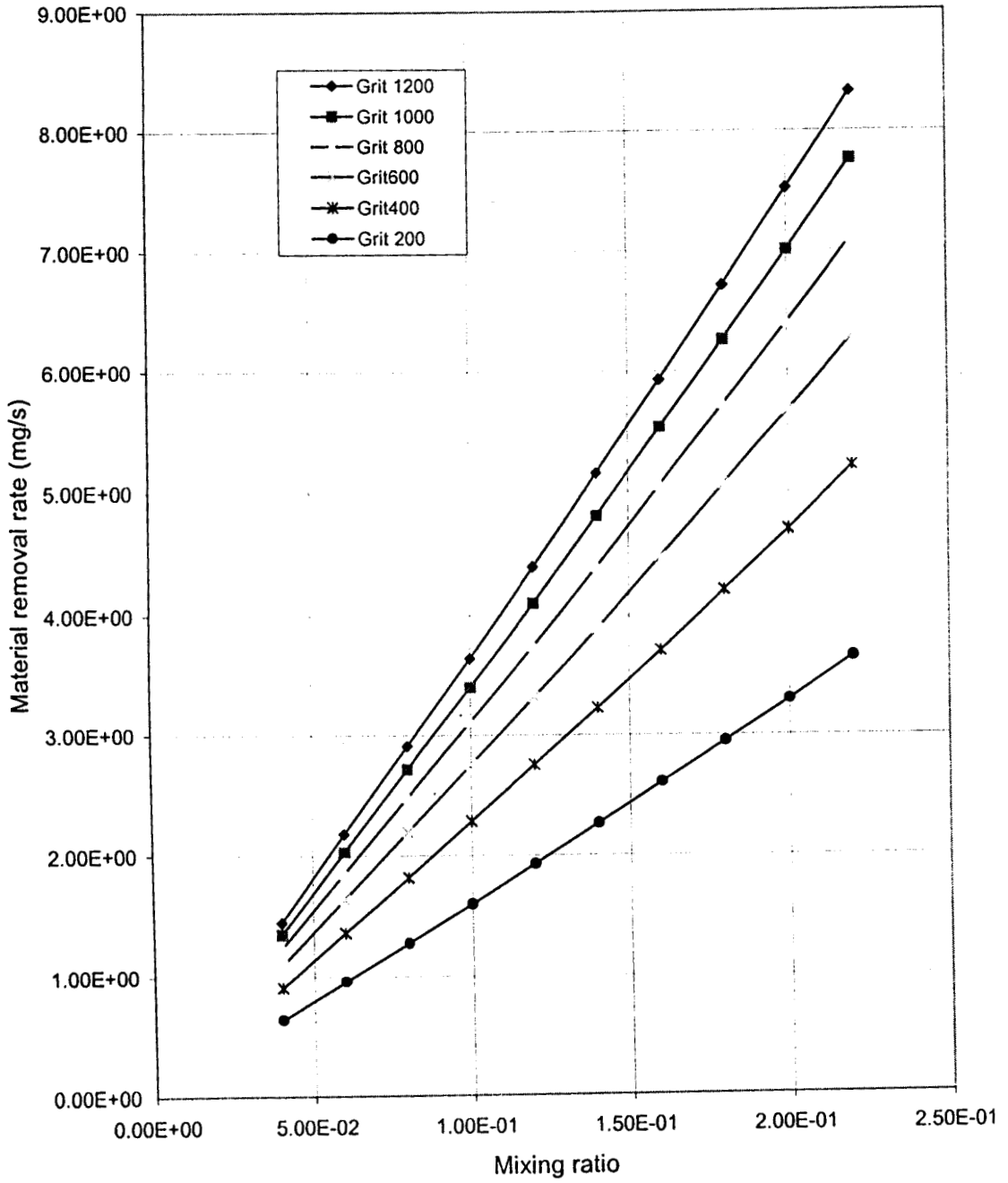


Figure 5.9 Theoretical prediction of the variation of material removal rate with mixing ratio (pressure =300kPa, stand off distance=20mm, diameter of nozzle=1.5 mm)

which means that the length of the potential core is about 10mm.

Figures 5.6 to 5.9 show the variation of material removal rate with mixing ratio. Figure 5.6 is plotted for different values of stand off distance. The values of the other parameters are pressure = 300kPa, diameter of nozzle = 1.5mm and grit size of 800. Figure 5.7 is drawn for different pressures at a stand off distance of 20 mm, a nozzle diameter of 1.5mm and grit size of 800. In figure 5.8 the varying parameter chosen is diameter of nozzle (pressure 300kPa, stand off distance=20mm and grit size=800), while in figure 5.9 the varying parameter is grit size (pressure = 300kPa, stand off distance =20mm and nozzle diameter = 1.5mm). It is seen that in all these cases the material removal rate monotonically increases with the mixing ratio. This could be explained as follows: a larger mixing ratio essentially means a larger rate of particle flow, which in turn increases the machining rate. However, a larger particle flow rate would ultimately result in a smaller velocity for the particles, because the momentum of the air stream reduces as it exchanges momentum with the particles. Therefore the velocity attained by the particles reduces due to an increase in the mixing ratio. In the range of mixing ratios considered in the analysis and used in practice the reduction in material removal rate due to reduction in velocity is compensated by the increase in the number of particles. Due to this reason it is possible that an optimum mixing ratio could also exist. The flow analysis does not preclude this possibility.

In literature, the effect of mixing ratio is not available explicitly. However, results of Verma and Lal [9] shown in Figure 2.4 indicate that the material removal rate is higher for higher mixing ratios.

Figures 5.10 to 5.13 show, how the material removal rate varies as the pressure of the system is changed. Figure 5.10 is drawn showing this variation with different values of stand off distance. The other parameters are constant for this plot. They are mixing ratio = 0.1, diameter of nozzle = 1.5mm and grit size = 800. In a similar fashion, in Figure 5.11, mixing ratio is the varying parameter while the stand off distance is 20mm, diameter of nozzle is 1.5mm and grit size is 800. In figure 5.12 the constant parameters are stand off distance = 20mm, mixing ratio = 0.1 and grit size = 800. And the varying parameter is diameter of nozzle. Figure 5.13 is drawn for different values of grit size, at a stand off distance of 20mm, mixing ratio = 0.1 and diameter of nozzle = 1.5mm. From these plots, it is seen that the material removal rate is nearly proportional to the pressure. This characteristic remains unaltered with change in the values of the other parameters. According to Pandey and Shan [8], the material removal rate is directly proportional to the system pressure as indicated in Figures 2.1 and 2.2.

The pressure of the system decides the mass flow through the system. It also compensates for the energy loss due to friction in the nozzle. The velocity of the gas is decided by the area of the nozzle and the exit Mach number. This gas flow rate in turn decides the abrasive flow rate. Therefore, the effect of the pressure on the material removal rate is similar to the effect of the mixing ratio. It is seen from the theory that, the pressure helps in accelerating the gas. For particles of diameter of the order of a few microns, the pressure gives rise to negligible force on them. Further there is no quantity equivalent to pressure in particle flows. In subsonic flows it is impossible for a free jet to have a pressure other than the ambient pressure. However, for sonic and supersonic gas

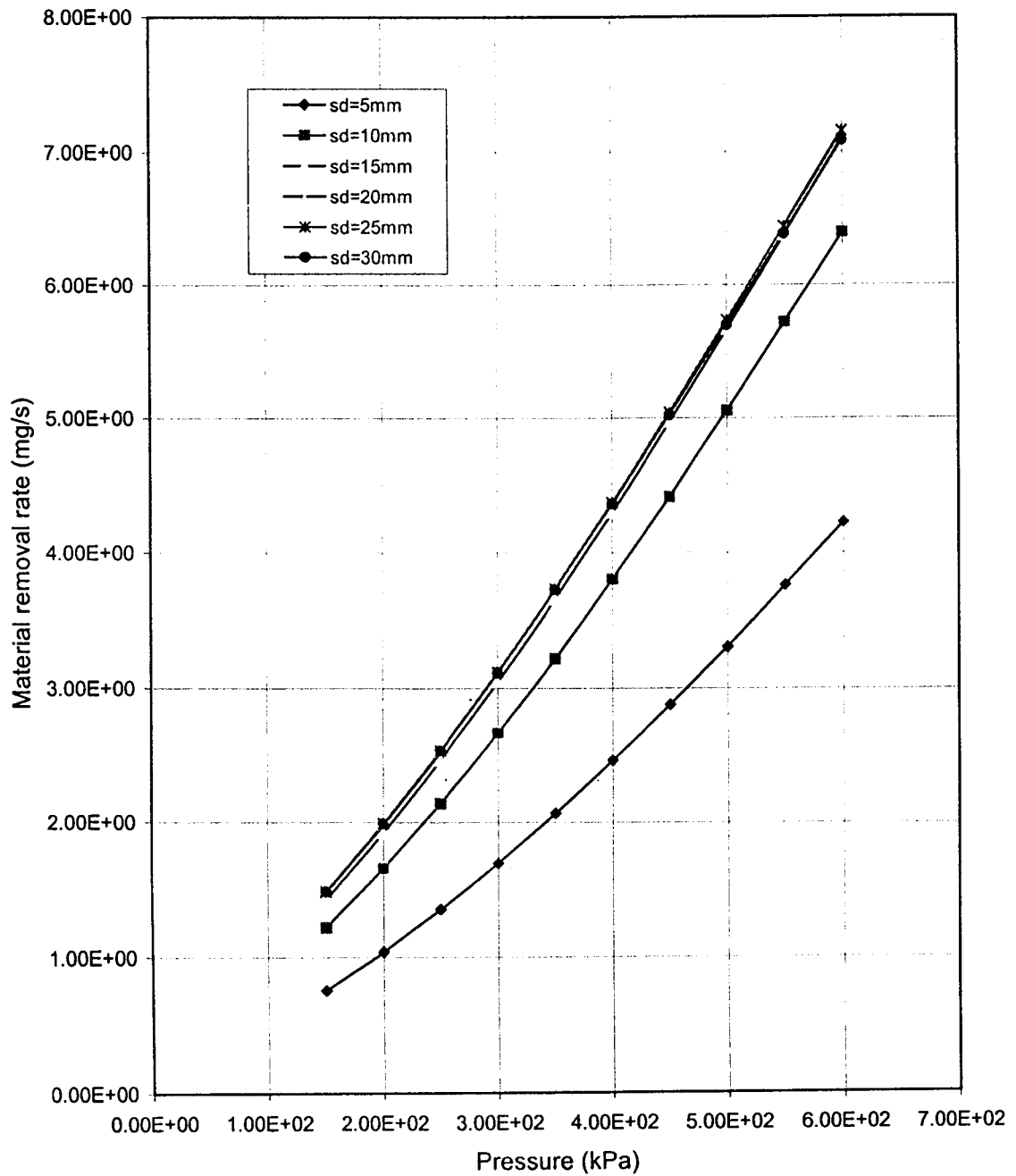


Figure 5.10 Theoretical prediction of the variation of material removal rate with pressure (mixing ratio=0.1, nozzle diameter=1.5mm, grit Size=800)

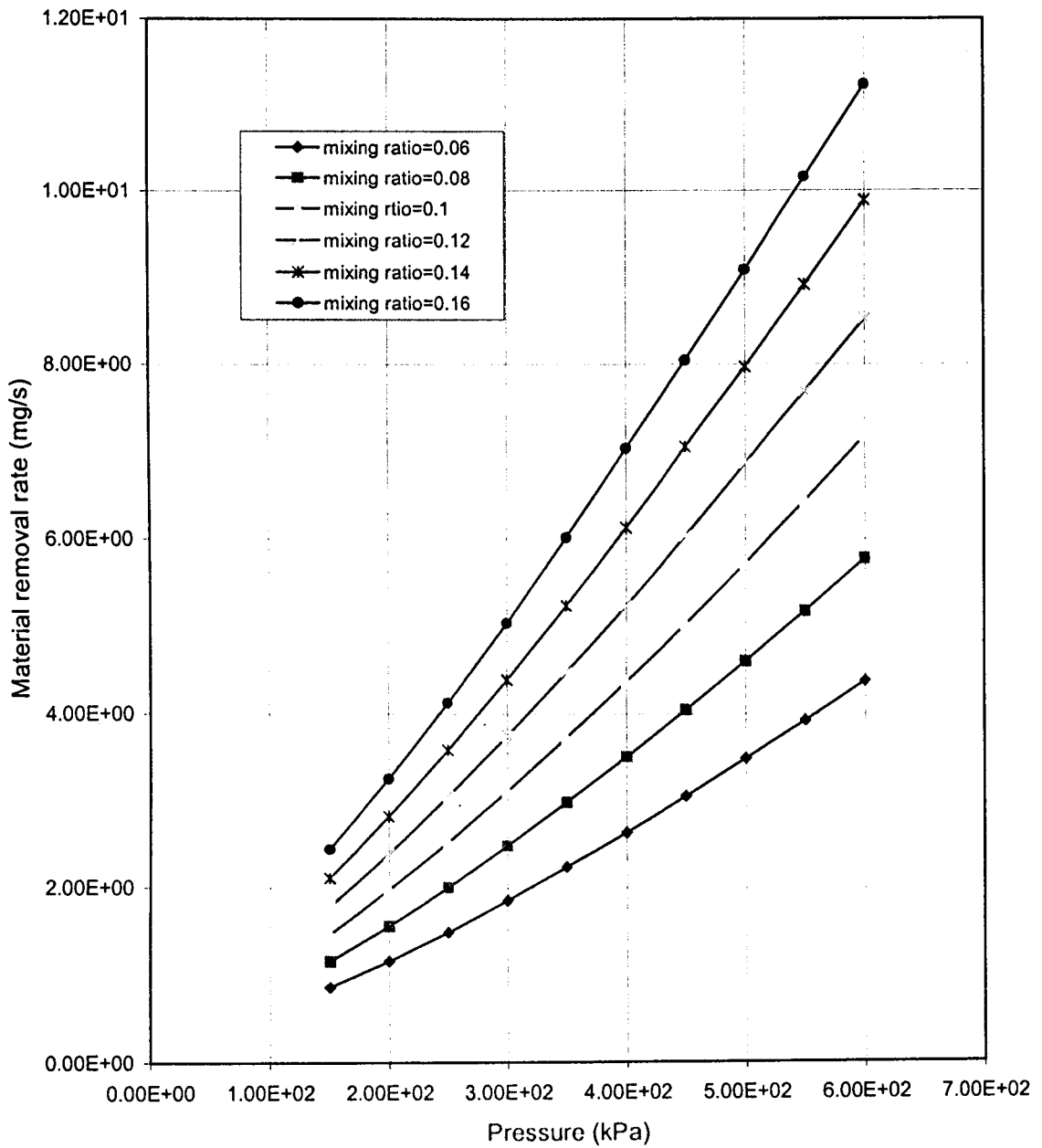


Figure 5.11 Theoretical prediction of the variation of material removal rate with pressure (stand off distance=20mm, nozzle diameter=1.5mm, grit size=800)

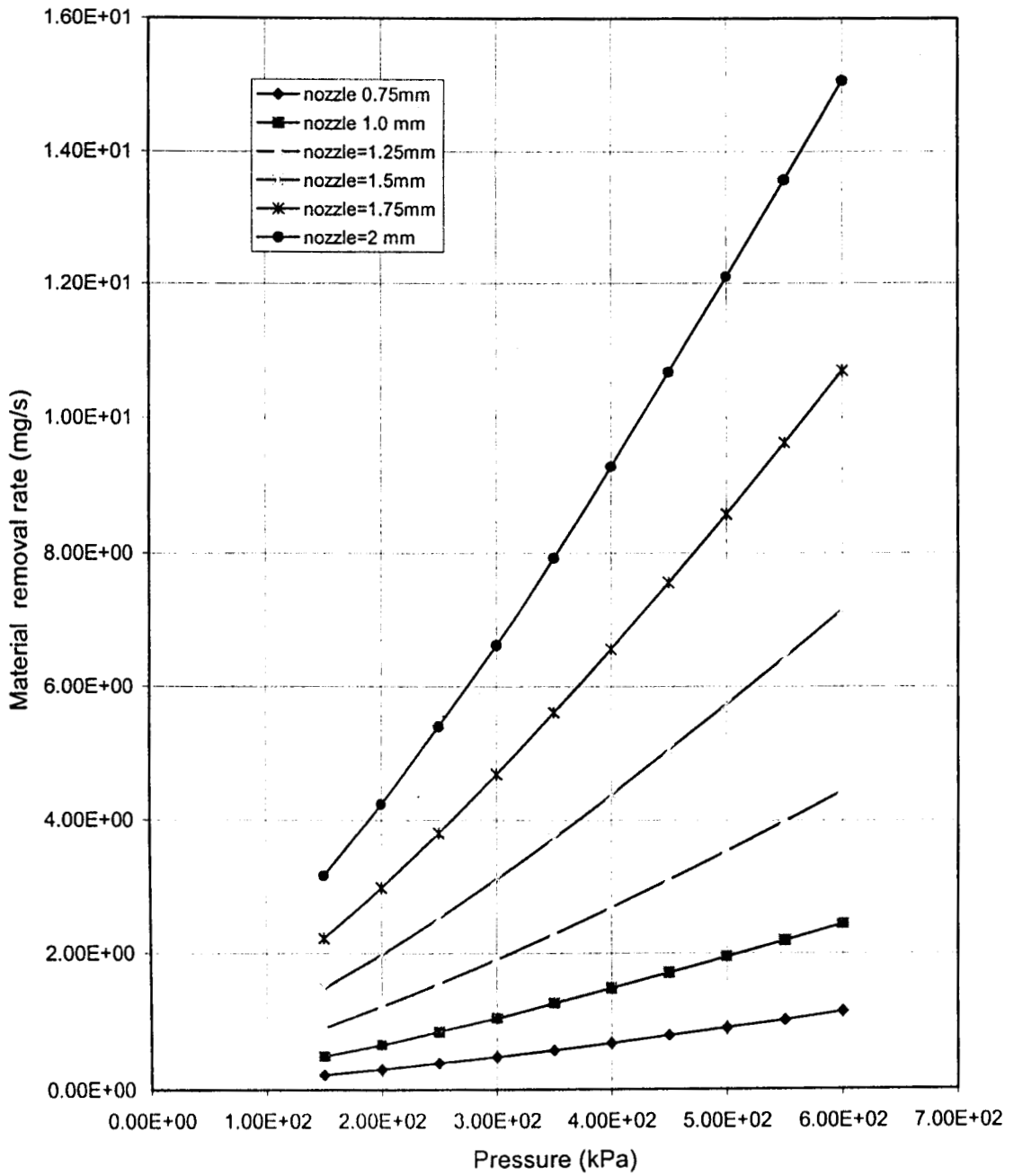


Figure 5.12 Theoretical prediction of the variation of material removal rate with pressure (stand off distance=20mm, mixing ratio=0.1, grit size=800)

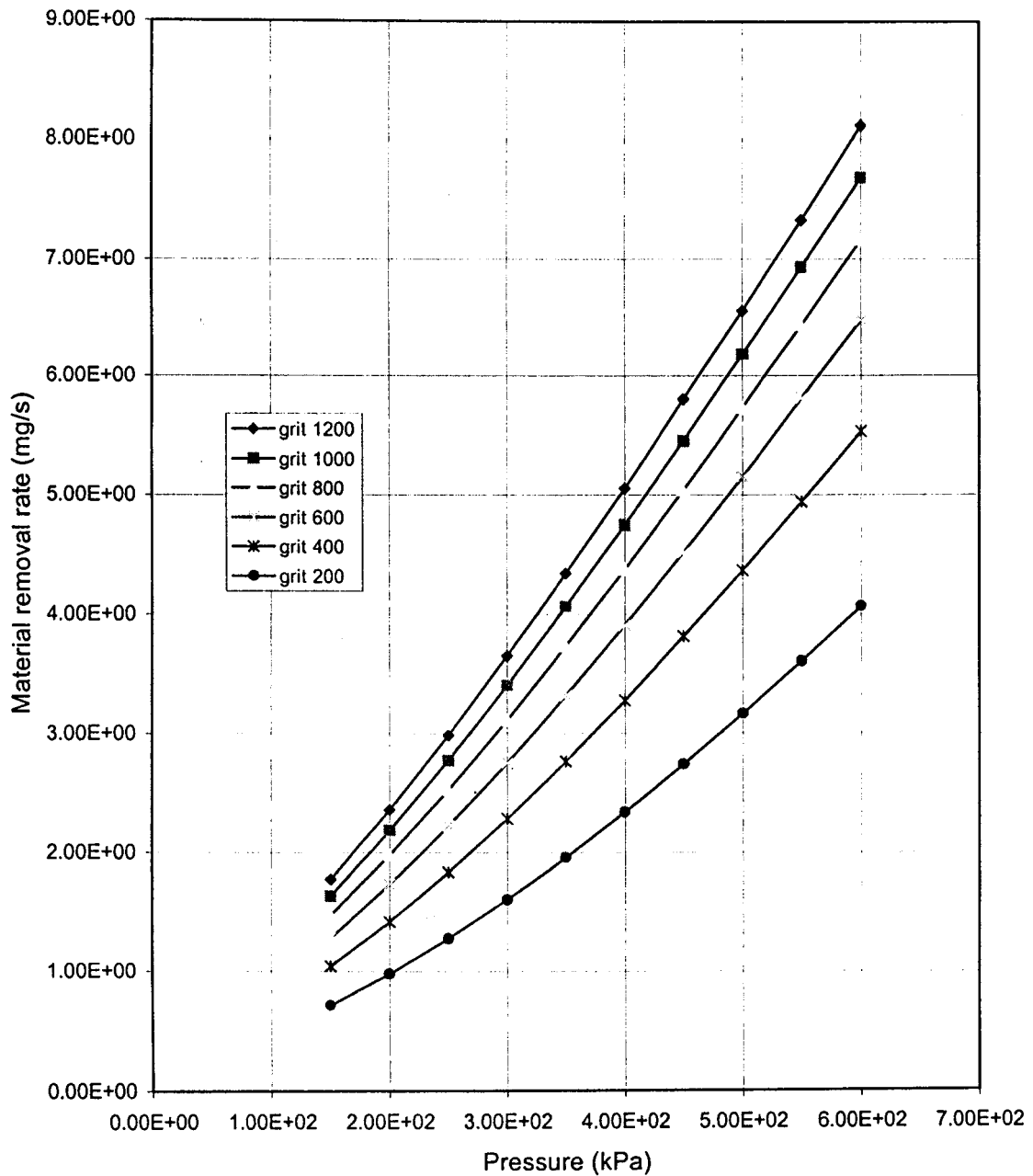


Figure 5.13 Theoretical prediction of the variation of material removal rate with pressure (stand off distance=20mm, mixing ratio=0.1, nozzle diameter=1.5mm)

jets the pressure inside the jet could be different from the ambient pressure. This pressure difference dies out as the jet flows.

Verification of whether the flow is sonic or subsonic is done by calculating the pressure ratio across the nozzle to see whether this pressure ratio is less than or equal to the critical pressure ratio. Once the system pressure is sufficiently large such that the pressure ratio across the nozzle is less than or equal to the critical pressure ratio (which is 0.528 for air), the velocity of the gas at the exit can not be controlled by the inlet pressure. Thus, for system pressures above 189 kPa, the effect of system pressure on material removal rate is restricted to the control of the air flow rate (and hence the particle flow rate).

Thus, it can be explained that the material removal rate is proportional to the pressure, at pressures above 189kPa (absolute), while the variation is non-linear for pressures below this. As pointed out earlier it is seen from Figures 2.1 and 2.2 that the material removal rate is proportional to the pressure showing very good agreement with this theory.

Early experimental work in the field did not take into account the role of nozzle diameter on the machining rate of the AJM process. The present work takes this aspect also into consideration. The set of figures, (Figures 5.14 to 5.17) show the dependence of material removal rate on the diameter of nozzle. Figure 5.14 is drawn for different values of stand off distance. The constant parameters are pressure (= 300kPa), mixing ratio (= 0.1) and grit size (= 800). In Figure 5.15, the curves are drawn with pressure as the varying parameter. Stand off distance (= 20mm), mixing ratio (= 0.1) and grit size (= 800) are the constant parameters. While Figure 5.16 is plotted for different values of the

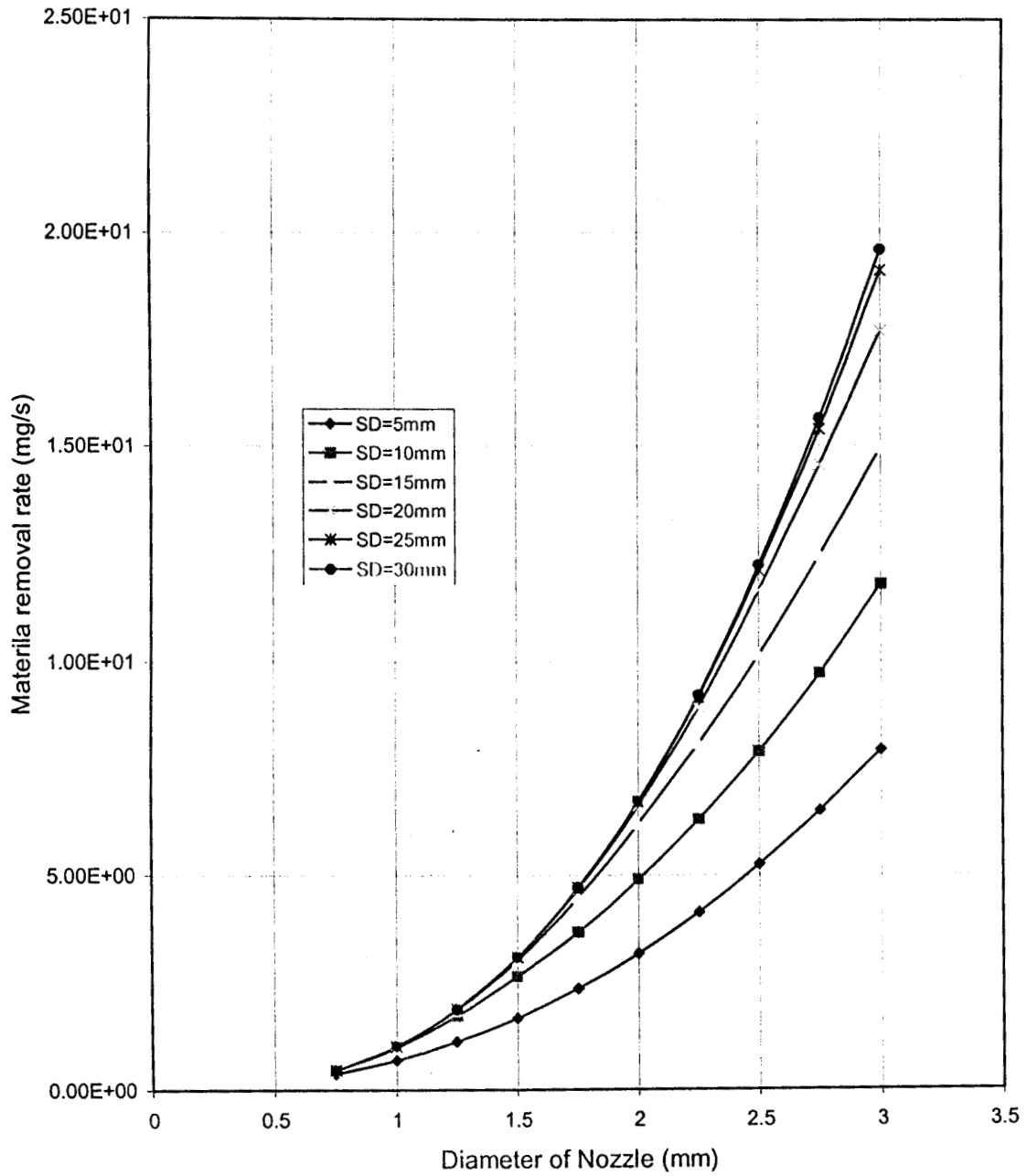


Figure 5.14 Theoretical prediction of the variation of material removal rate with diameter of nozzle (pressure=300kPa, mixing ratio=0.1, grit size=800)

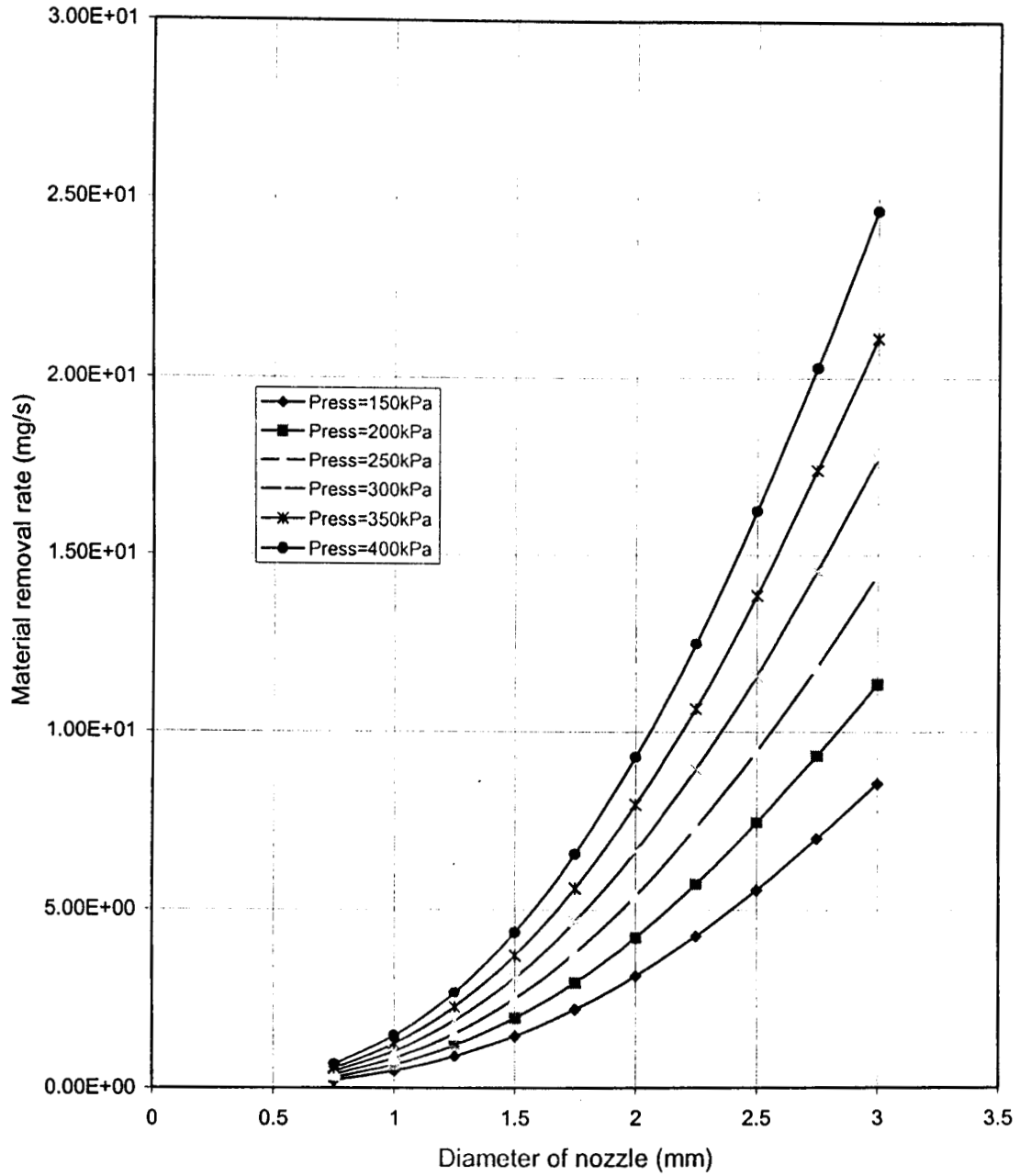


Figure 5.15 Theoretical prediction of the variation of material removal rate with diameter of nozzle (stand off distance=20mm, mixing ratio=0.1, grit size=800)

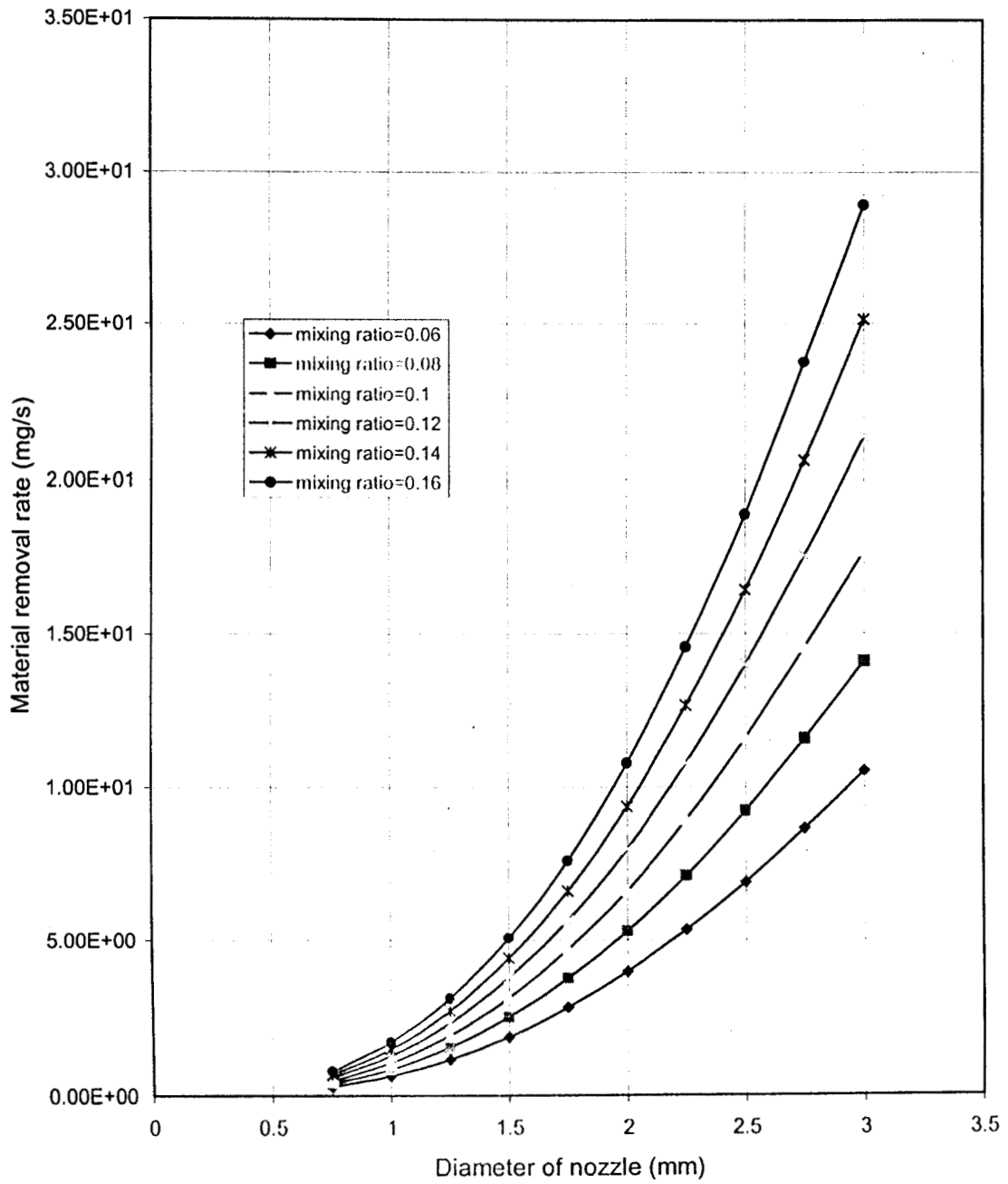


Figure 5.16 Theoretical prediction of the variation of material removal rate with diameter of nozzle (pressure=300kPa, stand off distance=20mm, grit size=800)

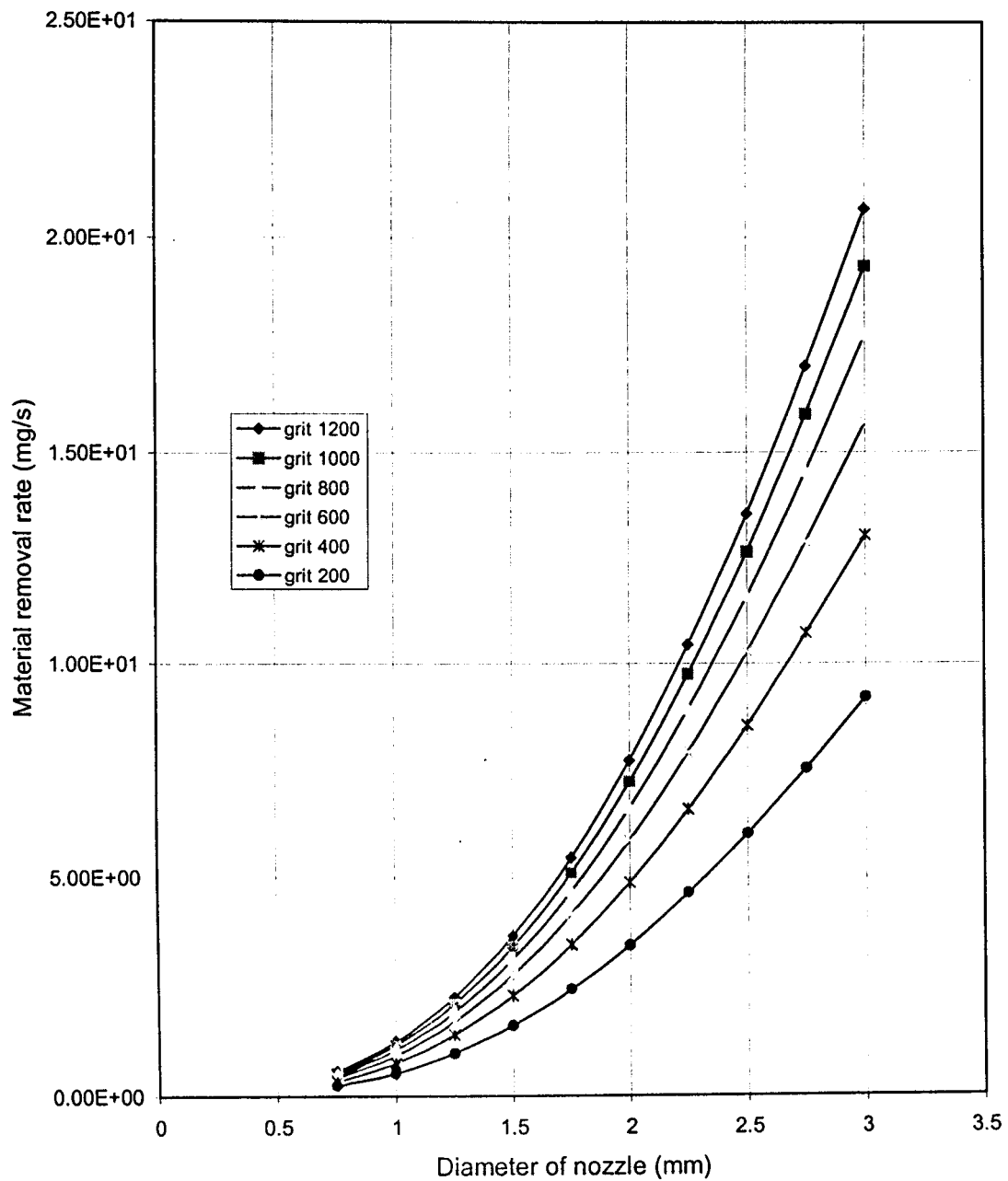


Figure 5.17 Theoretical prediction of the variation of material removal rate with diameter of nozzle (pressure=300kPa, stand off distance=20mm, mixing ratio=0.1)

mixing ratio (pressure = 300kPa, stand off distance = 20mm and grit size = 800), Figure 5.17 is plotted for various values of grit size. (pressure = 300 kPa, stand off distance = 20 mm and mixing ratio = 0.1). In all these cases, the variation of material removal rate with the nozzle diameter is parabolic (non-linear). This pattern is unchanged for different values of all other parameters in the range investigated. This characteristic could be explained as given below, from a theoretical standpoint.

The diameter of the nozzle does not affect the jet velocity so long as the ratio of the area of the nozzle to the area of the supply pipe is smaller than the critical area ratio. The inlet velocity is such that the Mach number is very small. (≈ 0.02). Therefore the inlet conditions are nearly the stagnation conditions. An area ratio less than 0.01 is below the critical area ratio for this condition. Therefore for most practical situations, the velocity at the exit of the nozzle is nearly sonic. At sonic conditions, the mass flow rate of air is $0.0404 \frac{P_0}{\sqrt{T_0}} A^*$ where A^* is the area of the passage at which sonic conditions prevail. Thus, the air flow rate and hence the particle flow rate is proportional to the area of the nozzle. Outside the nozzle, the length of the potential core increases as the nozzle diameter increases and therefore particles have a better chance of acquiring more kinetic energy in the jet. Thus the material removal rate is higher for larger nozzles due to larger flow rate and higher velocity attained by the particles. If the diameter of the nozzle is too large, the gas velocity and the velocity of particles become very small so that the machining rate decreases. Nozzles of such large diameters are not commonly employed and have not been considered in this analysis.

The variation of material removal rate with the grit size is shown in Figure 5.18. This is drawn for various stand off distances. The pressure is 300 kPa , the mixing ratio is

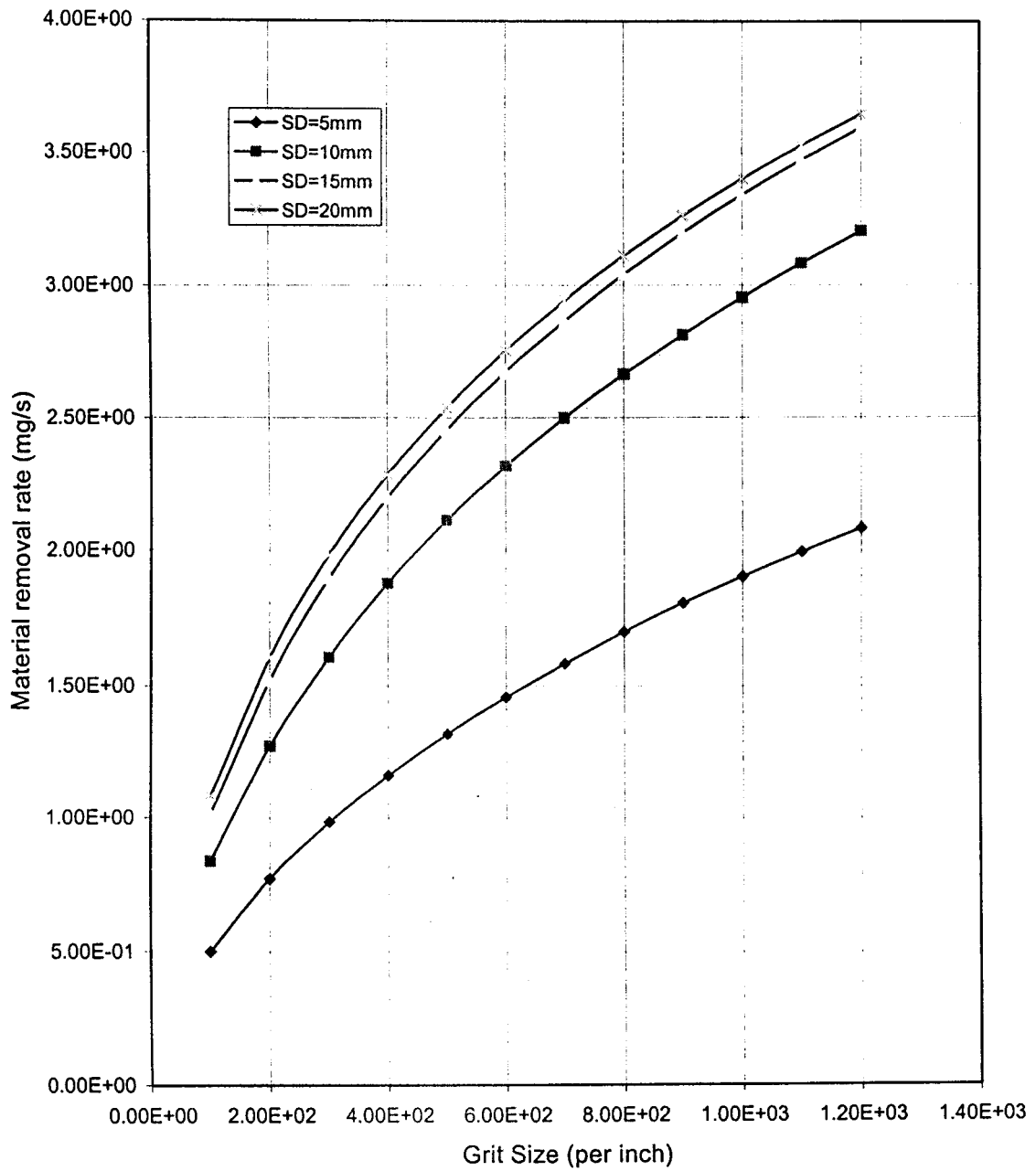


Figure 5.18 Theoretical prediction of the variation of material removal rate with grit Size (pressure =300kPa, mixing ratio=0.1, diameter of nozzle=1.5mm)

0.1 and the diameter of nozzle is 1.5 mm. It is seen that the material removal rate increases as the grit size increases. This variation can be explained by considering how the fracture volume is related to the radius of the particle. The volume of material removed by the impact of a single particle (the fracture volume) is proportional to the cube of the radius (volume) of the particles. Thus, intuitively, one might expect a higher material removal rate when the average diameter of the abrasive powder is larger. However, the velocity of the particles must also be taken into consideration. It is easy to visualize that, under the action of the same force, the acceleration of smaller bodies is larger than that of larger bodies. Therefore particles having comparatively smaller diameters get higher velocity than particles with larger diameters, when both travel through the same velocity field. Added to this is the situation that, the number of particles in a given flow rate is inversely proportional to the cube of the radius of the particles. Therefore the number of impacts per second is higher for abrasive powder of small diameter (high grit size) than the number of impacts per second for powder of larger diameter (small grit size). These two effects together may compensate the effect of material removal indicated above in a single impact. Thus the theoretical prediction as illustrated by the Figure 5.18 is justifiable. However, experimental observations point to an exactly opposite trend. This could be due to the fact that, during experimentation, fine abrasive powder was found to show very poor flowing characteristics. The particles of small average size cling together and form larger chunks. Further, they tend to stick to the walls of the mixing chamber and the hose connecting the mixing chamber to the nozzle. By borrowing the concept of viscosity of fluids, powder with smaller particles may be thought of as having a larger viscosity. This effect can be observed in sieve analysis also.

Particles retained in a sieve usually contain finer particles also. Thus, in practice, abrasives of relatively larger particle diameters have been found to flow better than that with very small particle sizes.

5.3 Experimental Investigations

The experiments have been done with a view to validating the theoretical findings, to propose an empirical relationship for the material removal rate and to study the surface roughness of parts machined by AJM. The theoretical predictions agree qualitatively with experimental findings already published as indicated in the previous section. In the experimental data reported by Verma and Lal [9] and Pandey and Shan [8], the material removal rates are very small. This may be because; in these experiments the diameter of the nozzle used is very small. From the analysis reported in chapter 4, it is seen that the length of the nozzle also is a parameter of the process. In most of the studies on AJM, this parameter is not identified and is not investigated in the present set of experiments as well. The photograph of the experimental set up is shown in figure 5.19.

In the experiments reported herein, ordinary glass slides of 6mm thickness are used as work pieces. These are held on a fixture beneath the nozzle. The parameters of the process are set on the machining set up. Each run of the machine was for a period of 30s. The abrasive used is Aluminium oxide of grit size 200, 400, 600, 800, 1000 and 1200. (The abrasive powder was supplied by M/s Emery India Ltd. Jamnagar). Nozzles of diameters ranging from 1.00 mm to 2.75 mm were used for the experimentation. The nozzles employed are converging conical nozzles of stainless steel body with a tungsten

carbide insert serving as the tip of the nozzle. The overall length of the nozzle is 100mm.

These experimental parameters are summarized in the Table 5.2 below:

Work material	Glass slides 6mm thick
Abrasive used	Aluminium oxide
Size of abrasives (grit size)	200, 400, 600, 800, 1000 and 1200
Time of run	30 s
Nozzle material	Stainless steel body with tungsten carbide insert
Nozzle size (diameter at exit)	1.0mm, 1.25mm, 1.5mm, 1.75mm, 2mm, 2.25mm, 2.5mm and 2.75mm
Stand off Distance	2 mm to 50 mm

Table 5.2 Experimental parameters

5.3.1 Validation of the Theoretical Predictions

In the first part, experiments were done for the purpose of comparing the results with the theoretical predictions, with a view to validating them. In this, the pressure was maintained at 250 kPa, a nozzle of diameter 2.0 mm and aluminium oxide abrasive of grit size 800 were used for machining. The stand off distance was set at discrete values from 2 mm to 25 mm. The mixing ratio was allowed to vary. The material removed is measured by measuring the weight loss of the glass pieces. The abrasive flow rate is

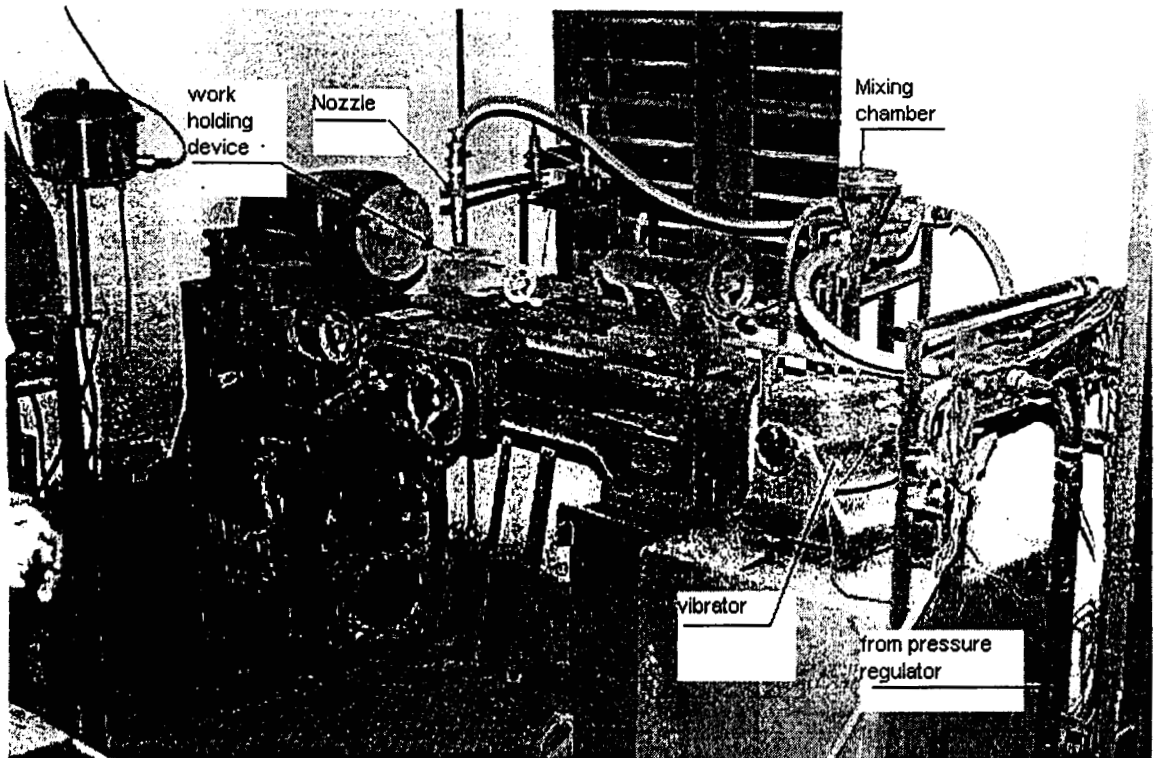
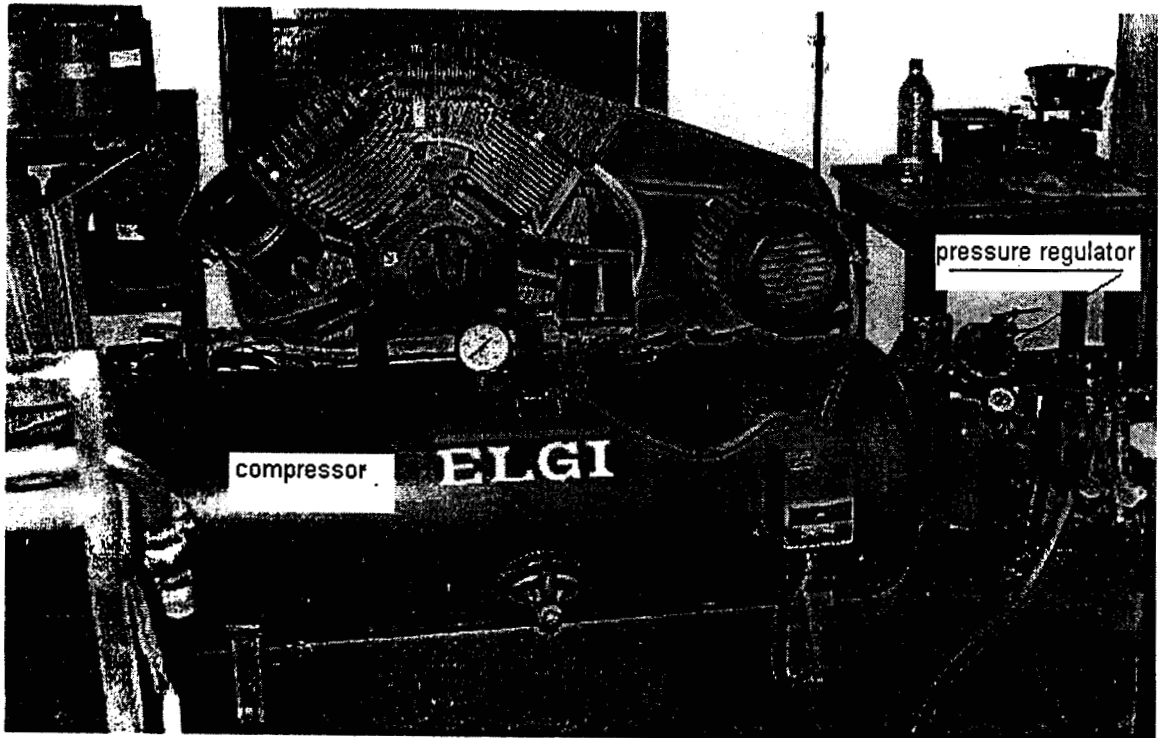


Figure 5.19 Experimental set up (Compressor at the top and experimental station at the bottom)

measured by actually finding the amount of abrasive used in a test run, and the flow rate of air is measured with the help of a previously calibrated orifice meter. The results of these experiments are tabulated in table 5.3 below.

Stand off dist.		1	2	3	4	5	6	7
2 mm	m_r	0.009	0.02	0.04	0.06	0.085	0.1	0.146
	m_{rr} (mg/s)	0.8	0.56	0.6	0.8	0.7	1.0	1.1
4 mm	m_r	0.03	0.057	0.066	0.076	0.10	0.128	0.133
	m_{rr}	1.0	1.4	1.3	1.6	1.6	1.8	1.7
6 mm	m_r	0.036	0.045	0.05	0.06	0.09	0.095	0.126
	m_{rr}	1.8	2.2	1.9	2.2	2.1	2.3	2.9
12 mm	m_r	0.028	0.04	0.065	0.07	0.106	0.146	0.17
	m_{rr}	2.3	2.5	2.6	2.8	3.0	3.6	3.8
15 mm	m_r	0.023	0.033	0.05	0.081	0.102	0.124	0.14
	m_{rr}	1.75	2.0	3.0	3.20	4.3	5.0	5.6
20 mm	m_r	0.018	0.024	0.062	0.09	0.1	0.155	0.176
	m_{rr}	1.8	3.0	4.0	5.4	5.4	6.5	7.2
25 mm	m_r	0.02	0.045	0.062	0.08	0.10	0.12	0.146
	m_{rr}	1.9	2.3	4.0	5.2	5.0	6.2	6.0

Table 5.3 Data obtained on the AJM set up for comparison with theory

These data are plotted in figure 5.20 as plots of material removal rate vs. mixing ratio for various values of stand off distances. Best-fit curves are drawn alongside the experimental points. The best fits are found by hypothesizing that the relationship between m_{rr} and m_r is of the form $m_{rr} = Cm_r^n$ where C is a constant. This is done with the MATLAB software. The variation of material removal rate with stand off distance is found from these curves. The experimentally obtained data and the curves fitted through these points are shown in figure 5.20.

For verification with theoretical predictions, the variation of m_{rr} with stand off distance (for $m_r = 0.1$) is taken. This curve is shown in figure 5.21. In this also the best-fit line is found using MATLAB. The same is compared with theoretical results in figure 5.22. It can be seen that the trend as predicted by analytical methods is in very good agreement with the experimental observation. The theoretically predicted values of material removal rate are larger than the experimentally obtained values, in general. The mean deviation of theoretical values from experimental results is **0.36 mg/s**. This variation would mainly be due to the over estimate of the material removal rate from theory since, the analysis does not take into account the particles bouncing off the work surface and the possibility of the reduction in machining rate as machining proceeds. Some of these aspects are discussed by Nair and Vijayakumar [67].

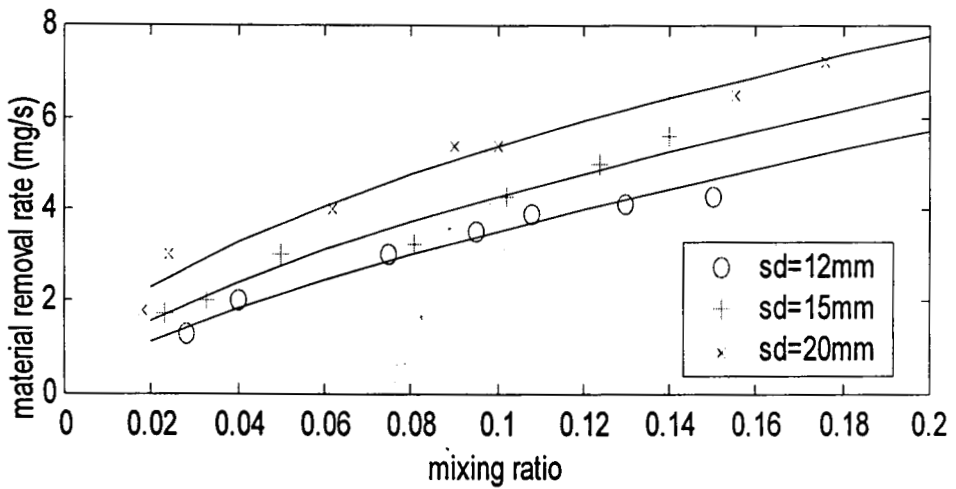
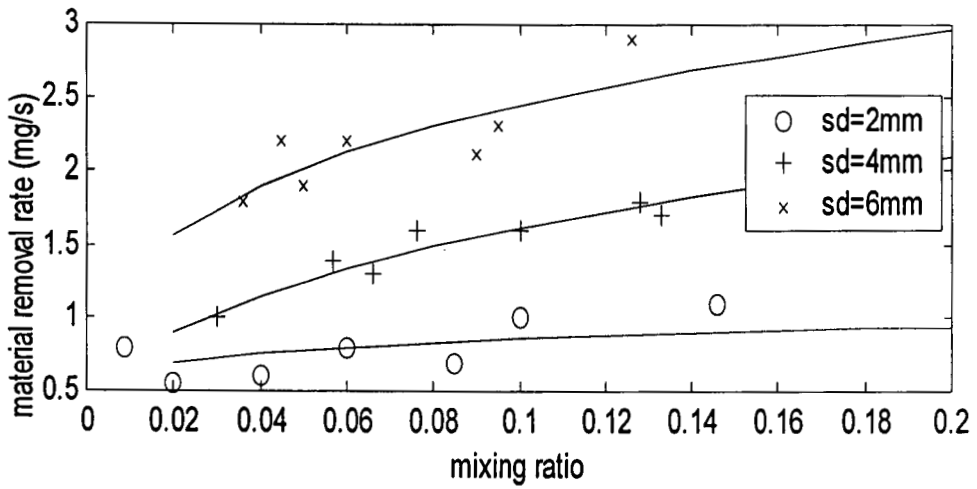


Figure 5.20 Experimental data and best-fit curves:

Material removal rate vs. mixing ratio

(From experiments at pressure=250kPa, diameter of nozzle=2mm and grit size=800)

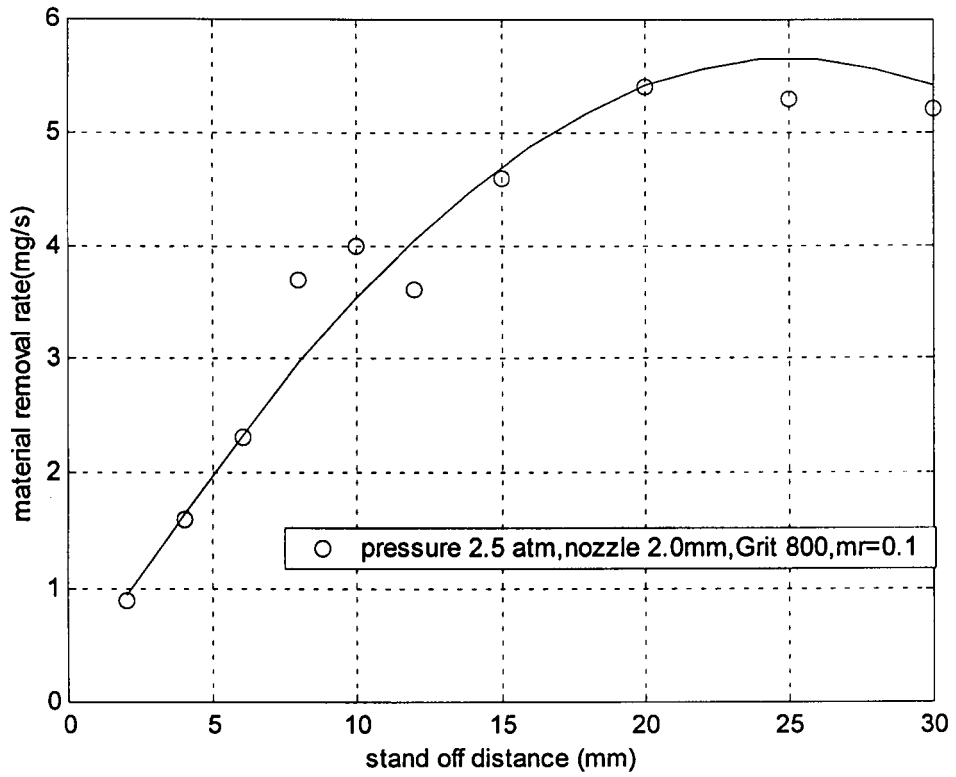


Figure 5.21 Experimental points and best-fit curve for the variation of material removal rate with stand off distance
(Pressure=250 kPa, mixing ratio=0.1, grit size=800)

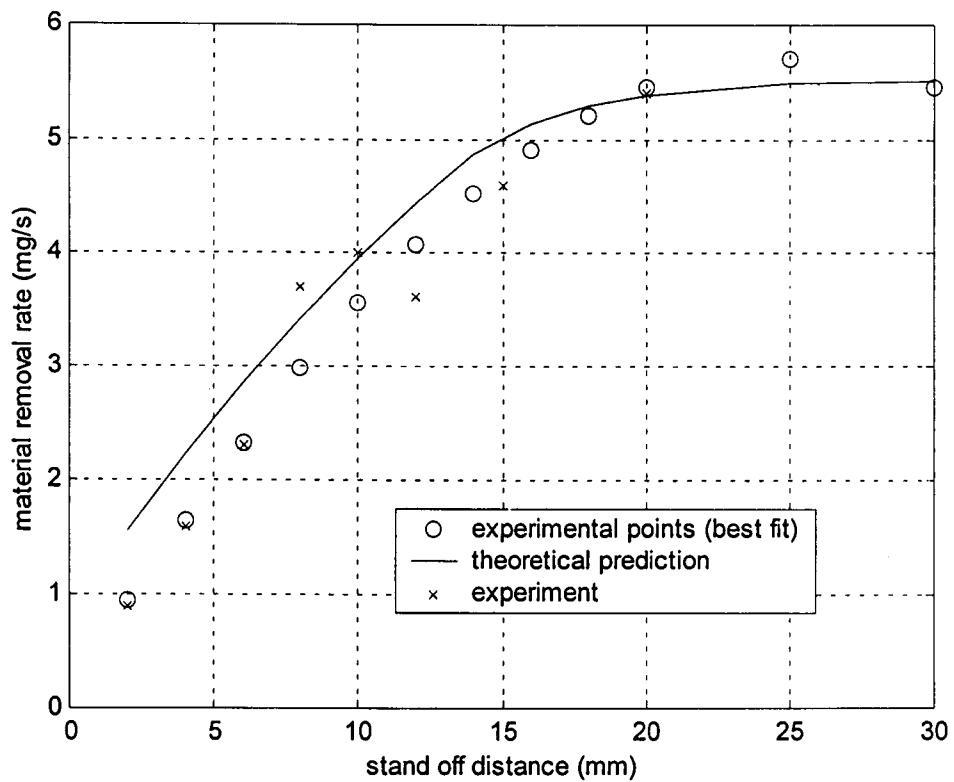


Figure 5.22 Experimental validation of the theory

**(Data from theory and experiments for pressure=250kPa, mixing ratio=0.1,
grit size=800, diameter of nozzle=2 mm)**

5.3.2 An Empirical Relation for Material Removal Rate

The second part of the experiments has been carried out with a view to formulating a correlation for material removal rate. The main parameters of the process viz. the pressure (p), the stand off distance (sd), the mixing ratio (m_r), the size of the abrasive particles (Grit Size G), and the diameter of nozzle (d_n) are treated as variables. To cover the full range of variation of all the parameters of the process and to reduce the number of experiments, a completely randomized combination of the parameters [68] is chosen for experimental data generation. Pressure is selected in the range from 100 kPa to 550 kPa. Nozzles of diameters 1.75mm, 2mm, 2.25mm 2.5 mm and 2.75 mm are used. Aluminium oxide of Grit sizes 200, 400, 600, 800 and 1200 are employed for machining. Stand off distance in the range from 2mm to 55 mm was set. At each of the combination of the parameters, the experiment is repeated thrice and the average value of the material removal rate is taken. The random combinations and the results of experiments are given in Table 5.4

Sl.No.	Stand off distance Sd (mm)	Pressure p (kPa)	Grit Size	Nozzle dia d_n (mm)	Mixing ratio m_r	Material removal rate m_{rr} (mg/s)
1	7	300	200	2.25	0.181	3.853
2	45	250	200	1.75	0.310	4.816
3	15	500	200	1.75	0.063	4.993

4	25	400	200	2.75	0.128	16.582
5	2	100	200	2.75	0.045	0.462
6	30	150	200	1.75	0.079	1.073
7	15	500	400	2.75	0.01	1.404
8	25	550	400	1.75	0.071	8.189
9	35	150	400	2.25	0.012	0.507
10	50	250	400	2.75	0.172	10.755
11	30	350	400	2.25	0.156	10.73
12	7	350	400	1.75	0.280	4.235
13	20	150	600	1.75	0.208	1.284
14	2	550	600	2.25	0.048	1.415
15	30	500	600	2.75	0.130	13.855
16	35	350	600	2.75	0.092	9.815
17	50	200	600	2.25	0.150	3.291
18	40	400	600	2.75	0.005	1.58
19	10	100	800	1.75	0.039	0.14
20	45	400	800	2.25	0.095	9.76
21	10	300	800	2.75	0.032	2.39
22	4	250	800	1.75	0.0960	2.118
23	20	200	800	2.25	0.072	3.14
24	35	450	800	2.75	0.209	18.95
25	4	450	1200	2.75	0.002	0.953
26	40	300	1200	2.25	0.167	7.589

27	2	200	1200	1.75	0.003	0.133
28	25	500	1200	2.25	0.004	2.32
29	2	550	1200	2.25	0.0047	0.587
30	7	100	1200	2.75	0.007	0.198

Table 5.4 Experimental data for empirical correlation for material removal rate

The above results are used to find an empirical relation of the material removal rate in terms of the other process parameters. The form of the best fit for material removal rate with stand off distance obtained from the earlier experiments is used in this also. The dependence of mrr with the other parameters is chosen to be of the form $\prod_{i=1}^n Cx_i^{m_i}$. The result of a 'least square fit' obtained from the above experimental results is

$$mrr = 1.2014(1 + sd - 0.02sd^2)^{1.1951} m_r^{0.5176} p^{1.0112} dn^{1.3929} G^{-0.3473} \quad (5.2)$$

In this, mrr is in **mg/s**, stand off distance sd is in **mm**, pressure p is the gauge pressure in **kg/cm²**, the nozzle diameter dn is in **mm** and the grit size G is **per inch**. The suggested fit gave a correlation coefficient of **0.91** and the mean deviation is **0.9mg/s**.

The variation of mrr with the main parameters of the process as computed from the above experimental correlation is presented in the form of graphs in Figures 5.23 to 5.42. Figures 5.23, 5.24, 5.25 and 5.26 illustrate how the material removal rate varies as the stand off distance is varied. Figure 5.23 is drawn with mixing ratio as parameter. The other parameters are pressure = 300kPa, Nozzle diameter = 1.5mm and grit size = 800.

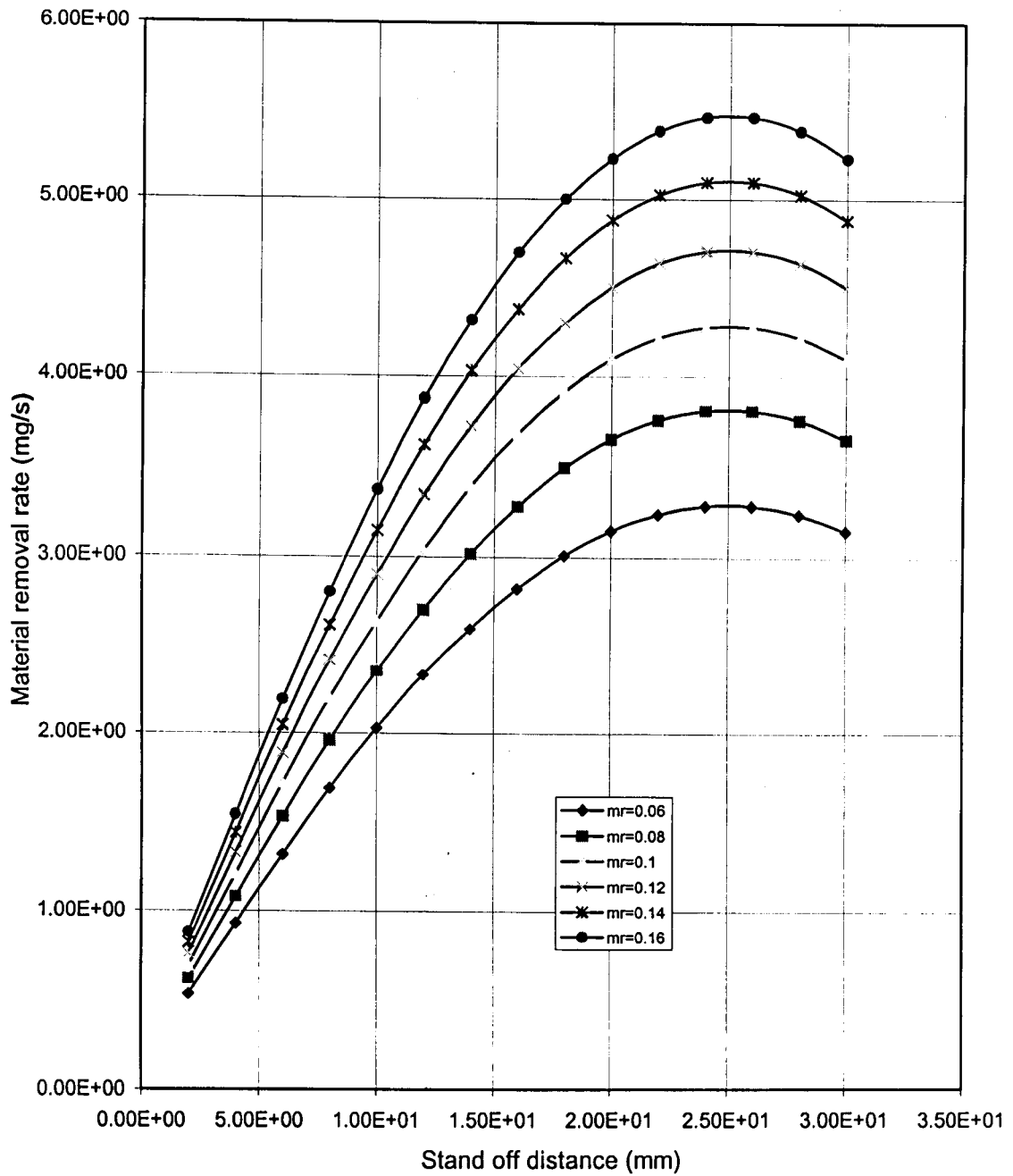


Figure 5.23 Variation of material removal rate with stand off distance (from experiment)(pressure=300kPa, diameter of nozzle=1.5mm, grit size=800)

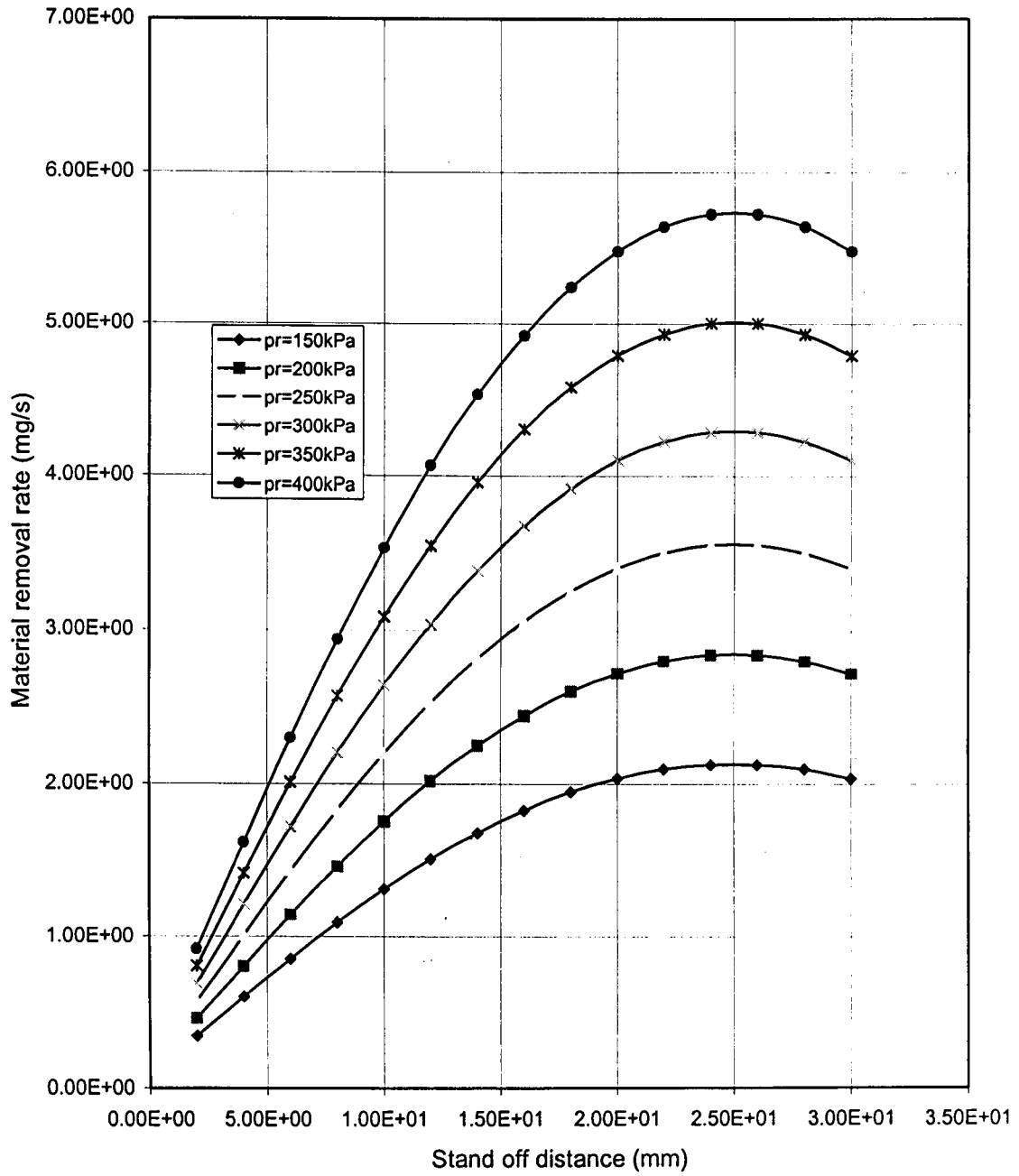


Figure 5.24 Variation of material removal rate with stand off distance (from experiment) (mixing ratio=0.1, diameter of nozzle=1.5mm, grit size=800)

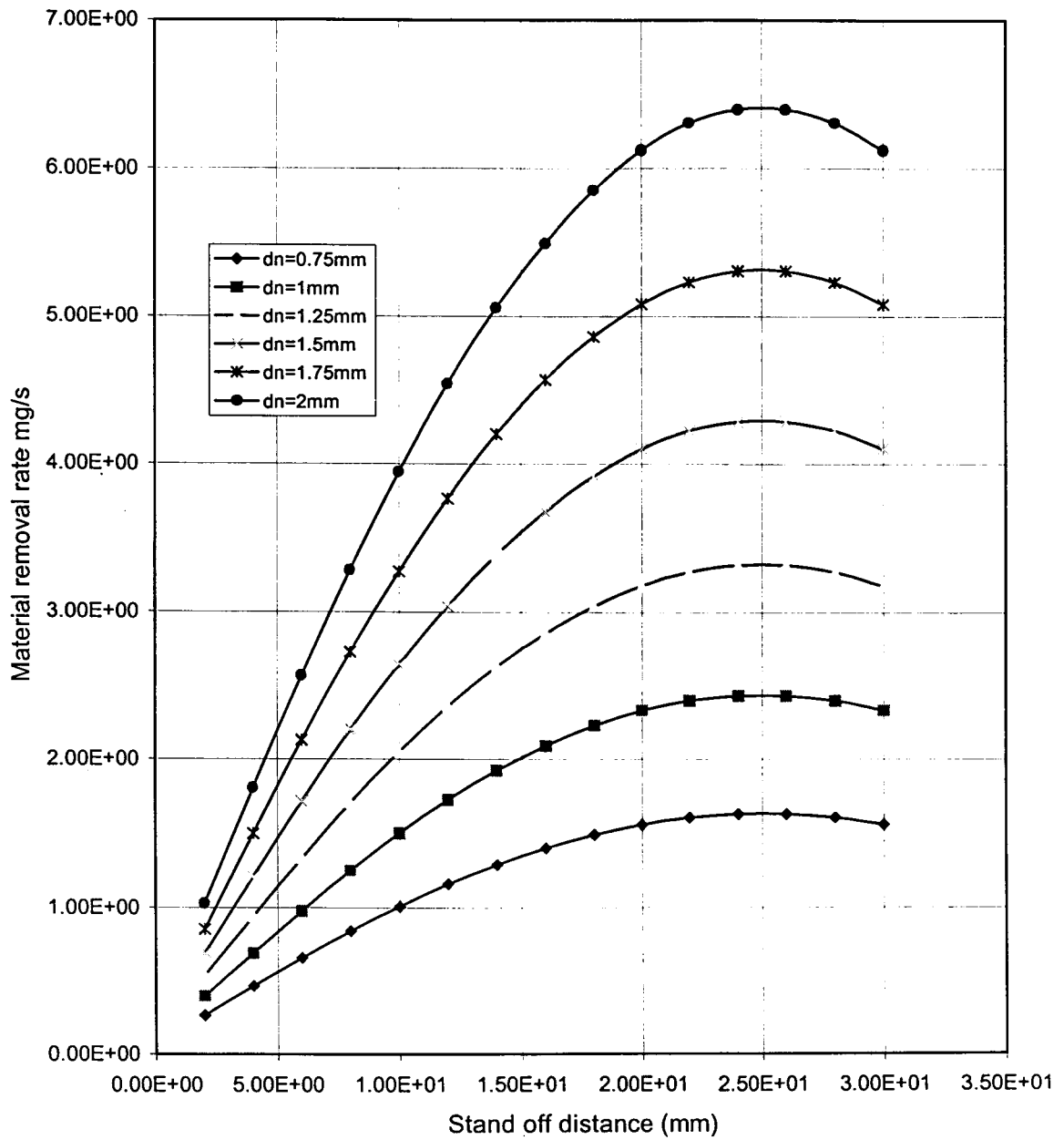


Figure 5.25 Variation of material removal rate with stand off distance (from experiment) (pressure=300kPa, mixing ratio=0.1, grit size=800)

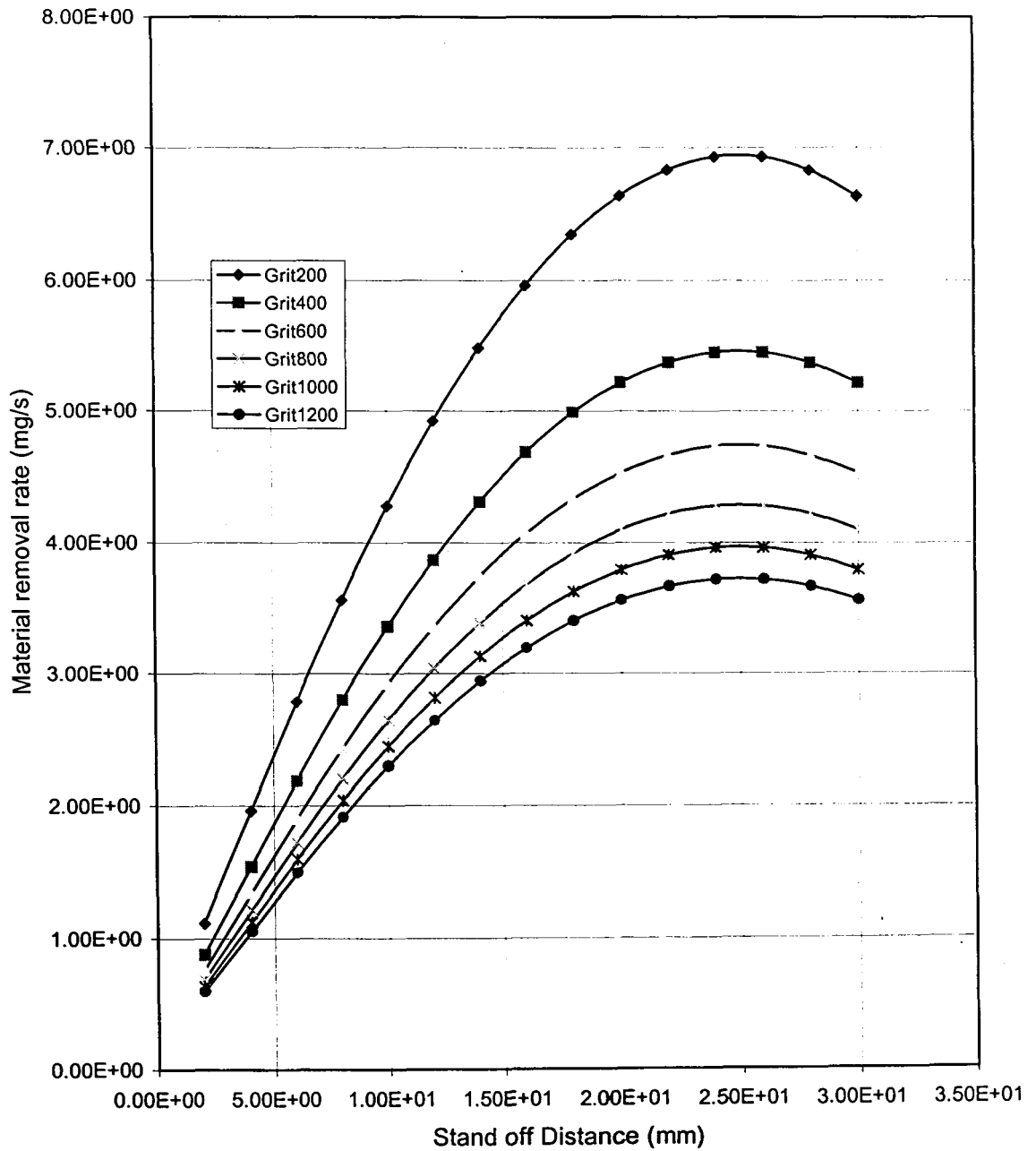


Figure 5.26 Variation of material removal rate with stand off distance (from experiments) (pressure=300kPa, mixing ratio=0.1, diameter of nozzle=1.5mm)

Figure 5.24 is drawn with pressure as the changing parameter. The mixing ratio is 0.1, the nozzle diameter is 1.5mm and the grit size is 800. In Figure 5.25 the changing parameter is nozzle diameter, while the pressure is 300kPa, the mixing ratio is 0.1 and the grit size is 800. The curves in Figure 5.26 are drawn for different values of the grit size with the pressure = 300kPa, the mixing ratio =0.1 and the diameter of nozzle = 1.5mm.

These curves indicate the existence of an optimum stand off distance, irrespective of the pressure, mixing ratio, nozzle diameter and grit size. However, the curves are flatter for low values of Pressure (150kPa) and Diameter of nozzle (0.75mm), indicating that the maximum machining rate can be obtained over a range of stand off distances when these parameters are comparatively small whereas the change in material removal rate is sharp at large values of the parameters. It is apparent that, for obtaining good machining rates, the machining is to be done at a stand off distance of 20mm or above, and at a pressure as large as possible. The inter relationship between these parameters are not brought into focus, because of the type of relationship suggested in equation (5.2).

The variation of material removal rate with mixing ratio is presented in Figures 5.27, 5.28, 5.29 and 5.30. In Figure 5.27 the curves are drawn for different values of the stand off distance, at a pressure of 300 kPa, nozzle diameter of 1.5 mm and grit size of 800. In a similar way Figure 5.28 is for different values of pressure. The stand off distance is 20mm, the nozzle diameter is 1.5mm and the grit size is 800. The diameter of the nozzle is the changing parameter for Figure 5.29. The constant parameters are pressure (300 kPa), stand off distance (20mm) and grit Size (800). Figure 5.30 shows the effect of variation of Grit size as a parameter. The other parameters for the plot are: pressure = 300kPa, stand off distance = 20mm and nozzle diameter = 1.5 mm.

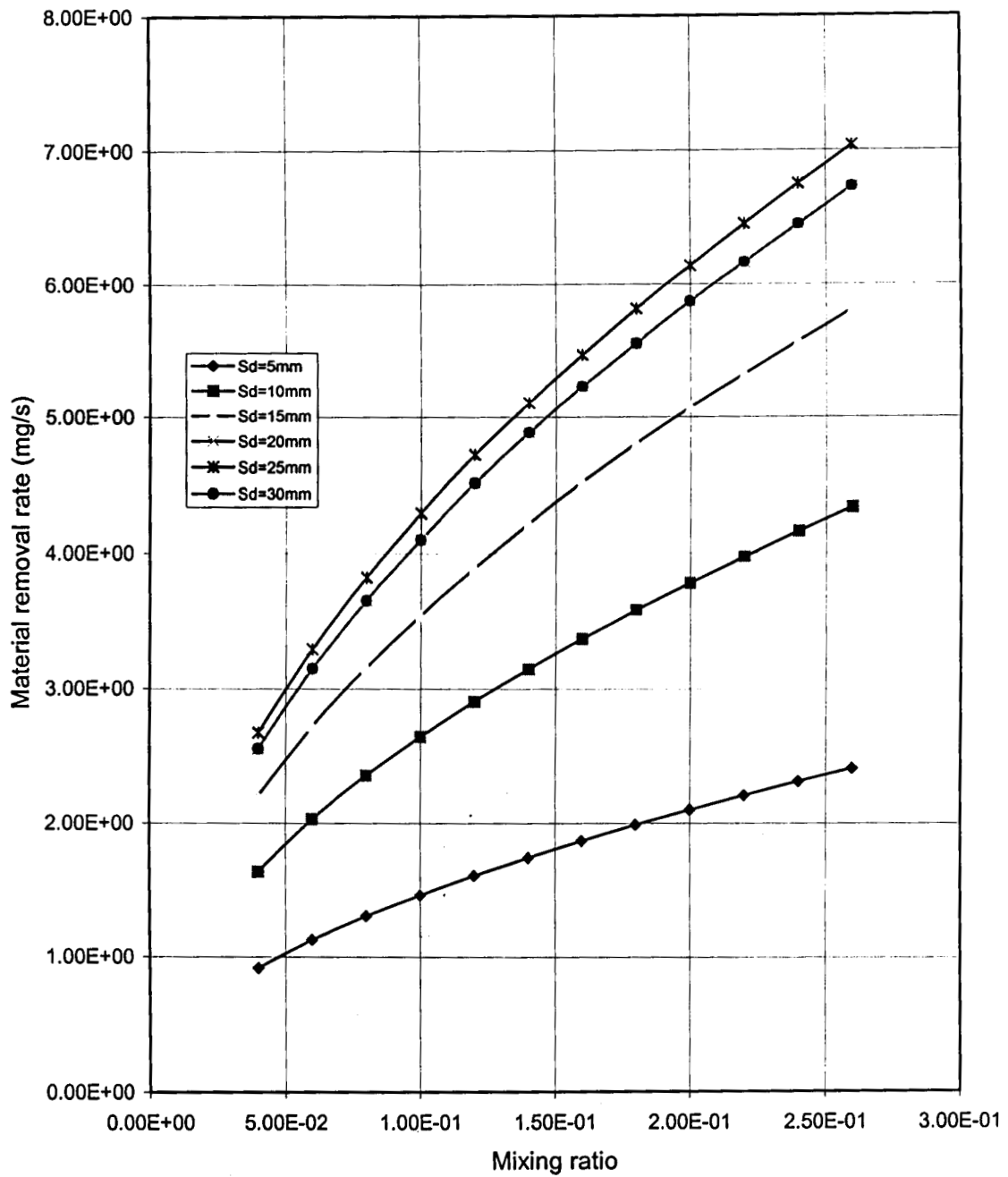


Figure 5.27 Variation of material removal rate with mixing ratio (from experiment) (pressure = 300kPa, diameter of nozzle = 1.5mm, grit size = 800)

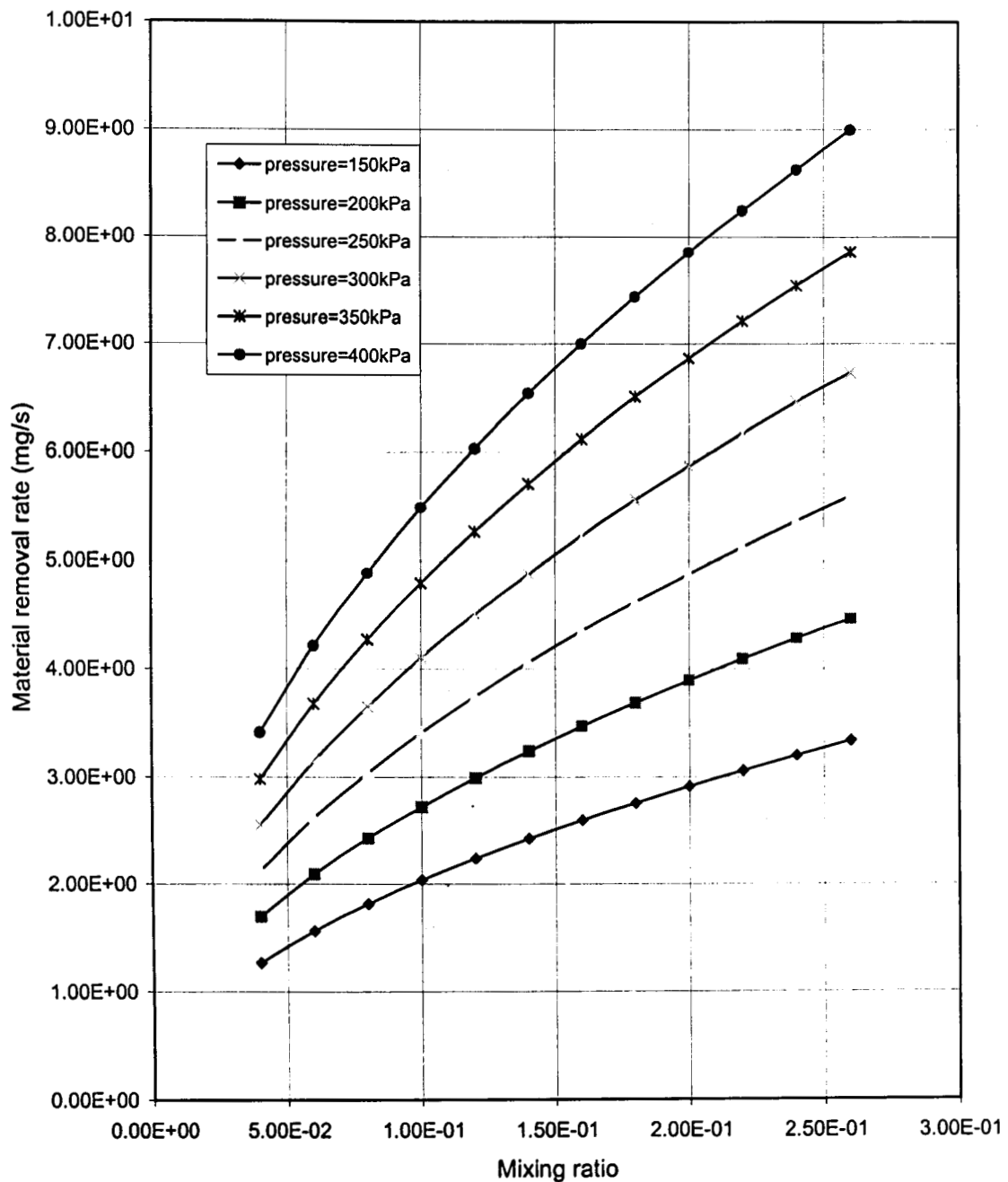


Figure 5.28 Variation of material removal rate with mixing ratio (from experiments) (stand off distance=20mm, diameter of nozzle=1.5mm, grit size=800)

601-4350

78
JRS/3

NB 3260

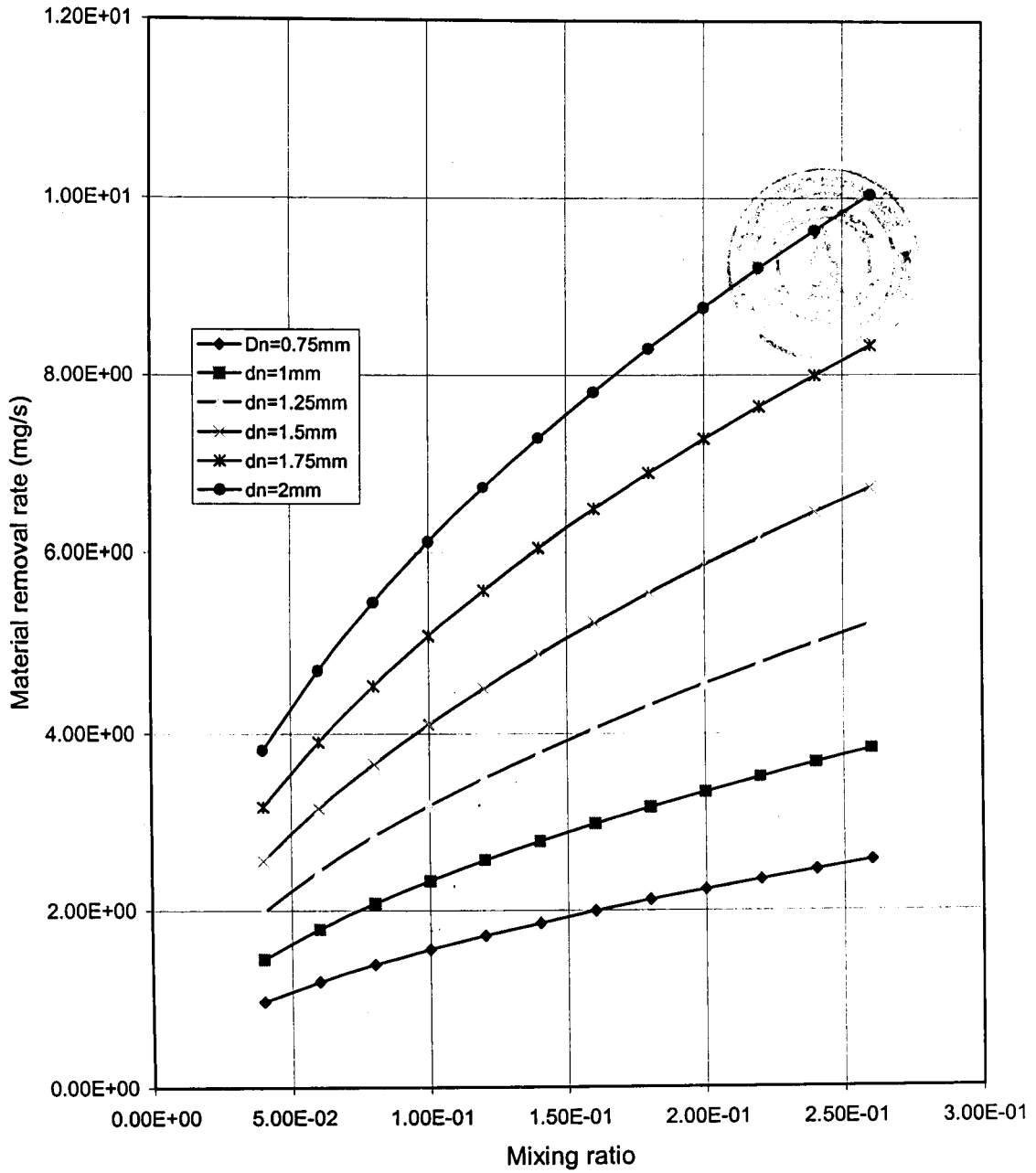


Figure 5.29 Variation of material removal rate with mixing ratio (from experiments) (stand off distance=20mm, pressure=300kPa, grit size=800)

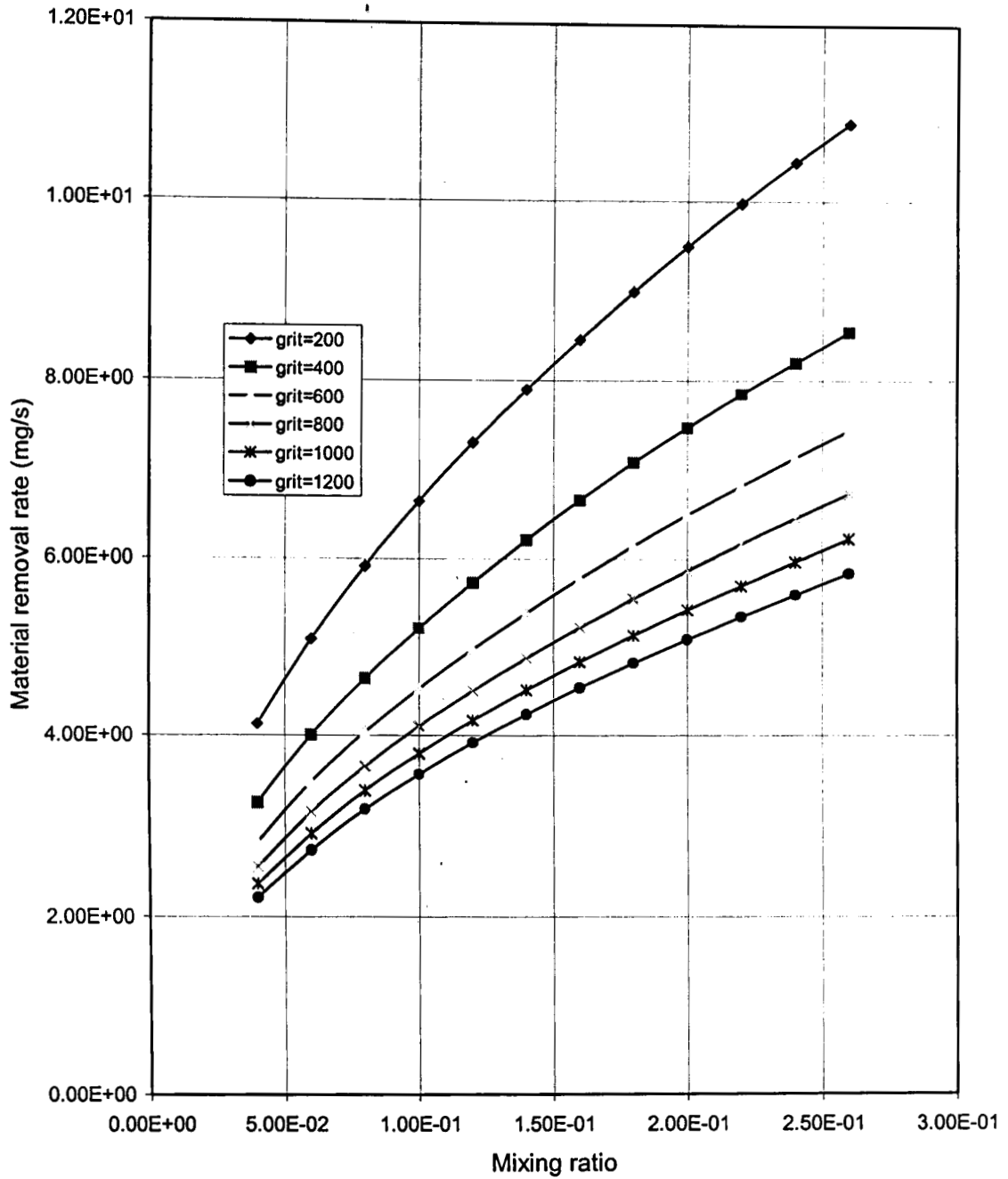


Figure 5.30 Variation of material removal rate with mixing ratio (from experiments) (pressure=300kPa, stand off distance=20mm, diameter of nozzle=1.5mm)

As expected, the material removal rate shows a monotonic increase with the mixing ratio, which agrees with the prediction by the theory also. The variation of the Material removal rate with mixing ratio is nearly parabolic. (The term *mixture ratio* used in literature is slightly different). At higher values of mixing ratio the powder flow rate is higher. This would result in a reduction of the velocity acquired by the particles. This reduction in particle velocity is more than compensated by the number of particles striking the surface. Thus, the increase in the material removal rate with mixing ratio is justifiable. At zero mixing ratios, the material removal rate is zero. Similarly at mixing ratio=1.0 also the material removal rate must be zero because the powder cannot get any velocity with out a source of energy. Thus intuitively, one feels that there must be an optimum mixing ratio for which $m r r$ is a maximum. But however, this is not predicted by the theory and the correlation. Since the experiments are done for low and moderate values of mixing ratios, an optimum mixing ratio, if any, is outside the range. The largest mixing ratio at which the experiments were done is 0.30. Therefore the above fit is valid only in the range of mixing ratios from 0 to 0.30.

Figures 5.31, 5.32, 5.33 and 5.34 show the variation of material removal rate with pressure. The other parameters considered in these curves are stand off distance, mixing ratio, diameter of nozzle and grit size respectively. In Figure 5.31 the curves are plotted for a mixing ratio = 0.1, Nozzle diameter 1.5mm and grit size 800. Figure 5.32 is drawn with stand off distance = 20mm, nozzle diameter = 1.5mm and grit size = 800. The constant parameters in Figure 5.33 are stand off distance = 20mm, mixing ratio = 0.1 and grit size = 800 while that in figure 5.34 are stand off distance = 20mm, mixing ratio = 0.1 and nozzle diameter = 1.5mm. It can be seen that the variation of material removal rate

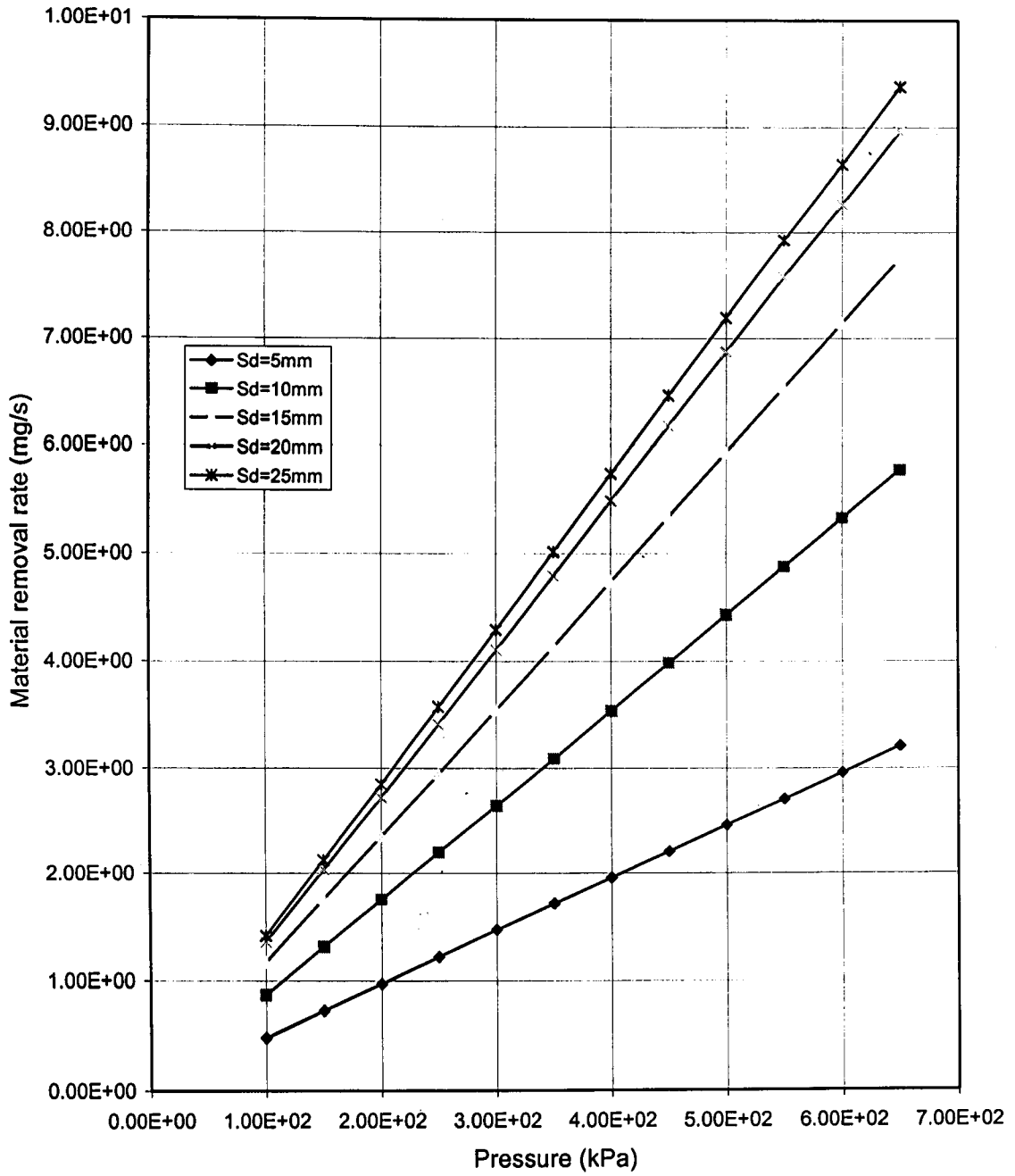


Figure 5.31 Variation of material removal rate with pressure (from experiments) (mixing ratio=0.1, diameter of nozzle=1.5mm, grit size=800)

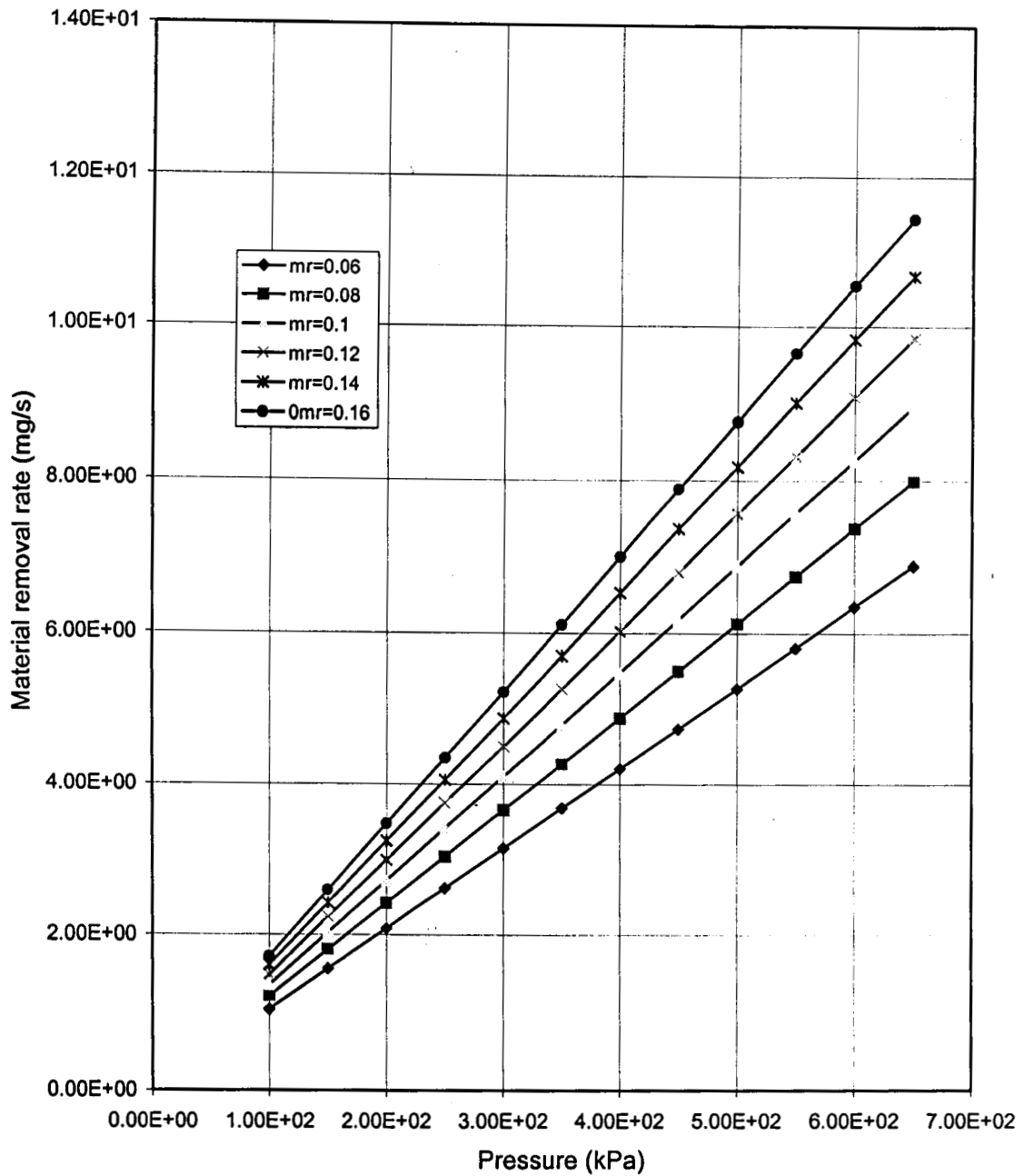


Figure 5.32 Variation of material removal rate with pressure (from experiments) (stand off distance=20mm, diameter of ozzle=1.5mm, grit Size=800)

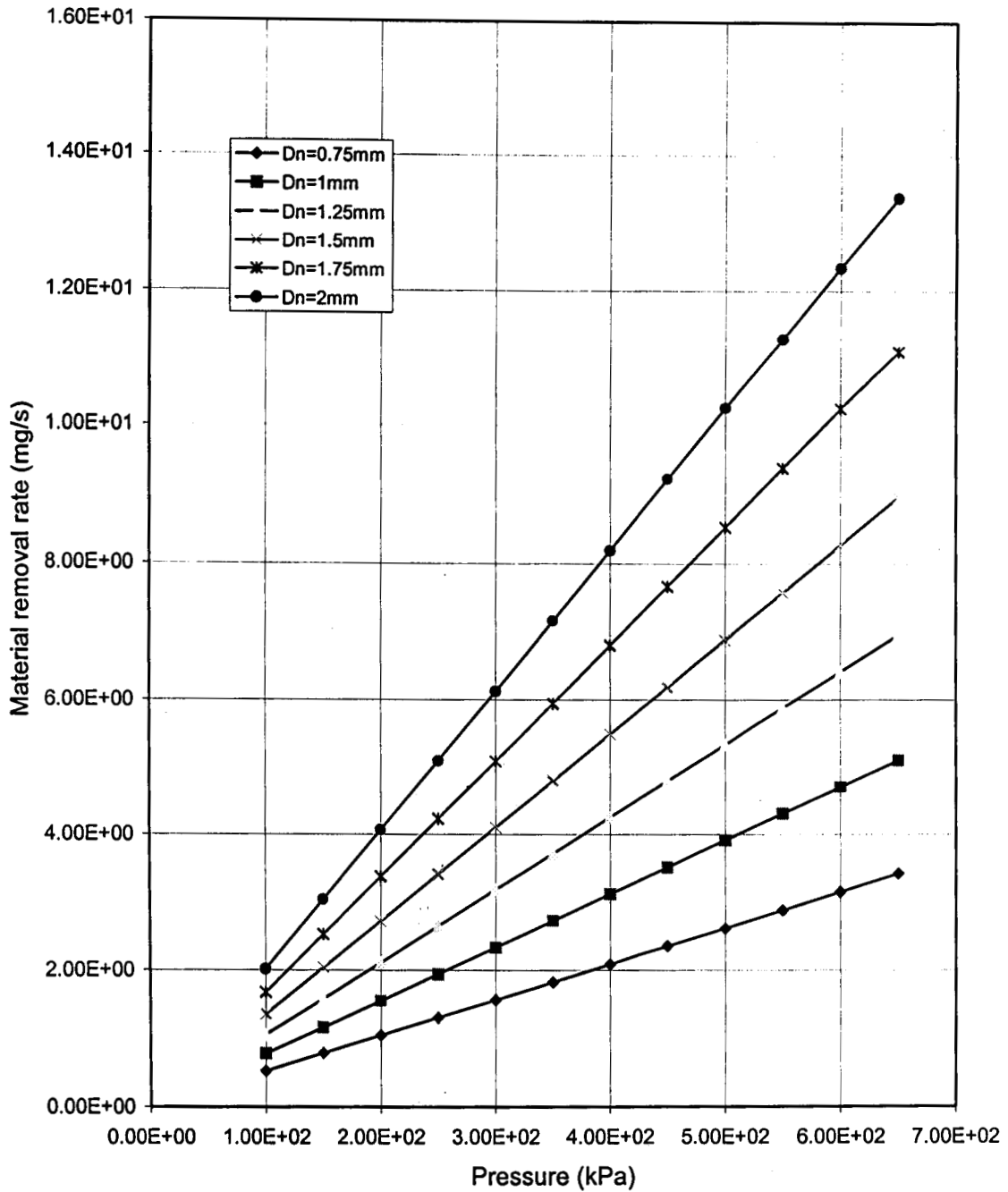


Figure 5.33 Variation of material removal rate with pressure (from experiments) (stand off distance=20mm, mixing ratio=0.1, grit Size=800)

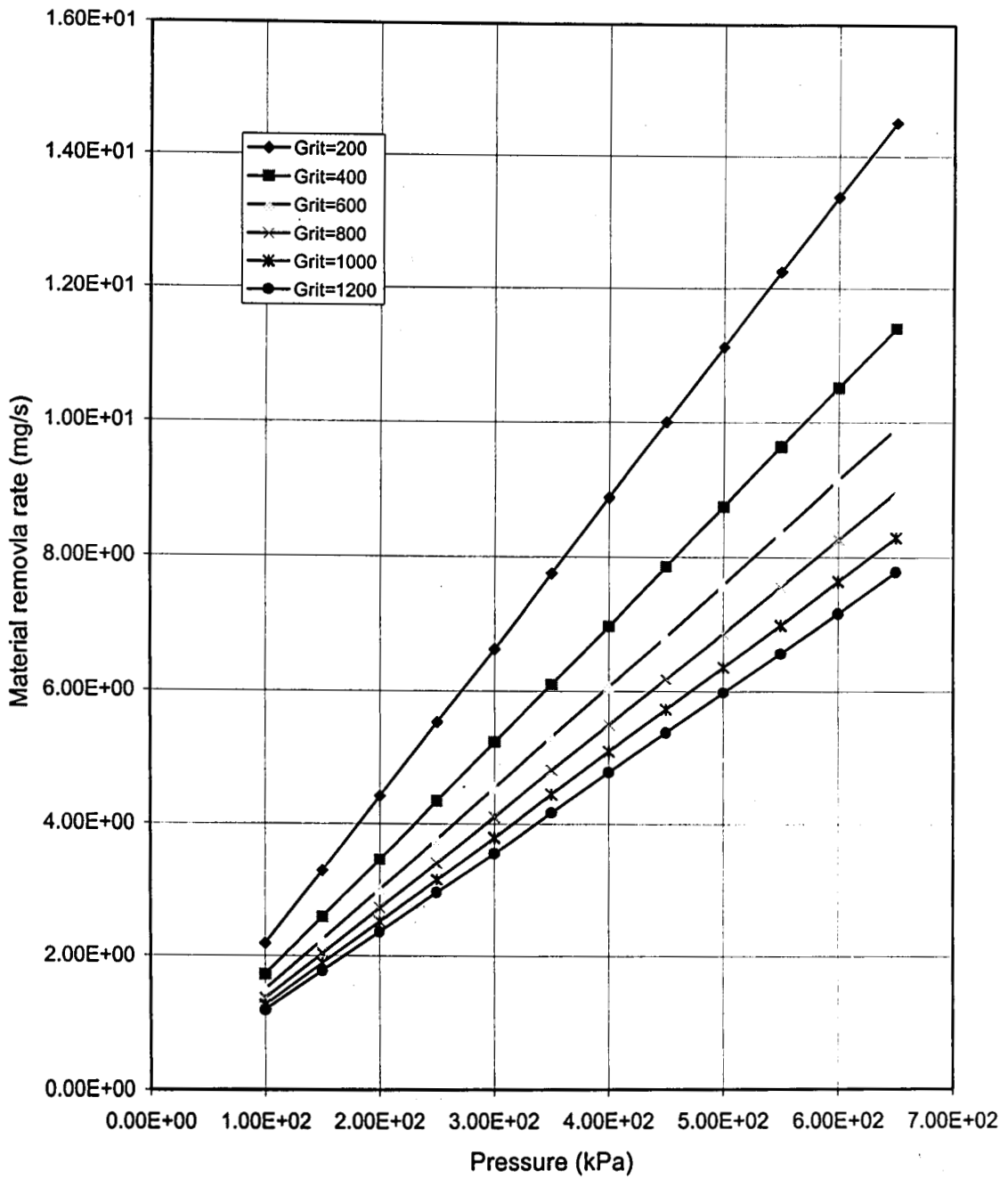


Figure 5.34 Variation of material removal rate with pressure (from experiments) (stand off distance=20mm, mixing ratio=0.10, diameter of nozzle=1.5mm)

with pressure found in these curves is in agreement with published results of other investigators (References [8] and [9]) and the theoretical predictions made earlier in this thesis. In all these, the material removal rate varies almost linearly with pressure.

The variation of material removal rate with nozzle diameter is given in Figures 5.35, 5.36, 5.37, and 5.38. Figure 5.35 has the stand off distance as the changing parameter, with pressure = 300kPa, mixing ratio = 0.1 and grit size = 800. In figure 5.36, mixing ratio is the changing parameter with pressure = 300kPa, Stand off distance = 20mm and grit size = 800. Figure 5.37 is drawn for different values of the pressure, at a stand off distance of 20mm, mixing ratio = 0.1 and grit size = 800. Figure 5.38 has these curves drawn for abrasive grit sizes 200, 400, 600, 800, 1000, and 1200. The values of the other parameters are pressure = 300kPa, stand off distance = 20mm and mixing ratio = 0.1.

It is seen from these experimental curves (Figures 5.35 to 5.38) that, the material removal rate increases with diameter of nozzle. Theoretically it is possible to operate nozzles with very large exit areas and use such devices for AJM applications. However, if the expansion takes place from the (supply) pipe area (corresponding to 25.4mm diameter) to the area of the nozzle, practical considerations will limit the largest nozzle that can be used. Early researchers employed nozzles of diameter of the order of tenths of millimeters. The material removal rate reported by them was very small. In the present experiments, the author used nozzles as big as 2.75 mm in diameter and was successful in obtaining considerably high machining rates with them. Thus it can be safely concluded that, so long as the diameter of the hole to be drilled or the width of the cut are unimportant, large nozzles are to be recommended. Then the machining can be performed

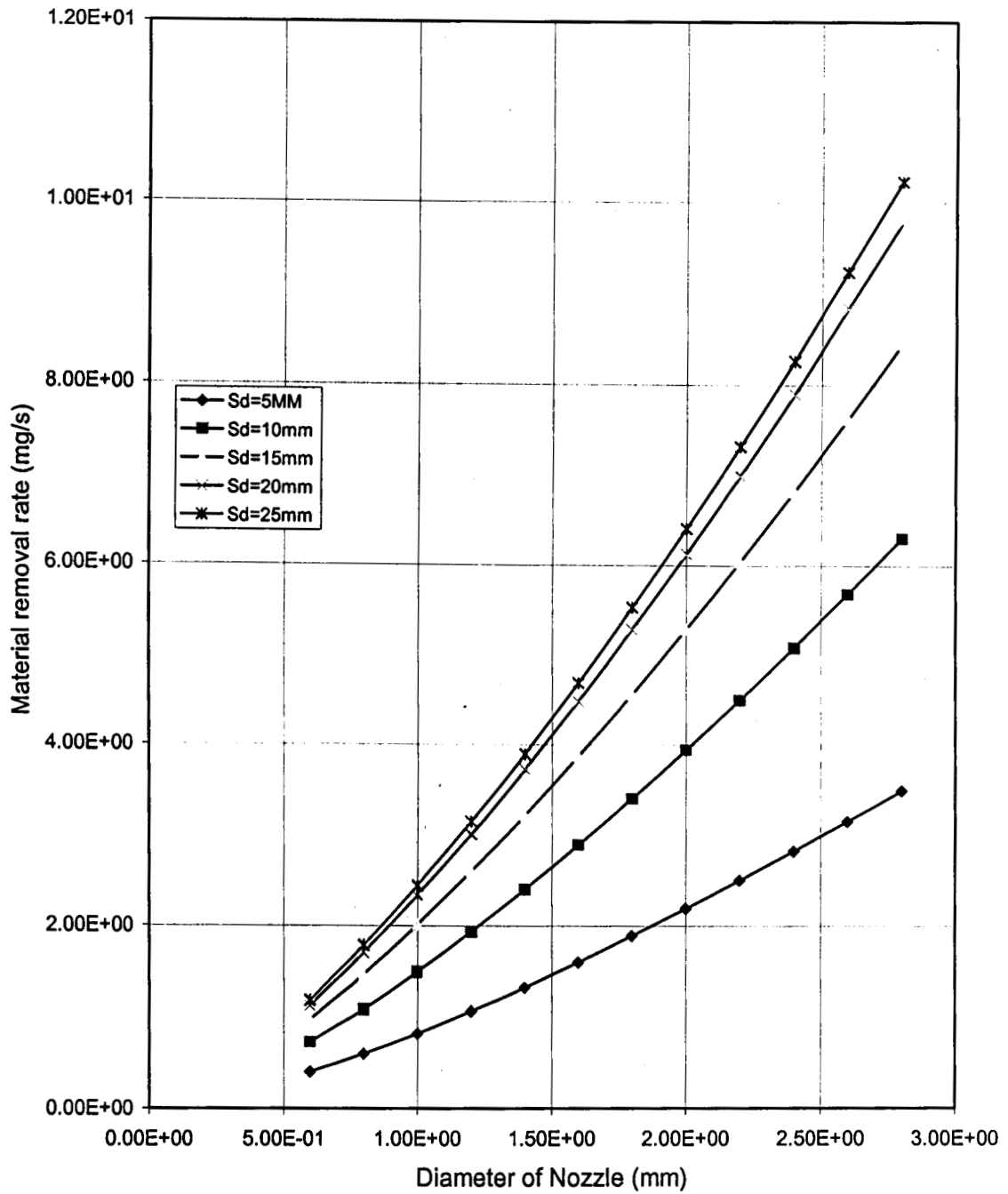


Figure 5.35 Variation of material removal rate with diameter of nozzle (from experiments)(pressure=300kPa, mixing ratio=0.1, grit Size=800)

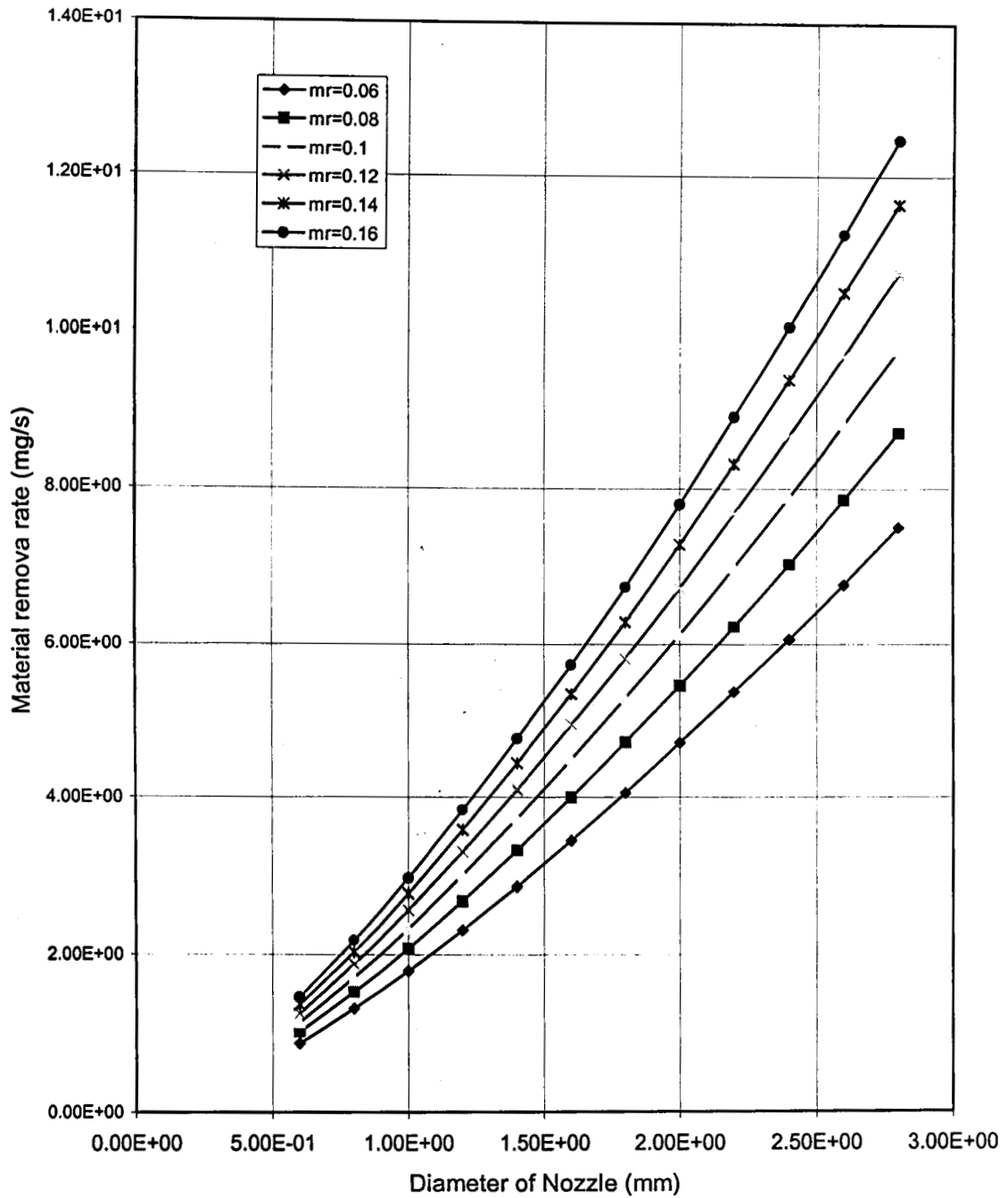


Figure 5.36 Variation of material removal rate with diameter of nozzle (from experiments)
 (pressure =300kPa, stand off distance = 20mm, gritsize = 800)

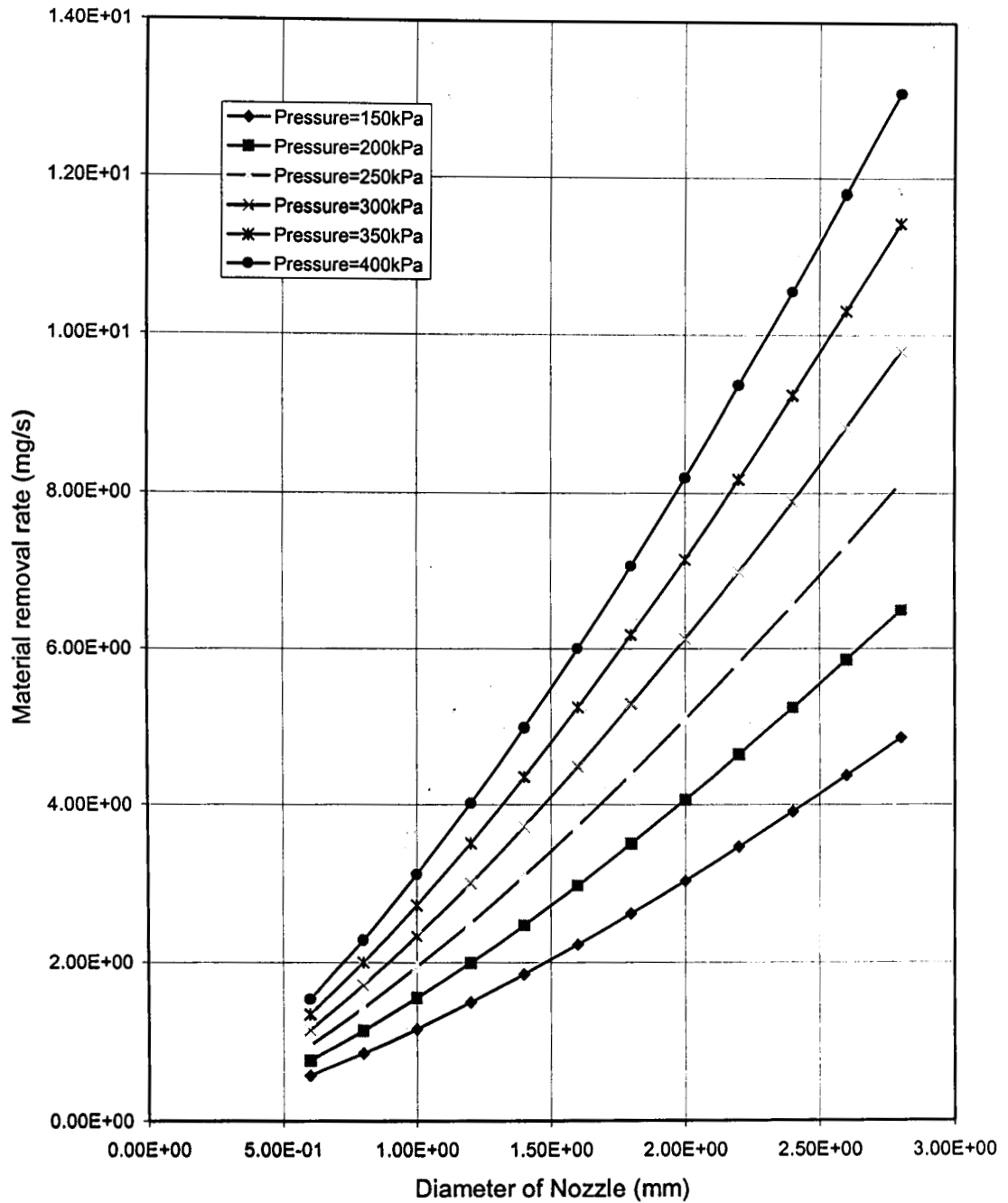


Figure 5.37 Variation of material removal rate with diameter of nozzle (from experiments)
 (stand off distance = 20mm, mixing ratio = 0.1, grit Size = 800)

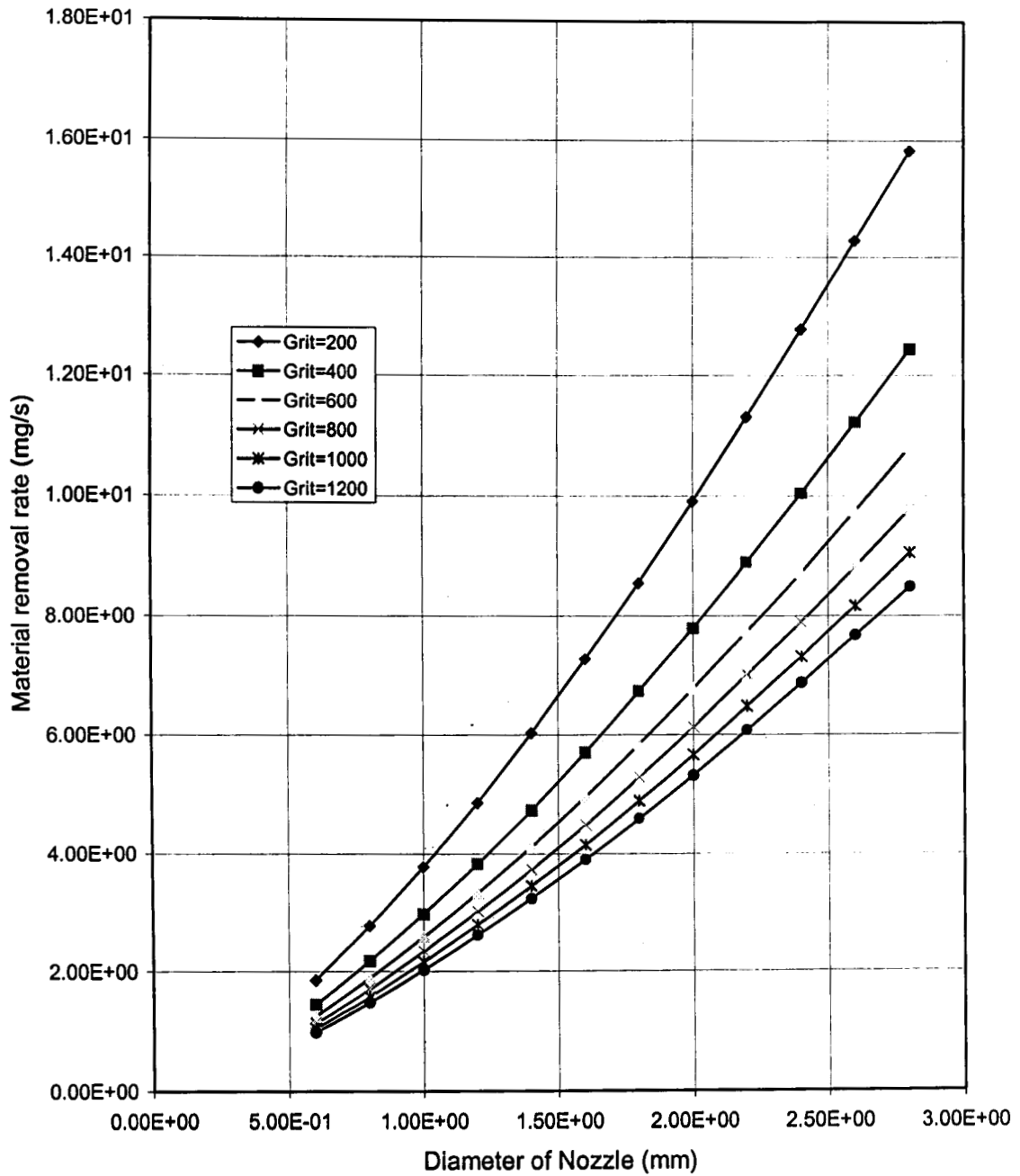


Figure 5.38 Variation of material removal rate with diameter of nozzle (from experiments)
 (stand off distance = 20mm, mixing ratio = 0.1, pressure = 300kPa)

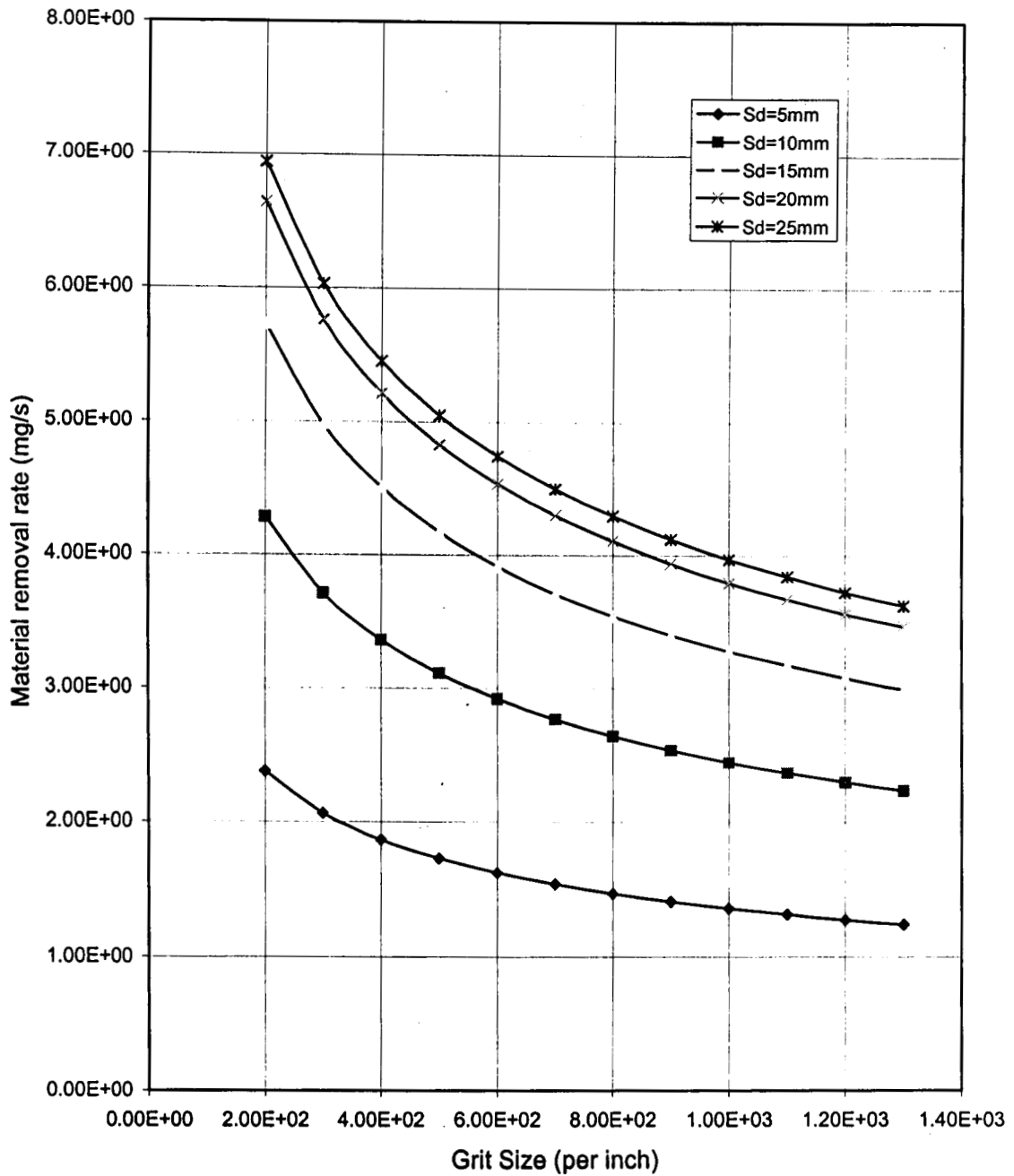


Figure 5.39 Variation of material removal rate with grit size (from experiments)
 (pressure = 300kPa, mixing ratio = 0.1, diameter of nozzle = 1.5mm)

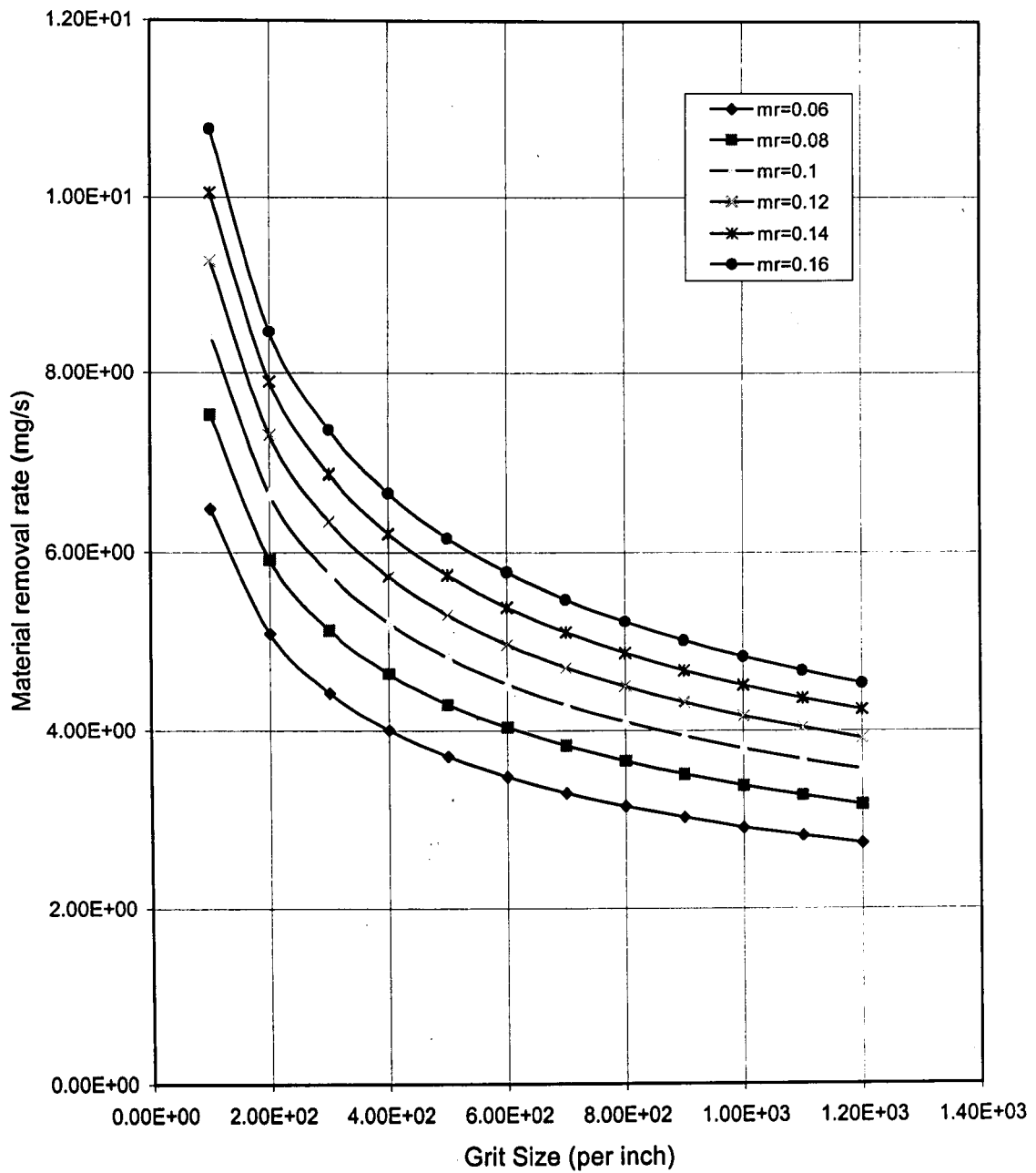


Figure 5.40 Variation of material removal rate with grit size (from experiments)
 (stand off distance = 20mm, pressure =300 kPa, diameter of nozzle = 1.5mm)

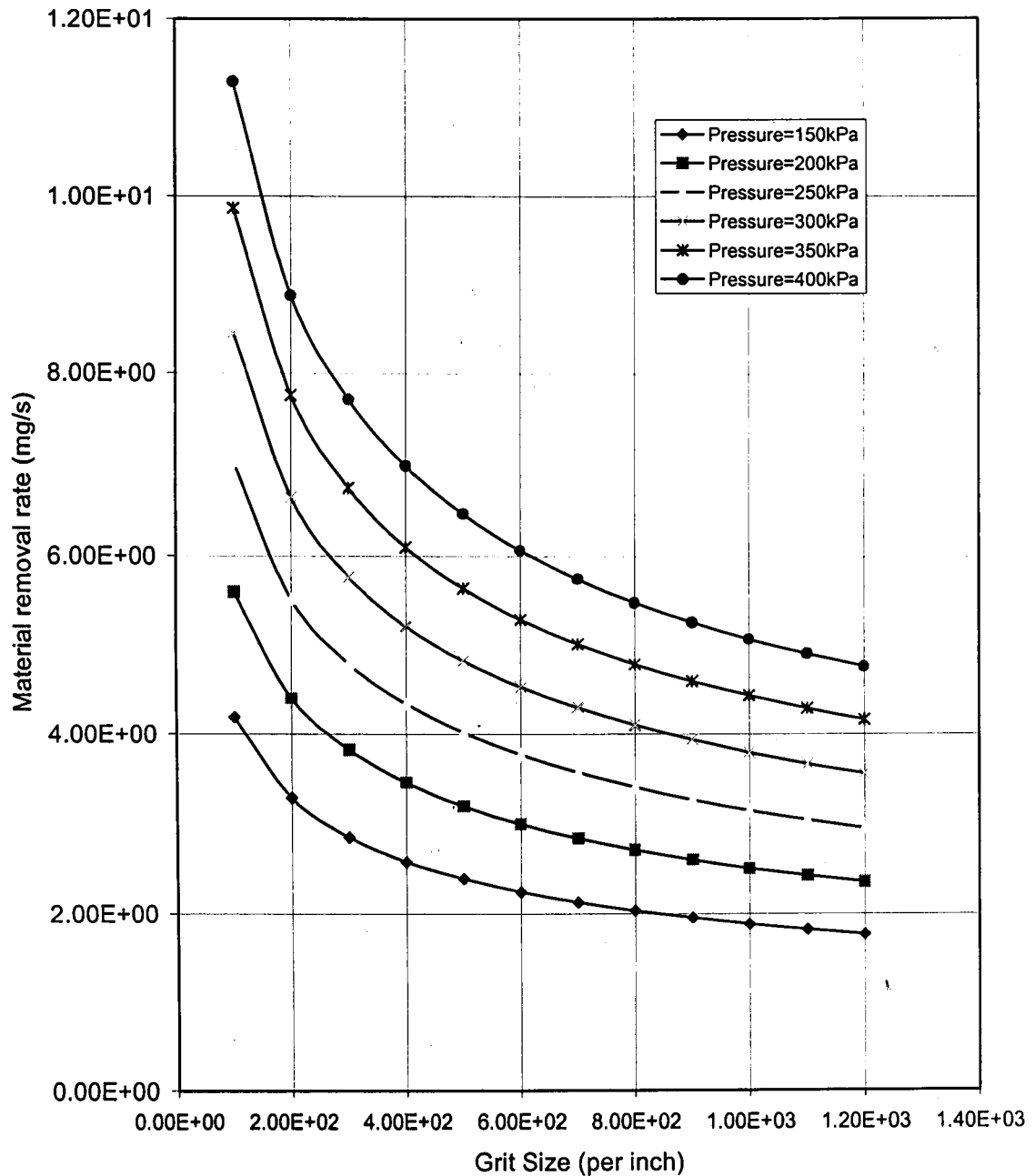


Figure 5.41 Variation of material removal rate with grit size (from experiments)(stand off distance = 20mm, mixing ratio = 0.1, diameter of nozzle = 1.5mm)

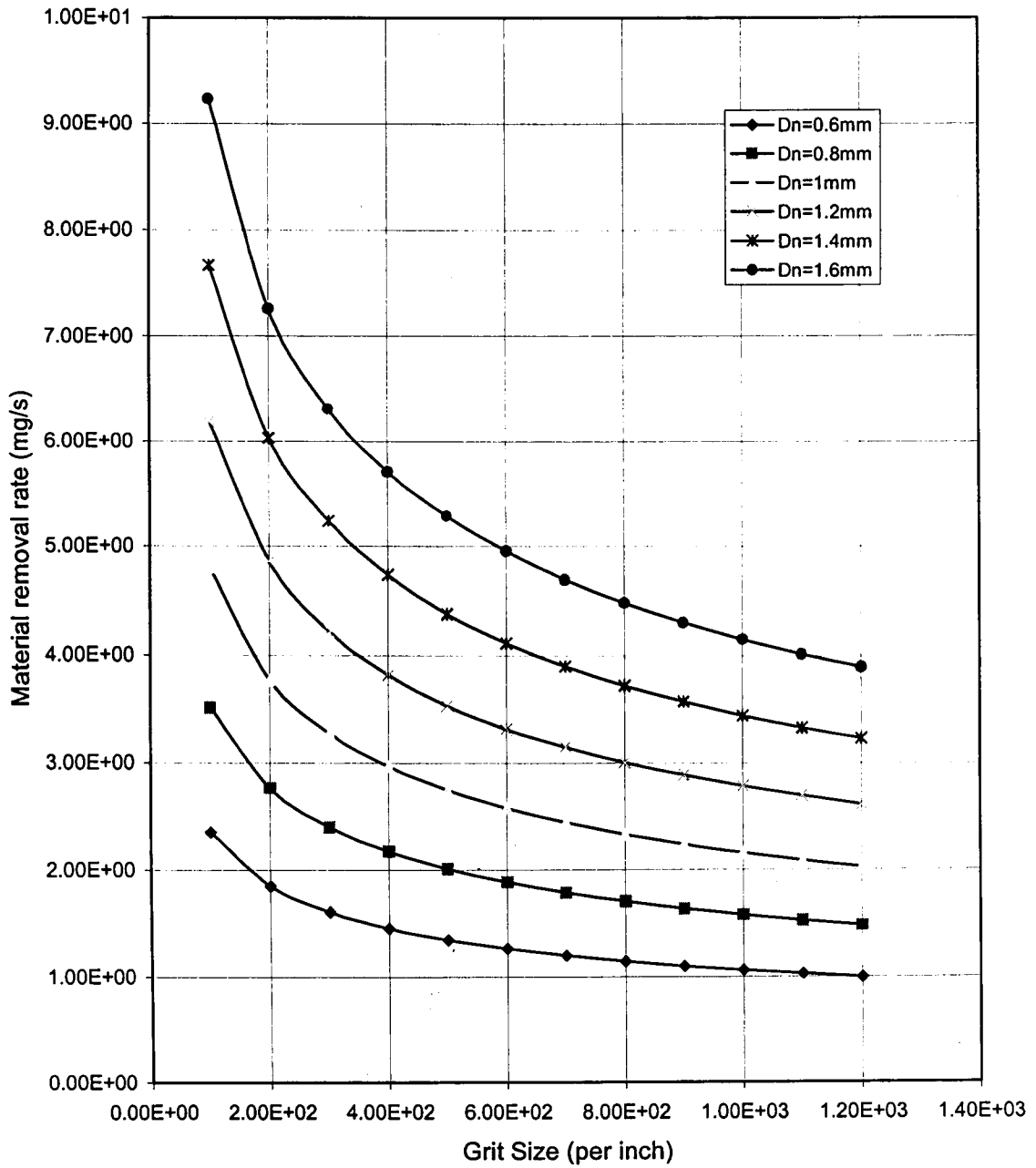


Figure 5.42 Variation of material removal rate with grit size (from experiments) (stand off distance = 20mm, pressure = 300kPa, mixing ratio = 0.1)

at satisfactory rates even at moderate pressures. The practical limitations are the large air - abrasive flow rate, resulting in the wastage of too much of the abrasive powder.

The variation of material removal rate with grit size is shown in figure 5.39, 5.40, 5.41 and 5.42. In figure 5.39 the curves are drawn for different values of stand off distance when the pressure is kept at 300kPa, the mixing ratio at 0.1 and the nozzle diameter at 1.5mm. The next set of curves (Figure 5.40) is plotted for various values of mixing ratio with a stand off distance = 20mm, pressure = 330kPa and diameter of nozzle = 1.5mm. Figure 5.41 is drawn for different values of pressure, at a constant value of stand off distance (20mm), mixing ratio (0.1) and grit size (800). Figure 5.42 shows the variation of material removal rate with grit size for constant values of stand off distance (20mm), mixing ratio (0.1) and pressure (300kPa). It is seen in these cases that the machining rate increases with the size of the particle (inversely proportional to the grit size). However, this variation of material removal rate with particle size, does not agree with theoretically predicted variations as given in Figure 5.18. The probable reasons to which this observation could be attributed to were given in section 5.2 of this chapter.

Considering only three parameters in their experimental study, Rani and Seshan [69] found the following best fit for the material removal rate. The parameters included in their study were, the pressure p , the mixture flow rate m and nozzle stand off distance sd . The equations obtained by them are

$$mrr = 97.75 + 53.99p + 68.46m + 51.43sd + 39.23p \cdot m + 30.29p \cdot sd + 41.89m \cdot sd + 23.13p \cdot m \cdot sd \quad \text{for } 0 \leq sd \leq 35 \quad \text{and}$$

$$mrr = 138.16 + 60.65p + 105.22m - 11.02sd + 44.8p \cdot m - 23.63p \cdot sd - 51.13m \cdot sd - 17.55p \cdot sd \cdot m \quad \text{for } 35 \leq sd \leq 70$$

(5.3)

In this equation the * denotes non-dimensional variables. The predicted optimum stand off distance is 35 mm. The above equation takes the inter-relationship between the parameters into account. However, the correlation is a linear fit which does not take into account the mechanics of the problem. The optimum stand off distance also is arbitrarily fixed. The results of Rani and Seshan are reproduced in figure 5.43 and 5.44 for the purpose of comparison with the experimental results presented by the author.

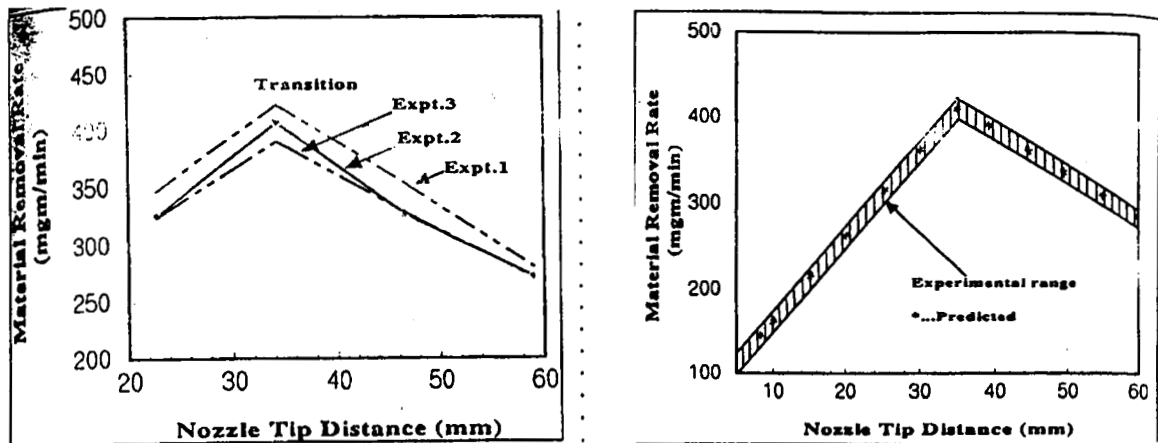


Figure 5.43 Variation of Material removal rate with Stand off Distance

(Results of Experiments by Rani and Seshan [69])

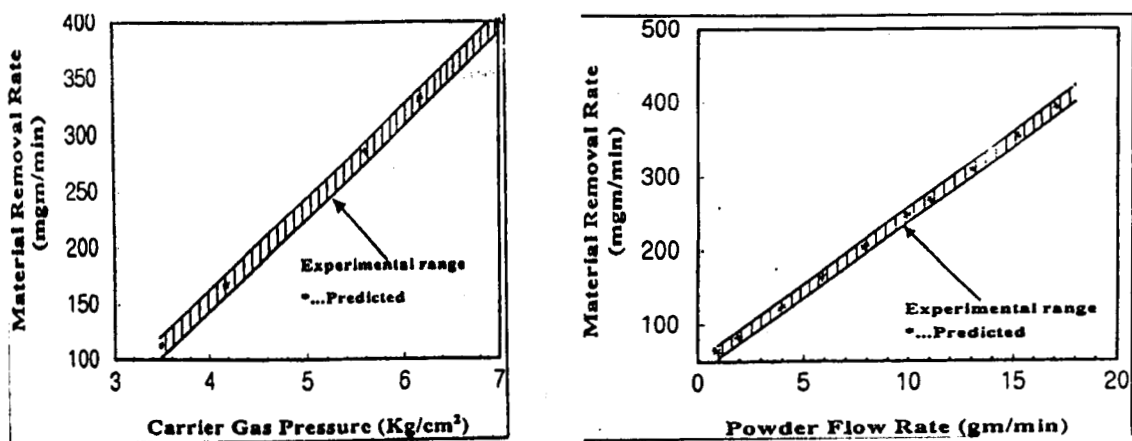


Figure 5.44 Variation of material removal rate with carrier gas pressure and

powder flow rate (Results of experiments by Rani and Seshan[69])

From the results indicated above, Rani and Seshan conclude that the effect of powder flow rate on material removal rate is more significant than the other parameters and that there exists relationship among the parameters. The experimental results presented by the author do not agree with all their conclusions. While it is certain that some of the parameters of the process are inter dependant, the effect of stand off distance and the pressure on material removal rate is found to be more significant than the flow rate of the abrasives, as is evident from the powers of these parameters in the empirical relation arrived at in this thesis. The experimental data does indicate the dependence of the material removal rate on these parameters of the process. During the experiments, at some of the operating conditions, the orange yellow glow reported by Venkatesh et.al. [11] was observed. This was found at small stand off distances and for 400 grit and 200 grit (for comparatively bigger particles).

5.3.3 Surface Studies

The flat surfaces generated by the machining process have been tested to study the topological aspects of the surface. Several samples are machined for the purpose of determination of the surface roughness parameters, namely CLA and RMS values. To generate plane surfaces while machining on an AJM set up, the work piece is fed past the nozzle tip at a steady speed. In the experimental set up this is achieved by mounting the work holding device on the cross slide of a lathe built into the set up. The surface roughness of the glass slides machined is measured on the SURFTEST SJ 301 surface tester supplied by MITUTOYO. The software SURFPAK supplied by Mitutoyo is used

to analyze the measurement data in the form of primary profile, roughness profile, autocorrelation plot and amplitude distribution plots. The software also gives the values of the necessary parameters of the measurement.

To study the dependence of the roughness on the stand off distance, pressure and particle size, a set of 30 random combinations of the three parameters are selected. Pieces are machined at these combinations. A nozzle of 0.1m length and 1.5mm exit diameter is used for the purpose. A view of the nozzle and slides (after machining) are shown in Figure 5.45

The data obtained for the 30 samples are as shown in Table 5.5 below:

No.	Pressure in kPa	Grit Size	Stand off distance mm	Ra(CLA) μm	Rq(RMS) μm
1	100	200	12	4.133	5.164
2	600	200	12	4.81	5.86
3	700	400	12	5.125	6.287
4	600	400	12	3.668	4.478
5	100	1000	12	2.931	3.642
6	300	1000	12	2.768	3.484
7	700	1000	12	3.87	4.703
8	500	200	16	4.648	5.8
9	700	200	16	4.75	5.9
10	600	400	16	5.4	6.5
11	200	800	16	3.063	3.873
12	400	1000	16	4.04	4.9
13	600	1000	16	3.428	4.227

14	100	200	20	4.183	5.027
15	700	200	20	5.786	7.065
16	500	400	20	6.861	8.095
17	400	600	20	4.761	5.816
18	200	800	20	2.39	3.029
19	400	8000	20	3.034	3.78
20	500	1000	20	3.013	3.722
21	300	200	24	3.857	4.845
22	200	400	24	4.238	5.233
23	300	400	24	5.363	6.476
24	400	400	24	4.039	4.933
25	400	1000	24	3.32	3.9
26	600	1000	24	4.641	5.675
27	200	1200	24	3.275	4.035
28	500	200	28	5.537	6.753
29	200	600	28	3.057	3.88
30	600	1000	28	3.293	4.342

Table 5.5 Data obtained from the measurements on SUFTEST SJ 301

A sample of the output provided by the surface tester is given in Figure 5.46. This is in the form of numerical data. Figure 5.47 is the graphical output. It is seen from the autocorrelation plot that, the surface generated is neither ergodic nor stationary. (This means that the machining process does have some periodic component in it and the roughness as measured from the samples may not represent the average of the ensemble.

The power spectrum indicates the frequency/frequencies of these periodic component/components in the form of spikes at these frequencies.)

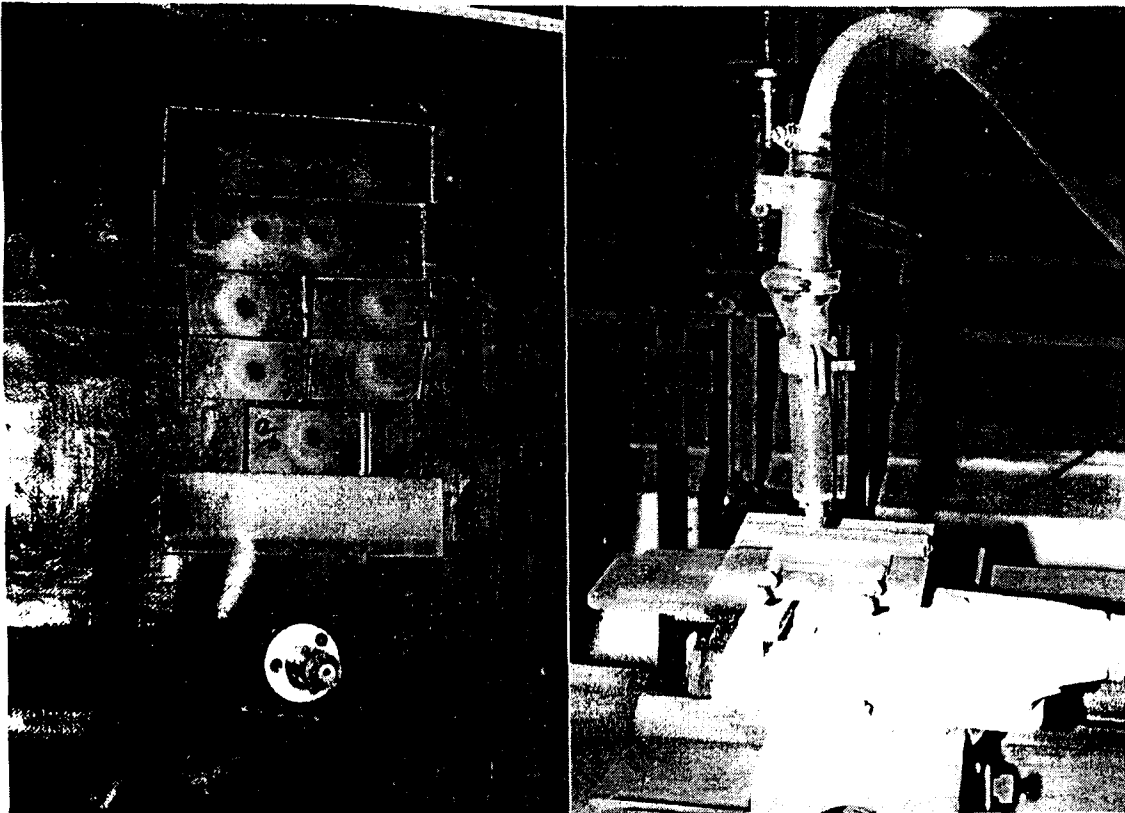


Figure 5.45 close up view of nozzle and some glass slides after machining

The data in Table 5.5 are assumed to be related to the three parameters by a power law. The best fit so obtained is:

$$Ra = 1.5162p^{0.1646}Sd^{-0.0295}GritSize^{0.0522} \quad (5.4)$$

$$Rq = 1.9025p^{0.162}Sd^{-0.0374}GritSize^{0.0624} \quad (5.5)$$

These equations are presented in the form of plots of Ra and Rq values against pressure, grit size and stand off distance in figures 5.48, 5.49 and 5.50. In figure 5.48 the grit size is 800 and the stand off distance is 20mm.

Measurement Condition

Measurement Length	4.8 mm	Range	AUTO
Speed	0.5 mm/s	Over Range	Abort
Pitch	0.5 um	Number of Points:	9600
Machine	SJ-300	Measurement Axis	Drive Unit(SJ-300)
Detector	for SJ-300	Stylus	for SJ-300
Polar Reversal	Off	Auto-Notch(+)	Off
Auto-Notch(-)	Off	Compensation Method	Off

Evaluate Condition List<<Profile=R_ISO - Section=[1]>>

Kind of Profile:	R_ISO
Smpig Length(1e):	0.8 mm
No of Smpig(n1e):	5
Ls	0.0025 mm
Lc	0.8 mm
Kind of Filter:	Gaussian
Evltn Length(1m):	4.0 mm
Pre-Travel:	0.4 mm
Post-Travel:	0.4 mm
Smooth Connection	Off

Parameter Calculation Result<<Profile=R_ISO - Section=[1]>>

Parameter	Result	Parameter	Result
Ra	2.742um	Ramax	2.883um
Rq	3.438um	Rqmax	3.689um
Rsk	-0.195	Rskmax	0.738
Rku	2.911	Rkumax	3.821
Rp	6.928um	Rpmax	8.113um
Rv	9.040um	Rvmax	10.581um
Rz	15.968um	Rzmax	17.556um
Rt	18.695um	Rc	9.598um
Rcmax	12.049um	RSm	0.158mm
RSmmax	0.214mm	Rdq	0.348
Rdqmax	0.367	Rk	8.779um
Rpk	2.303um	Rvk	4.216um
Mrl	10.708%	Mr2	90.225%

Figure 5.46 Typical Numerical output of SURFTEST SJ301

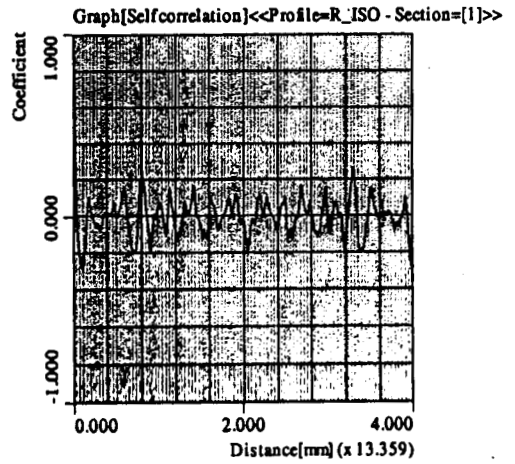
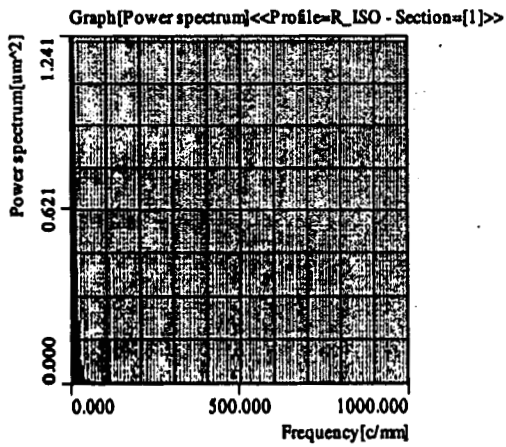
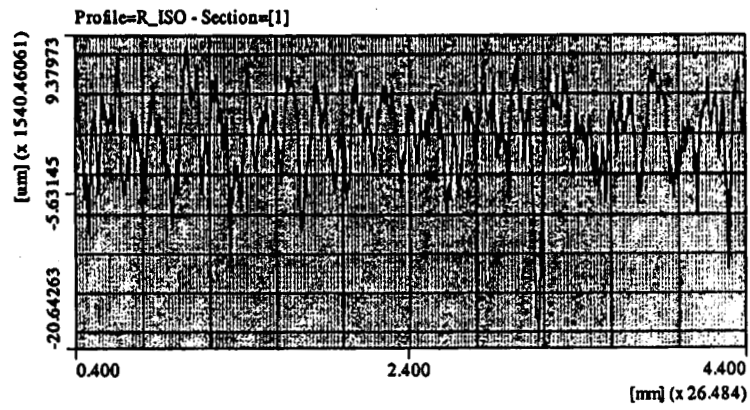
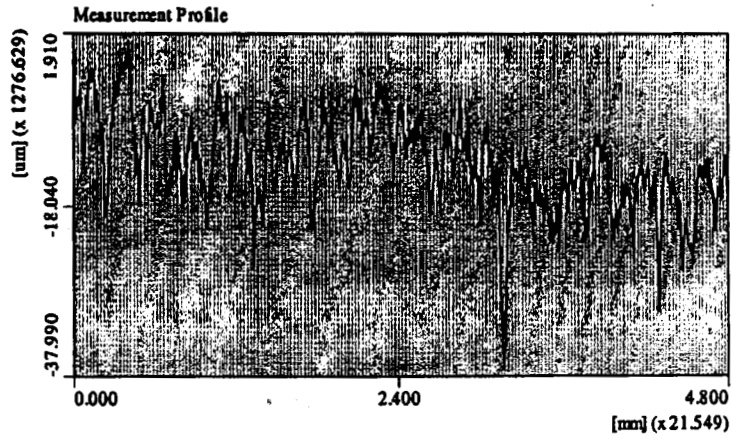
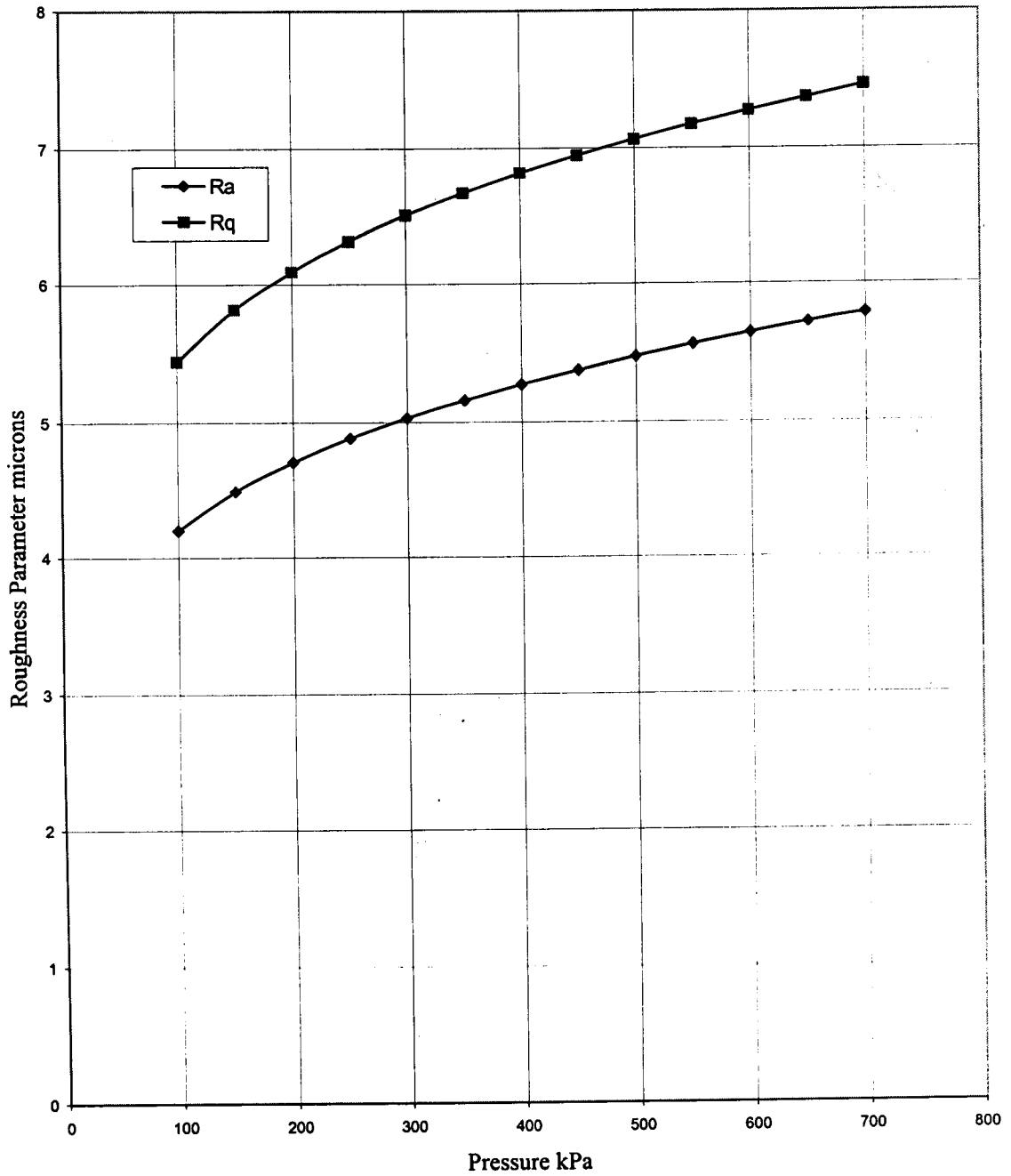
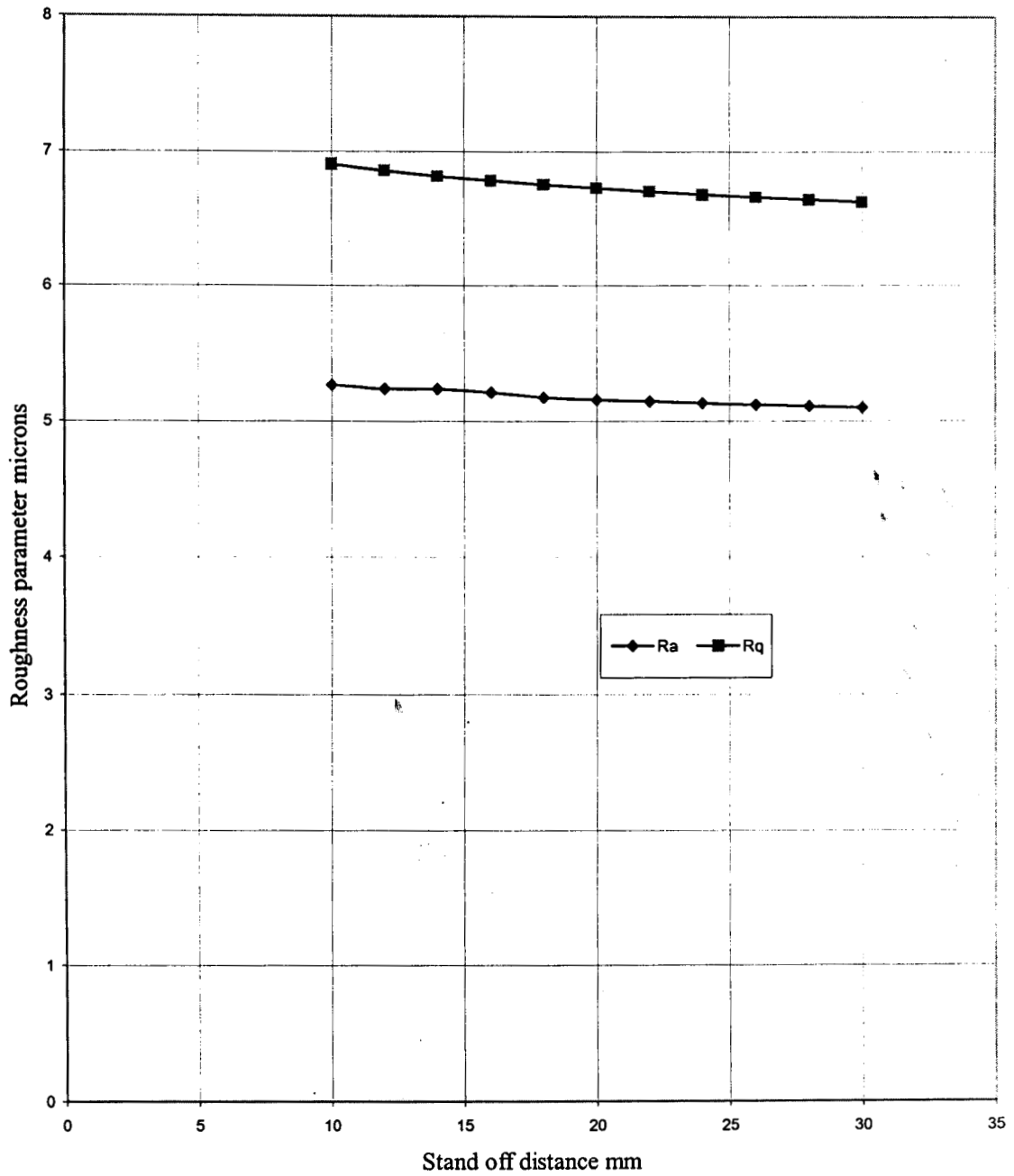


Figure 5.47 Typical Graphical output of SURFTEST SJ301



**Figure 5.48 Variation of roughness parameters with pressure
(Stand off distance 20 mm, grit size 800)**



**Figure 5.49 Variation of roughness parameters with stand off distance
(Pressure 350 kPa, grit size 800)**

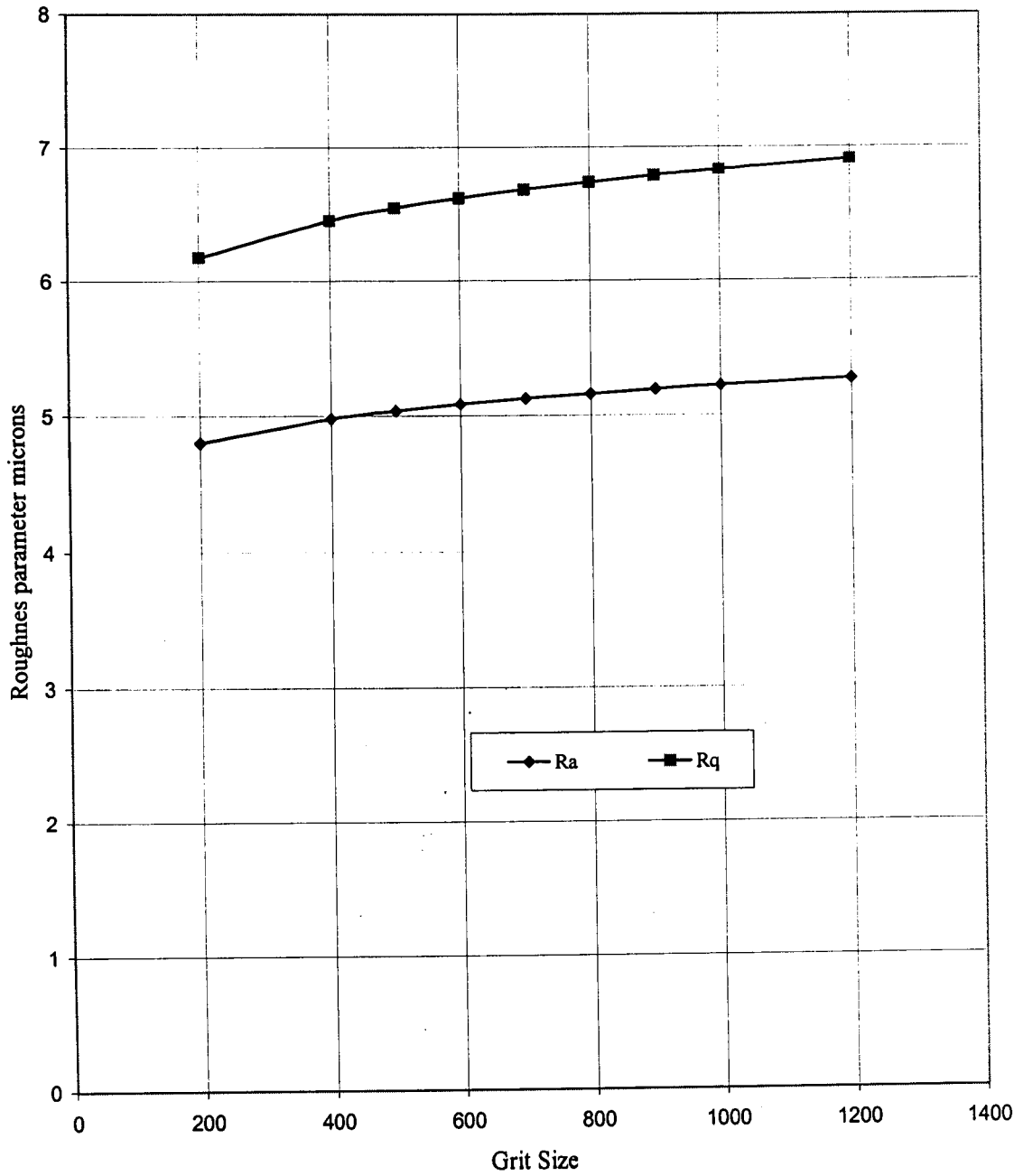


**Figure 5.50 Variation of roughness parameters with grit size
(Pressure 350 kPa, stand off distance 20mm)**

In Figure 5.49, the pressure is 350kPa and the grit size is 800. In figure 5.50 the pressure is 350kPa and the stand off distance is 20mm. It is observed from these plots that, the effect of stand off distance and grit size on the roughness is not significant. However the roughness is seen to increase with pressure.

Another set of measurements on a few specimens is carried out to study whether the feed given during the machining of a flat surface affects the surface roughness. During the specimen preparation, the pressure is set at 250 kPa and the average mixing ratio is found to be 0.3. All the samples were machined at the same stand off distance of 20 mm. During the specimen preparation, after each cut, the feed is given to the work piece. This is the only varying parameter, which is different from specimen to specimen. The measurements of R_a and R_q on five different locations on each of the sample are taken. The data obtained as the output of the SURFPAK is given in Table 5.6. The spread of these values are shown in Figure 5.51 while the averages of these five R_a and R_q values and their trends are plotted in Figure 5.52. These plots show a definite trend that the roughness is smaller at large feeds. This could be due to the fact that, at larger feeds, the number of particles causing further damage to an already damaged surface becomes smaller. Thus from a surface finish point of view, a large feed is desirable. However, to get a more or less uniform depth of cut, small feeds are desirable.

The surface studies undertaken in this investigation indicate that the periodic factor in the machining process has a frequency in the range between 10-20 Hz. The most probable source of this could be the vibration given to the mixing chamber. The mixing chamber is vibrated by an electromagnetic vibrator, which is excited by the signals from an amplifier. The signals generated are not necessarily random.

Pressure 250 kPa, Stand off distance 20 mm, Abrasive: Aluminium oxide of Grit 800							
Feed		Ra	Rq	Feed		Ra	Rq
0.5 mm	1	3.059	3.832	1 mm	1	3.151	4.018
	2	3.542	4.395		2	2.709	3.395
	3	3.630	4.503		3	3.135	3.989
	4	3.307	4.046		4	3.372	4.149
	5	3.874	4.686		5	3.113	3.844
Feed		Ra	Rq	Feed		Ra	Rq
2mm	1	2.742	3.438	2.5 mm	1	2.702	3.328
	2	2.681	3.37		2	2.939	3.593
	3	2.828	3.554		3	2.881	3.583
	4	2.736	3.390		4	2.807	3.517
	5	2.554	3.109		5	3.15	3.885
Feed		Ra	Rq				
5mm	1	2.248	2.743				
	2	2.385	3.026				
	3	2.385	2.918				
	4	2.660	3.365				
	5	2.93	3.74				

Table 5.6 Roughness data obtained for different feeds.

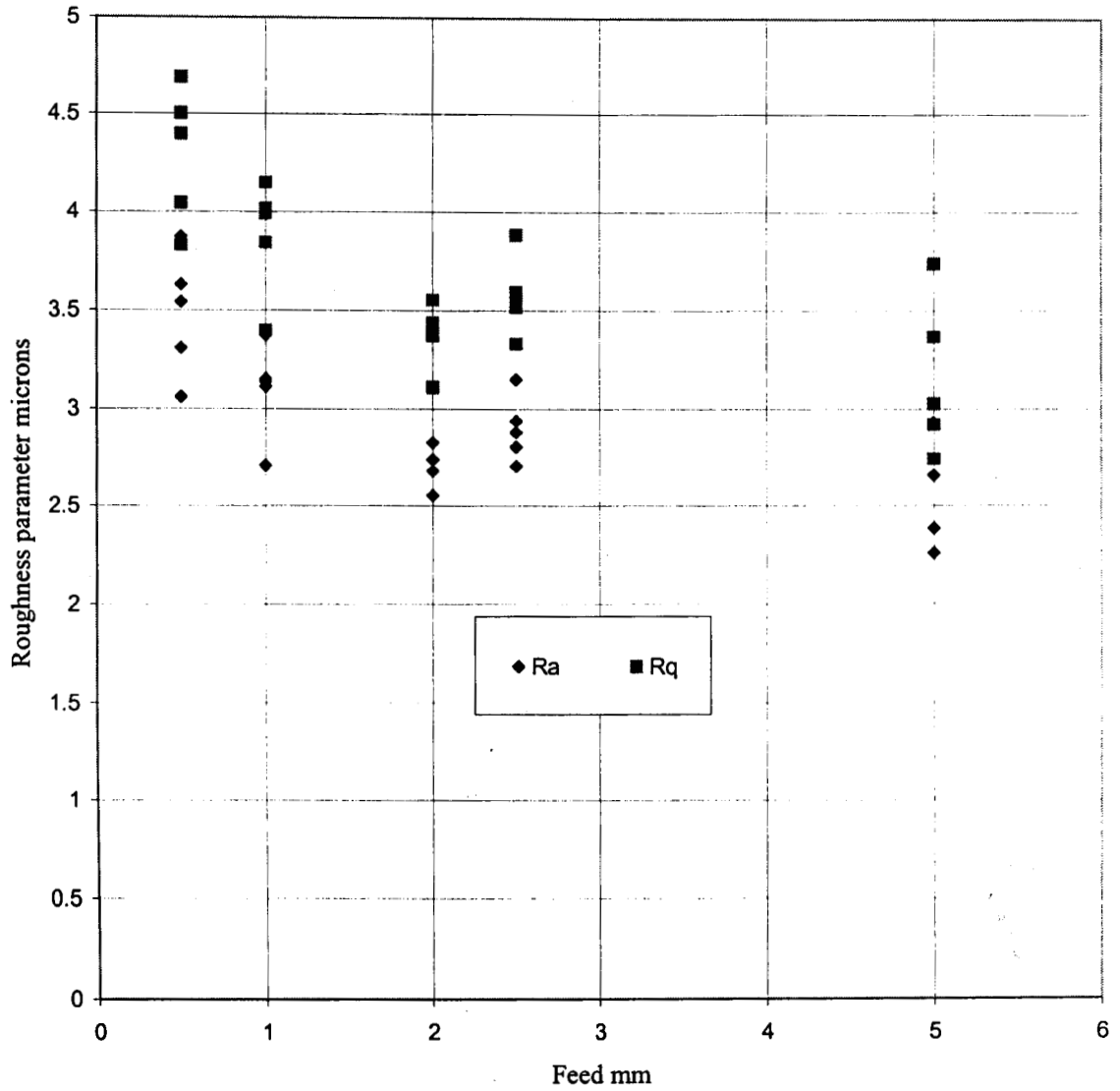


Figure 5.51 Scatter of Roughness parameters
 (Pressure 250 kPa, mixing ratio 0.3, stand off distance 20mm and grit size 400)

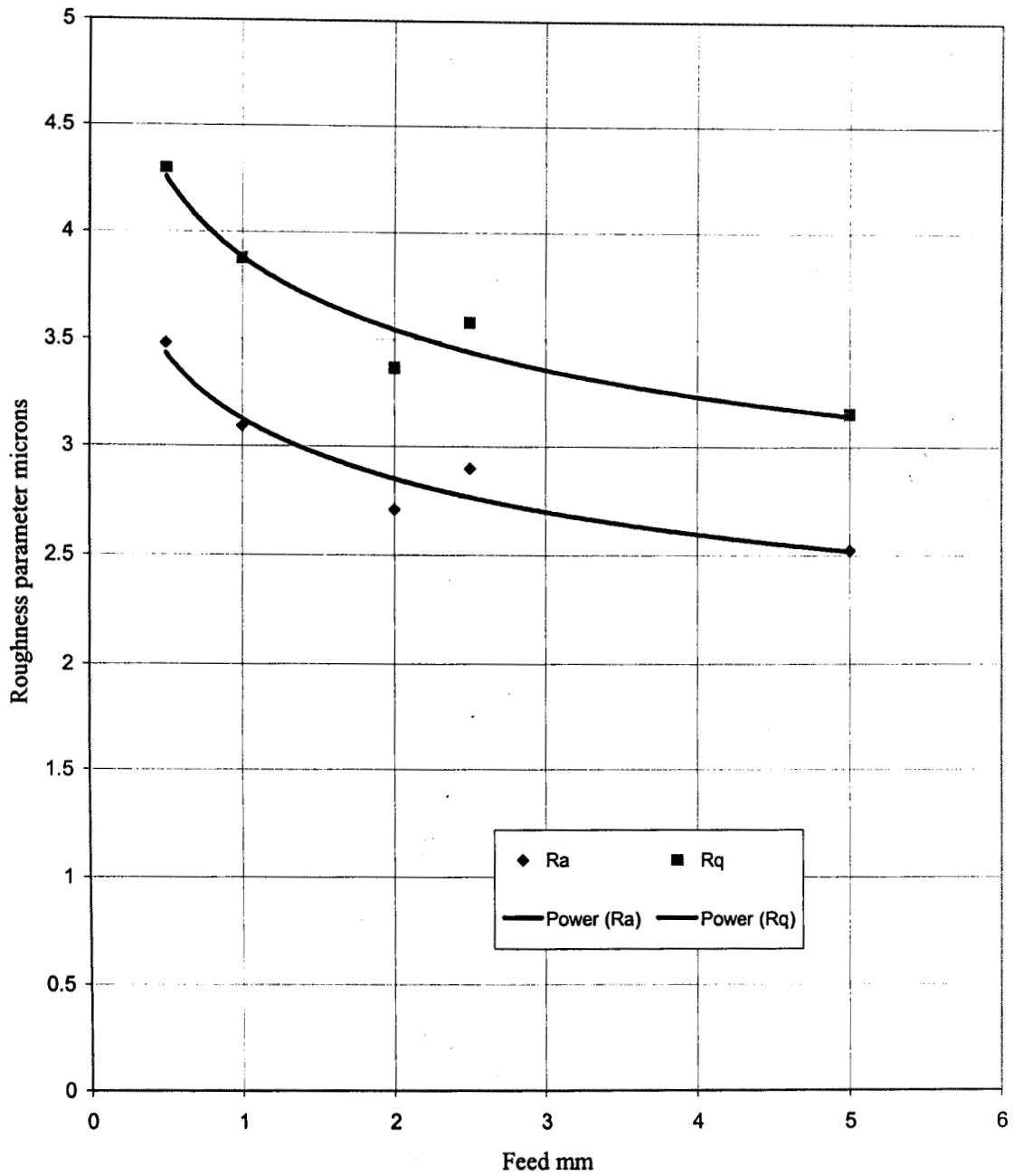


Figure 5.52 Variation of average roughness with feed
 (Pressure 250 kPa, stand off distance 20mm, grit size 800 and mixing ratio 0.3)

Owing to such a vibration, it is also possible that abrasive powder is not distributed with equal probability across a section. Further, the particles can agglomerate and disintegrate in a periodic fashion. This sort of a phenomenon is observed in turbulent flow of a fluid. Since the carrier gas is in a state of turbulent flow, the particles themselves will have turbulent fluctuations in velocity. When this agglomeration takes place with bias to particle size and space in the system, it tends to bring in an amount of deterministic effect in the machining.

Chapter 6

CONCLUSION

6.0 General

Starting from basic principles, an analytical approach to the mechanics of material removal in Abrasive Jet Machining is proposed in this thesis. The proposed theory is applied in the context of machining brittle materials like glass and ceramics. Using this theory, prediction of the material removal rate has been attempted. The results of these analytical predictions have been found to be in reasonable agreement with the experimental results arrived at by experimentation by the author, the standard deviation being 0.36 mg/s. The results also agree qualitatively with the results published earlier. The reasons for the theoretically predicted material removal rate to be more than the experimental results have been attributed to the non inclusion of inter-particle collisions and the variations of machining rate during drilling of holes. Since SED_{cr} is a material property for which no experimental procedure for its determination is yet available, it is suggested that the AJM process be used as a method for finding the SED_{cr} of brittle materials.

Transfer of energy from the particles to the medium causes removal of the material. This means that the material properties of the abrasive particles, like hardness, do not play any role in the mechanism of material removal. Therefore, theoretically, it is possible to machine harder materials using comparatively softer materials. During the experiments, this concept was put to test by attempting to machine brick by talcum powder. This has been found successful. However, the machining did not take place

when the work material was glass. The likely difference between the two situations is that, on impact with glass the particles in the powder breaks into fragments and is unable to cause micro cracks and material removal. But while using abrasive powder as a jet in AJM abrasive particles resist fragmentation before the material removal and hence it is able to cause micro cracks and thereby material removal.

6.1 Specific conclusions

The major conclusions that can be drawn from the results of this thesis can be summarized as follows:

- (i) An optimum stand off distance for AJM exists. This is found from theory to be within the range of 20-30 mm. The optimum stand off distance is more or less independent of the other parameters of the process.
- (ii) The material removal rate increases with increase in mixing ratio. This trend is unaffected by the other parameters.
- (iii) The material removal rate corresponding to the optimum stand off distance for the range of mixing ratios from 0.06 to 0.16 varies from about 2 to 6 mg/s.
- (iv) For the range of mixing ratios used in practice and investigated here, an optimum mixing ratio at which the material removal rate is a maximum does not exist.
- (v) The material removal rate increases almost linearly with the system pressure.
- (vi) The machining rate increases at a rate proportional to the area of the nozzle.
- (vii) Enhanced machining rates can be realized by the use of nozzles of diameter of the order of a few millimeters.

- (viii) An empirical relationship between the material removal rate and the process parameters is found. The relation is:

$$mrr = 1.2014(1 + sd - 0.02sd^2)^{1.1951} m_r^{0.5176} p^{1.0112} dn^{1.3929} G^{-0.3473}$$

In the relationship suggested, the inter-relationship among the parameters is not considered. Several other parameters of the process, like the frequency and amplitude of vibration of the mixing chamber are overlooked in the theory as well as in the experiments. The relationship predicts an optimum stand off distance of 25mm.

- (ix) The surface roughness shows an increasing trend as the pressure of the system is increased. There is no significant variation in the surface roughness as the grit size and stand off distance are changed.
- (x) The surface roughness decreases as the feed is increased.
- (xi) Many authors suggest the existence of a minimum velocity for machining to take place (Threshold velocity). Correspondingly there is a minimum pressure also below which machining is impossible (threshold pressure). These are true, so long as the mode of material removal is by plastic deformation and subsequent failure. However, the theory proposed in this thesis rejects this concept because failure for brittle materials takes place with little plastic deformation. The theory is used in the context of machining of brittle materials and the experiments are conducted only on glass. Thus, even for very small pressures, the particles do get some velocity and correspondingly a small volume of material is removed.
- (xii) The surface roughness (CLA) of the parts machined by the process is found to be in the range of 2 to 5 microns.

6.2 Suggestions for further research

One of the major assumptions of the theory is that each particle removes an equal volume of material so long as their velocities and radii are equal. There is no distinction between simultaneous impact and impacts succeeding one another. When particles impact a work surface on different locations, the fracture profiles at these sites are likely to overlap. The interplay of the stress field and subsequent cracks need further investigation. It is also possible to model the impact problem by converting the impact of particles (simultaneous and successive) into an average pressure over the contact zone. This requires statistical analysis of where each particle hits the target and how much its velocity is. Further modification of the model can be done by incorporating particle size distribution and introducing the probability of a particle of a specific diameter at any particular location of the jet.

The analysis of the flow can be made more rigorous by incorporating the following factors in the analysis.

- (1) The material properties and elasticity of the impacting abrasive particles can be incorporated in the analysis, thus bringing into picture the fragmentation of the abrasive particles.
- (2) The effect of inter-particle collision in the nozzle and in the free jet can be introduced in the analysis.

- (3) The flow near the target surface is affected by particles bouncing off the work material. In this thesis this effect is not considered. Further, the particles on impact might disintegrate. These effects also can be taken into account.
- (4) The main flow near the work surface is radially outwards. The full Navier-Stokes equations are to be solved in the vicinity of the plate for better results.
- (5) By introducing the complete histogram of particle size distribution, it is possible to modify the flow analysis.

The experimental set up used is conspicuous by the absence of sophisticated instruments for the measurement of the abrasive flow rate and airflow rate. The design of the mixing chamber, the mode of vibration of the chamber, the location of the abrasive hopper and the location of the nozzle are some of the aspects which need sophistication for a well designed experimental set up. Laser Doppler anemometry for the on line measurement of velocity of air and particles will help obtain better results. This in turn results in more refinement in the empirical correlation and the subsequent modification of the theory.

Another area in which experimental and theoretical studies are necessary is the relationship between the nozzle diameter and the radius of the hole drilled. During experiments, it was found that the holes are nearly conical in shape. The diameter of the hole is related to the diameter of the nozzle and the stand off distance. This is not attempted in this work. However, it is possible to arrive at such a relationship with the proposed theory.

REFERENCES

1. Anon, 'Abrasive Jet Machining', *ASTME Collected Papers*, Book 6, 1963.
2. Ingulli, C.N., 'Abrasive Jet Machining', *Tool and Manufacturing Engineers*, No. 5, vol. 59, 1967.
3. Lavoie, F.J., 'Abrasive Jet Machining', *Machine Design*, pp 135-139, Sept 1973.
4. Bhattacharya, A., 'New Technology', *Institution of Engineers (India)*, 1973.
5. Supra, I. L., 'Studies on Abrasive Jet Machining', ME dissertation, University of Roorkee, 1975.
6. Sakar, P.K., and Pandey, P.C., 'Some investigations on Abrasive Jet Machining', *Semi-annual meeting of the Mechanical Engineering Division, Institution of Engineers (India)*, 1975.
7. Pandey, P.C., and Neema, M.L., 'Erosion of glass when acted upon by an abrasive Jet', *Proceedings of the international Conference on Wear*, St. Louis, 1977.
8. Pandey, P.C., and Shan, H.S., 'Modern Machining processes', Tata Mc Graw Hill Co., 1980.
9. Verma, A.P., and Lal, G.K., 'An experimental study of Abrasive Jet Machining', *International Journal of Machine tool design Research*, vol. 24, No. 1, 1984.
10. Kumar, R., Verma, A.P., and Lal, G.K., 'Nozzle wear during the flow of a gas particle mixture', *Wear* 91, 1983.
11. Venkatesh, V.C., Goh, T.N., Wong, K. H., and Lin, M.J., 'Empirical study of parameters in Abrasive jet Machining', *Int. Journal of Machine tool Manufacture*, v 29, No.4, 1990.

12. Yankee, H.W., 'Manufacturing processes', Prentice Hall, N.J., 1921.
13. Ramachandran, N., and Ramakrishnan, S., 'A review of Abrasive Jet Machining', *Journal of Materials Processing Technology*, 39, Elsevier, 21-31, 1993.
14. Venkatesh, V.C., 'Parametric studies in Abrasive Jet Machining', *Annals of CIRP*, vol.33/1, 1984.
15. Hertz, H., 'Miscellaneous papers', Translated by Jones, P.E., and Schott, G.A., Mac Millen, New York, 1896.
16. Cherepanov, G.P., 'Mechanics of Brittle Fracture', Mc Graw Hill Book Co., 1979.
17. Finnie, I., 'Erosion of surfaces by solid particles', *Wear* 3, pp 87-103, 1960.
18. Finnie, I., and Kabil, Y. H., 'On the formation of surface ripples during erosion', *Wear*, 8, 1965
19. Finnie, I., 'Some Observations on the erosion of ductile materials', *Wear*, 19, 1972.
20. Finnie, I., and Mc Fadden, D.H., 'On the velocity dependence of the erosion of ductile materials by solid particles at low angles of incidence', *Wear*, 48, 1978.
21. Finnie, I., Stevick, G.R., and Ridgely, G.R., 'The influence of impingement angle on the erosion of ductile metals by angular abrasive particles', *Wear*, 152, 1992.
22. Tilly, G.P., 'A two stage mechanism of ductile erosion', *Wear* 23, 1973.
23. Tilly, G.P., and Sage W., 'The interaction of particles and material behavior in erosion process', *Wear* 16, 1970.

24. Sheldon, G.L., and Finnie, I., 'The mechanics of material removal in the erosive cutting of brittle materials', *Transactions of ASME, Journal of Engineering for Industry*, Nov. 66, p 393-400.
25. Lee, C.H., Masaki, S., and Shirokumayashi, 'Analysis of ball indentation', *Int. Jl. of Mech. Sciences*, 14,1972.
26. Evans, A.G., Golden, M.E., and Rosenblatt, M.E., 'Impact damage in brittle materials in the elastic plastic response regime', *Proceedings of the Royal Society of London, Ser. A*,1978.
27. Shaw, M.C., 'Ultrasonic grinding', *Microtechnic*, vol. 10, 1950.
28. Murthy, K.N., Roy, D.C., and Mishra, P.K., 'Material removal for brittle materials in Abrasive Jet machining', *12th AIMTDR conference*, I.I.T. New Delhi, 1986.
29. Ramachandran, N., 'Some investigations on Abrasive Jet Machining', *Ph.D. Thesis*, Department of Mechanical Engineering, I.I.T. Bombay, 1993.
30. Jain, P.K., Chitale, A.K., Nagar, N.K., 'Theoretical and experimental investigations for material removal rate in Abrasive Jet machining', *14th AIMTDR Conference*, I. I. T. Bombay 1990.
31. Bhoi, R.K., Mishra, P.K., 'Unsteady erosion in USM process', *14th AIMTDR conference*, I.I.T. Bombay 1990.
32. Engel Peter, A., 'Impact wear of materials', Elsevier publishing Co., 1976.
33. Nair, E. V., 'Mechanics of material removal in Ultrasonic machining and improvement of performance characteristics', *Ph.D. thesis*, Department of Mechanical Engineering, I. I. T. Kanpur, 1983.

34. Sih, G.C., 'Application of strain energy theory to fundamental fracture problems', *10th Annual meeting of the Society of Engineering Science*, Raleigh, NC, 1973.
35. Farber, L., 'The venturi as a meter for gas-solid mixtures', *Trans. ASME*, vol. 75, 1953.
36. Wallis, G.B., 'One dimensional two phase flow', Mc Graw Hill Book Co., New York, 1969.
37. Nelson, J.H., Gilchrist, A., 'An analytical and experimental investigation of the velocity of particles entrained by the gas flow in nozzles', *Journal of Fluid Mechanics*, vol. 33, 1968.
38. Sharma, M.P., Crowe, C.T., 'A computer mathematical model for gas-particle two phase flows', *Multiphase transport, fundamentals, reactor safety and applications*, vol. 4, Ed. **Veziroglu**, Hemisphere Publishing Co., Washington, 1980.
39. Crowe, C.T., 'Review-Numerical models for dilute gas particle flows', *Trans. Of ASME, Jl. Of Fluids Engg.*, vol. 104, 1982
40. Zuckrow, M.J., Hoffman, J.D., 'Gas dynamics', Vol. I & II, John Wiley and Sons, New York, 1977.
41. Arastoopour, H., Lin, S., Weil, S.A., 'Analysis of vertical pneumatic conveying of solids using multiphase flow models', *A.I.Ch.E Journal*, vol. 28, 1982.
42. Arastoopour, H., Lin, S., Weil, S.A., 'Particle particle interaction force in a dilute gas solid system', *Chem. Eng. Science*, vol. 37, 1982.
43. Doss, E.D., 'Analysis and application of Solid-Gas flow inside a venturi, with particle-particle interaction', *Int. Jl. Of Multiphase flow*, vol. 11, 1985.

44. Hatta, N., Ishii, R., Takuda, H., Ueda, K., Kokado, J., 'Analytical study on subsonic nozzle flows of gas particle mixture', *I.S.I.J. Intl.*, vol.28, 1988.
45. Hatta, N., Ishii, R., Takuda, H., Ueda, K., Kokado, J., 'Numerical study of Gas-particle flows in a de-Laval nozzle', *I. S. I. J. Intl.*, vol. 29, 1988.
46. Schlichting, H., 'Boundary layer theory', Mc Graw Hill Book Co. New York, 1979.
47. White, F.M., 'Viscous Fluid Flow', Mc Graw Hill Book Co., New York, 1991.
48. Al-Sanea, S., "A numerical study of the flow and heat transfer characteristics of an impinging laminar slot jet, including cross flow effects", *Int. Jl. Of Heat and Mass Transfer*, vol. 35, 1992.
49. Abramovich, G.N., 'The theory of turbulent jets', The MIT press, Cambridge, Mass. 1963.
50. Abramovich, G.N., 'Effect of solid particle or droplet on the structure of turbulent jets', *Int. Jl. Of Heat and Mass Transfer*, vol. 14, 1972.
51. Goldschmidt, V., Eskinazi, S., 'Two phase turbulent flow in a plane jet', *Trans. Of ASME, Jl of App. Mechanics*, vol. 88,1966.
52. Hetsroni, G., Sokolov, M., 'Distribution of mass velocity and intensity of turbulence in a two phase thin jet', *Trans ASME, Jl of App. Mech.*, vol. 38, 1971.
53. Danon, W. M., Hetsroni, G., 'Numerical calculation of a two phase turbulent round jet', *International Journal of Multiphase Flow*, vol. 3, 1977.
54. Laats, M.K., Frishman, F.A., 'Assumptions used in calculating the two-phase flow', *Transaction of the ASME, Jl. Of Basic Engineering*, vol. 92, 1970.

55. Elshorbagy, K.A., Mobbs, F.R., Cole, B.N., 'An investigation into the effect of particulate phase on the spreading of air- solid jets', *Multiphase transport, Fundamentals, Reactor safety and Applications*, Ed. Veziroglu, N.J., vol. 4, Hemisphere Publishing Co., Washington, 1980.
56. Hatta, N., Ishi, R., Takuda, H., Ueda, K., and Kokado, J., 'Numerical analysis of a gas-particle subsonic jet impinging on a flat plate', *ISIJ International*, vol. 31, 1991.
57. Kim, J.H., Aihara, T., 'A Numerical study of heat transfer due to an axisymmetric laminar impinging jet of supercritical carbon dioxide', *International Journal of Heat and Mass Transfer*, vol. 35, 1992.
58. Ozdemir, B.I., Whitelaw, J.H., 'impingement of an axisymmetric jet on unheated and heated flat plates', *Journal of Fluid Mechanics*, vol. 240, 1992.
59. Verma, A.P., Lal, G.K., 'A theoretical study of erosion phenomena in Abrasive Jet Machining', *Trans. of the ASME*, vol. 118, 1996.
60. Maurice Ewing, M., Jardetsky, W.S., 'Elastic waves in Layered media', Frank Press, *Mc Graw Hill Book Co.*, 1957.
61. Rao, S.S., 'Optimization, theory and application', *Wiley Eastern Ltd.* 1979.
62. Hinze, J.O., 'Turbulence', *Mc Graw Hill Book Co., Inc.*, New York, 1959.
63. Forestall, W. (Jr.), 'Material and momentum transfer in coaxial gas streams', *Ph.D. Thesis*, MIT Cambridge, 1949.
64. Churchill, R.V., 'Operational Mathematics', *Mc Graw Hill Kogakusha Ltd.*, International Student Edition, 1972.
65. Rawson, H., 'Properties and applications of glass', *Elsevier Publishing Co.*, 1980

66. Koves, G., 'Materials for Structural and Mechanical functions', *Hayden*, New York, 1970.
67. Nair, E. V., and Vijayakumar, R., 'Decrease in Machining rate in Abrasive Jet machining Process with increasing depth', *Technologies for the Nineties*, National Symposium , R.E.C . Warangal, India, Nov .1991.
68. Freund and Miller, 'Probability and statistics for Engineers', *Prentice Hall India*, 1980.
69. Rani, R.M., and Seshan, S., 'Studies on Abrasive Jet Machining through Statistical design of experiments', *Experimental Techniques*, pp 28-30, 1998.
70. Dieter, G. E., 'Mechanical Metallurgy', Mc Graw Hill Book Co., 1961.
71. Kittel, C., 'Introduction to solid state Physics', *Wiley Eastern Ltd.*, 1979.

Appendix A

SOLUTION OF THE WAVE EQUATION

The solutions of the wave equations 3.25 and 3.26 are found in the following

manner. The equations are
$$C_1^2 \nabla^{*2} \phi = \frac{\partial^2 \phi}{\partial t^{*2}} \quad (\text{A.1})$$

and
$$C_2^2 \nabla^{*2} \psi = \frac{\partial^2 \psi}{\partial t^{*2}}. \quad (\text{A.2})$$

Assuming a variable separable solution of these equations,

Let $\phi(r^*, z^*, t^*) = R(r^*) Z(z^*) T(t^*) \quad (\text{A.3})$

In this the function T is assumed to be of the form $T(t^*) = \exp\{-[\zeta_1 + j\omega]t^*\} \quad (\text{A.4})$

where ζ_1 corresponds to internal damping in the medium for the wave. When this is substituted in equation (A.1),

$$C_1^2 \left\{ Z \frac{d^2 R}{dr^{*2}} + \frac{Z}{r^*} \frac{dR}{dr^*} + R \frac{d^2 Z}{dz^{*2}} \right\} = RZ(\zeta_1 + j\omega)^2 \quad (\text{A.5})$$

On rearrangement this becomes:

$$\frac{1}{R} \left[\frac{d^2 R}{dr^{*2}} + \frac{1}{r^*} \frac{dR}{dr^*} \right] - \frac{(\zeta_1 + j\omega)^2}{C_1^2} = RZ\{\zeta_1 + j\omega\}^2 \quad (\text{A.6})$$

The LHS of the equation is a function of r^* alone and the RHS is a function of z^* alone.

Therefore, each side is equal to a constant say $-m^2$.

$$\frac{d^2 R}{dr^{*2}} + \frac{1}{r^*} \frac{dR}{dr^*} + R \left\{ m^2 - \frac{(\zeta_1 - j\omega)^2}{C_1^2} \right\} = 0 \quad (\text{A.7})$$

and
$$\frac{1}{Z} \frac{d^2 Z}{dz^{*2}} - m^2 = 0 \quad (\text{A.8})$$

Equation (A.7) is a special form of Bessel's equation. Its solution can be written in the

$$\text{form } R = J_0 \left[\left\{ m^2 - \frac{(\zeta_1 + j\omega)^2}{C_1^2} \right\}^{\frac{1}{2}} r^* \right] \quad (\text{A.9})$$

$$\text{Equation A.8 has the solution } Z = \exp(-mz^*) \quad (\text{A.10})$$

In these equations m can take values from 0 to ∞ . Since these are solutions of a pair of linear differential equations, the individual solutions for each value of m can be summed up to get a general solution. Thus the general solution is:

$$\phi = \int_0^\infty \int_0^\infty A(m, \omega) \exp(-mz^*) \cdot \exp\{-[\zeta_1 + j\omega]t^*\} J_0 \left[\left\{ m^2 - \left(\frac{\zeta_1 + j\omega}{C_1} \right)^2 \right\}^{\frac{1}{2}} r^* \right] dm d\omega \quad (\text{A.11})$$

$$\phi = 0 \text{ if } r^{*2} + z^{*2} > C_1 t^*$$

By a similar procedure

$$\psi = \int_0^\infty \int_0^\infty B(m, \omega) \exp[-\{mz^* + (\zeta_2 + j\omega)t^*\}] J_0 \left[\left\{ m^2 - \left(\frac{\zeta_2 + j\omega}{C_2} \right)^2 \right\}^{\frac{1}{2}} r^* \right] dm d\omega \quad (\text{A.12})$$

$$\psi = 0 \text{ if } r^{*2} + z^{*2} > C_1 t^*$$

The integrals in A.11 and A.12 are evaluated as follows: Consider equation A.11. The arbitrary function $A(m, \omega)$ may be assumed to be of the form $a_1 \exp(-(m+a_2\omega))$ where a_1 and a_2 are arbitrary constants. This assumption about the form of the function is justified, since the assumed function is a power series and any function can be expressed in a power series of the variables.

Thus

$$\phi = a_1 \int_0^{\infty} \exp[-a_2 \omega + j\omega t^* + \zeta_1 t^*] d\omega \int_0^{\infty} \exp(-m(1+z^*)) J_0 \left[\left\{ m^2 - \left(\frac{\zeta_1 + j\omega}{C_1} \right)^2 \right\}^{\frac{1}{2}} r^* \right] dm \quad (\text{A.13})$$

The integral $\int_0^{\infty} \exp(-m(1+z^*)) J_0 \left[\left\{ m^2 - \left(\frac{\zeta_1 + j\omega}{C_1} \right)^2 \right\}^{\frac{1}{2}} r^* \right] dm$ is given by

$$\frac{\exp \left[\frac{-j(\zeta_1 + j\omega) \sqrt{r^{*2} + (1+z^*)^2}}{C_1} \right]}{\sqrt{r^{*2} + (1+z^*)^2}}. \text{ After substituting this into equation A.13 the second}$$

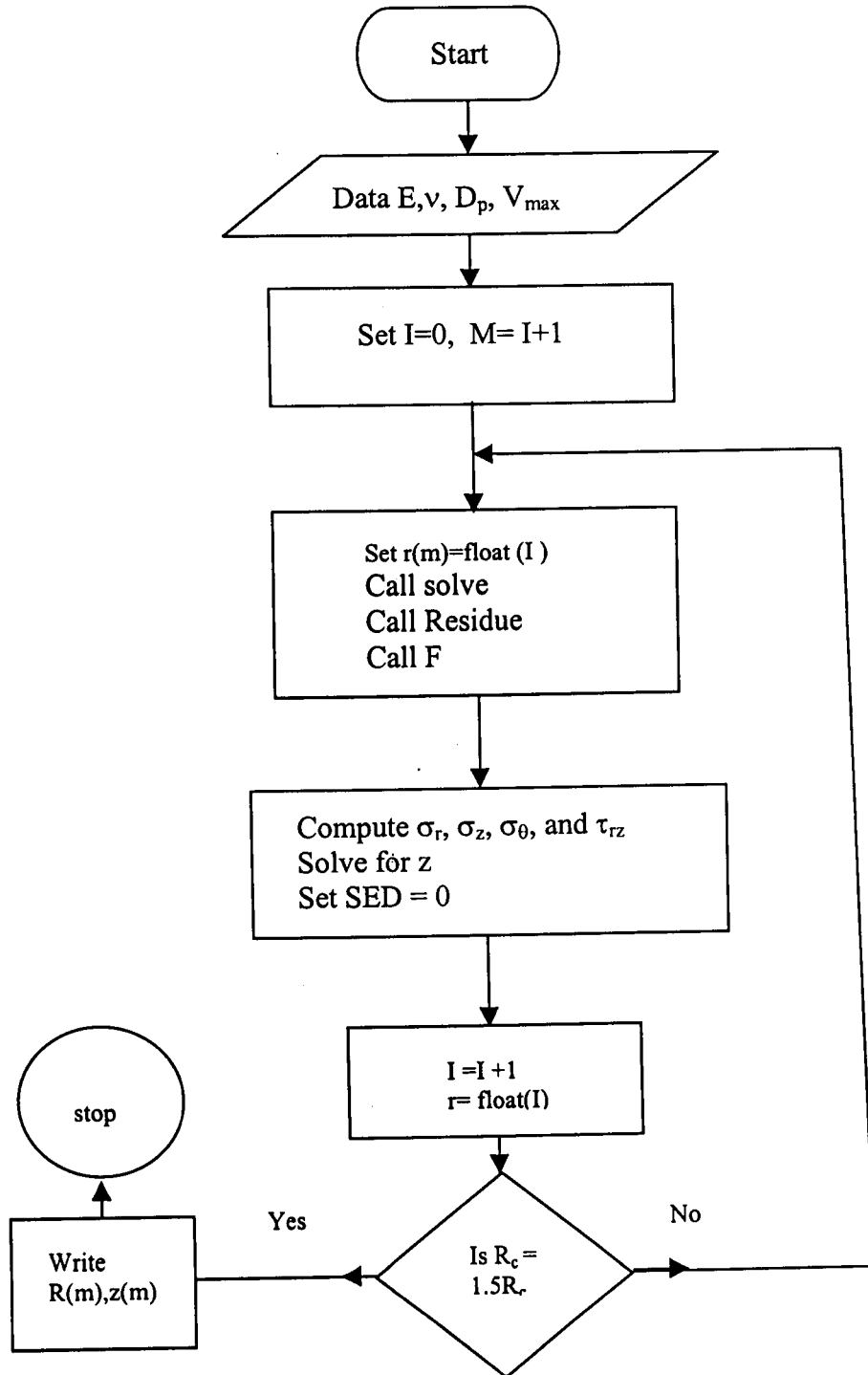
integral is evaluated. [64]. The result is;

$$\phi = \frac{a_1 \exp \left[-\zeta_1 \left\{ t^* - \left(\frac{r^{*2} + (1+z^*)^2}{C_1^2} \right)^{\frac{1}{2}} \right\} \right]}{\sqrt{r^{*2} + (1+z^*)^2} \left[a_2 + j \left\{ t^* - \left(\frac{r^{*2} + (1+z^*)^2}{C_1^2} \right)^{\frac{1}{2}} \right\} \right]} \quad (\text{A.14})$$

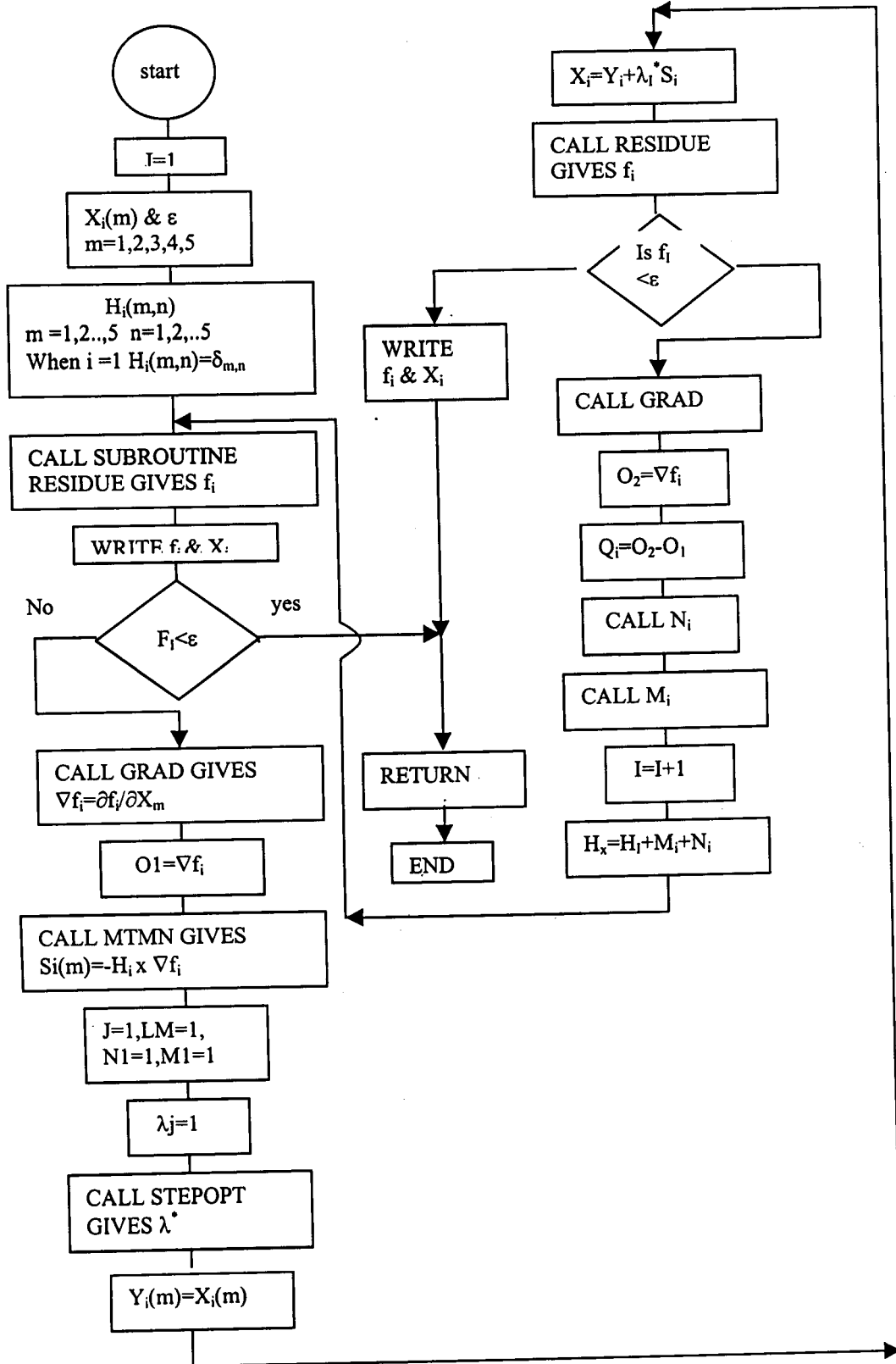
$$\text{and } \psi = \frac{b_1 \exp \left[-\zeta_2 \left\{ t^* - \left(\frac{r^{*2} + (1+z^*)^2}{C_2^2} \right)^{\frac{1}{2}} \right\} \right]}{\sqrt{r^{*2} + (1+z^*)^2} \left[b_2 + j \left\{ t^* - \left(\frac{r^{*2} + (1+z^*)^2}{C_2^2} \right)^{\frac{1}{2}} \right\} \right]} \quad (\text{A.15})$$

APPENDIX B

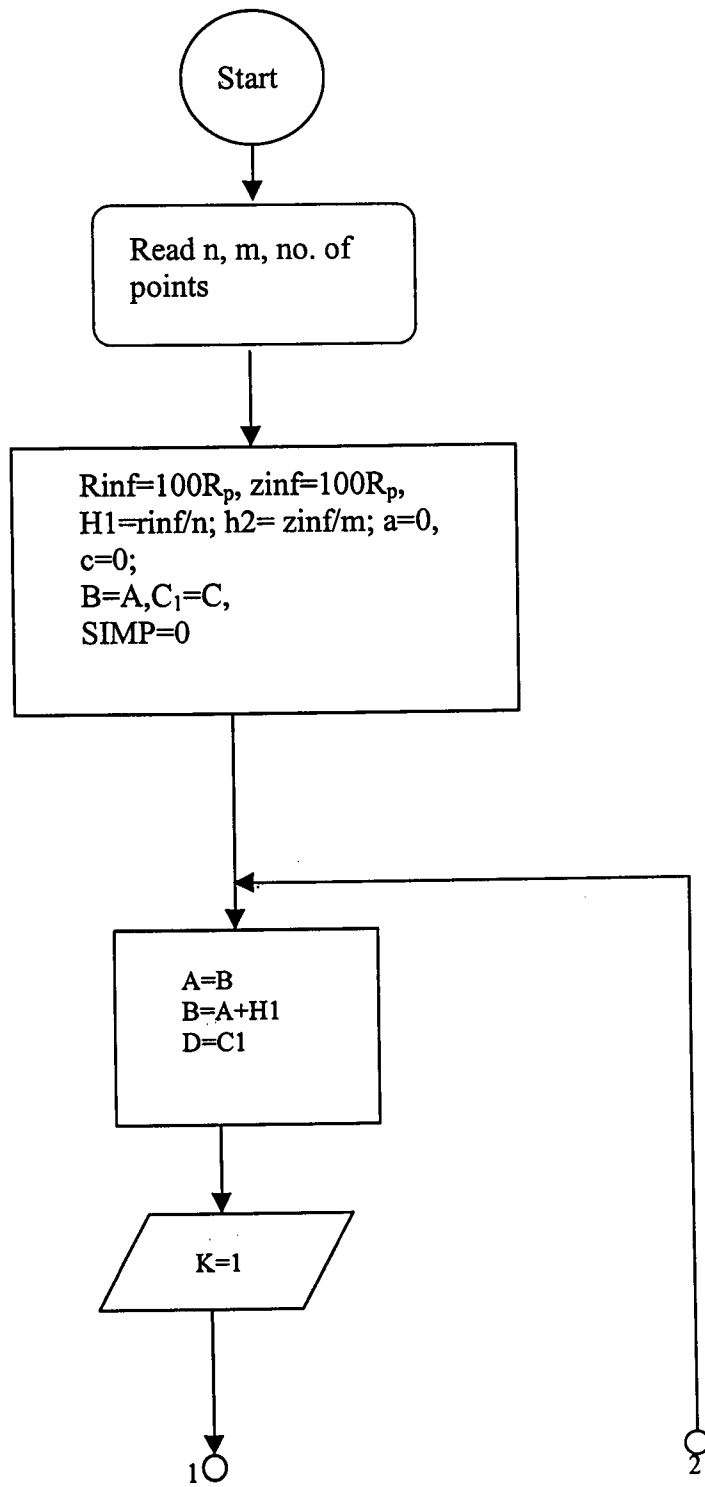
FLOW CHART FOR STRESS ANALYSIS AND CALCULATION OF CONSTANTS MAIN PROGRAM

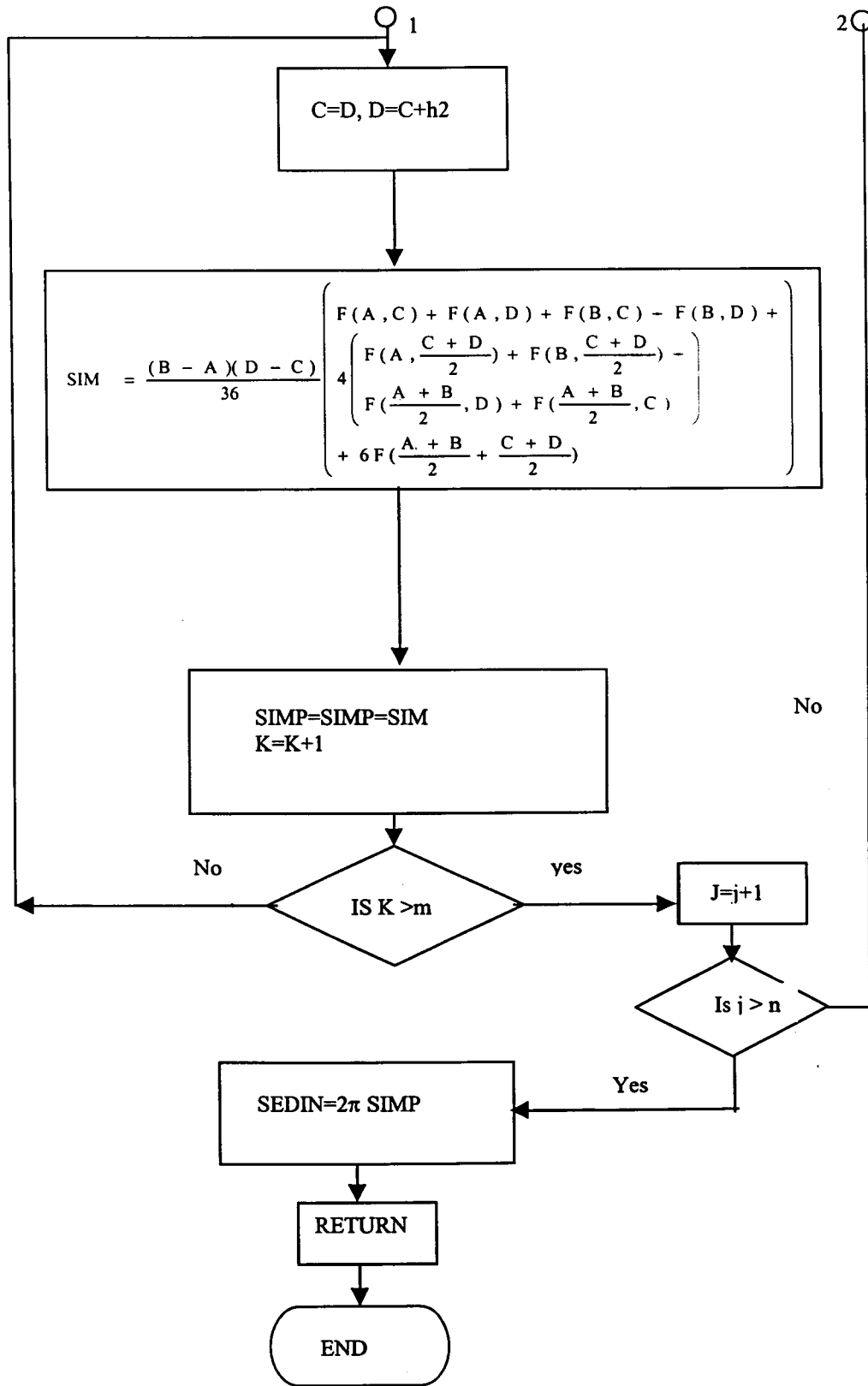


SUBROUTINE SOLVE

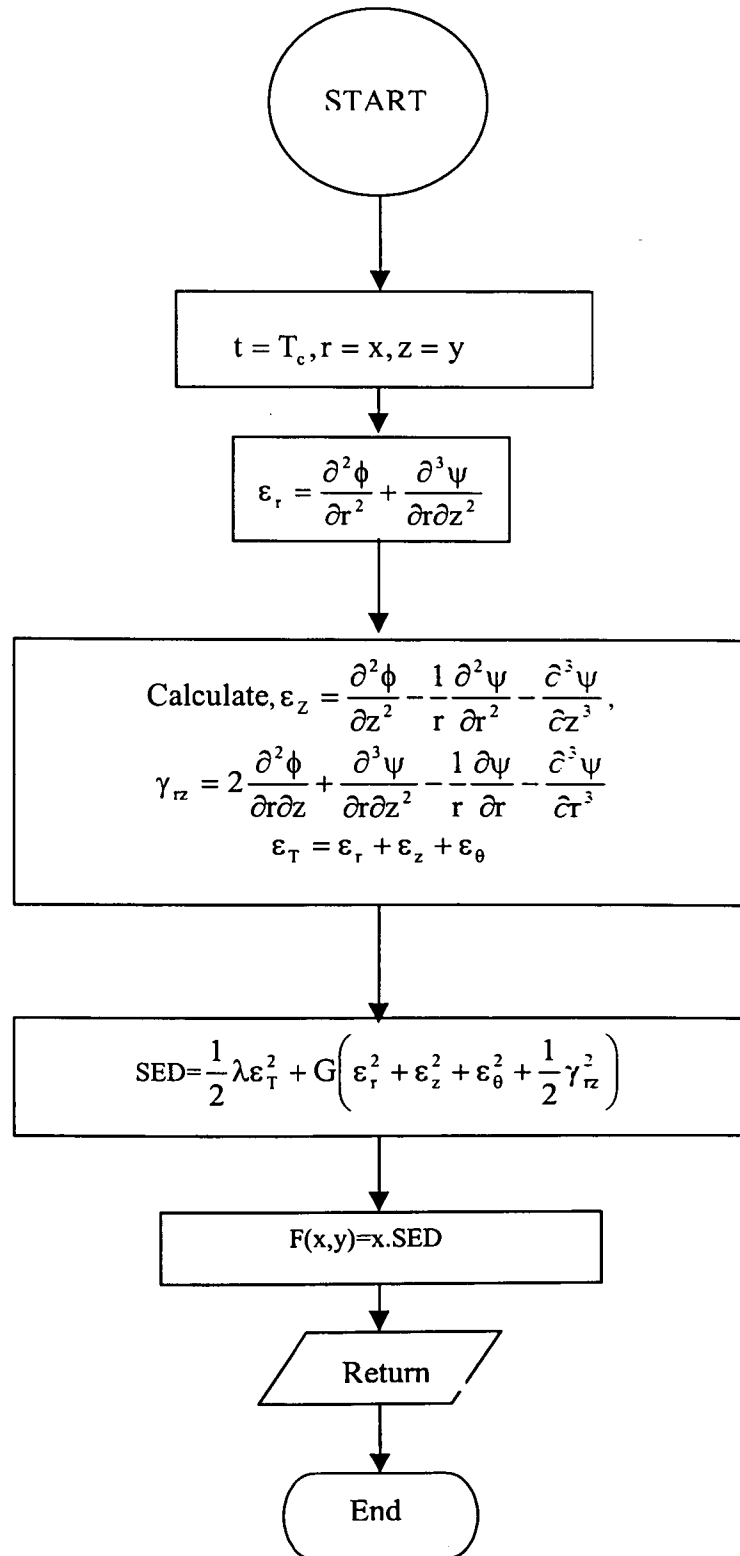


SUBROUTINE SIMPSON

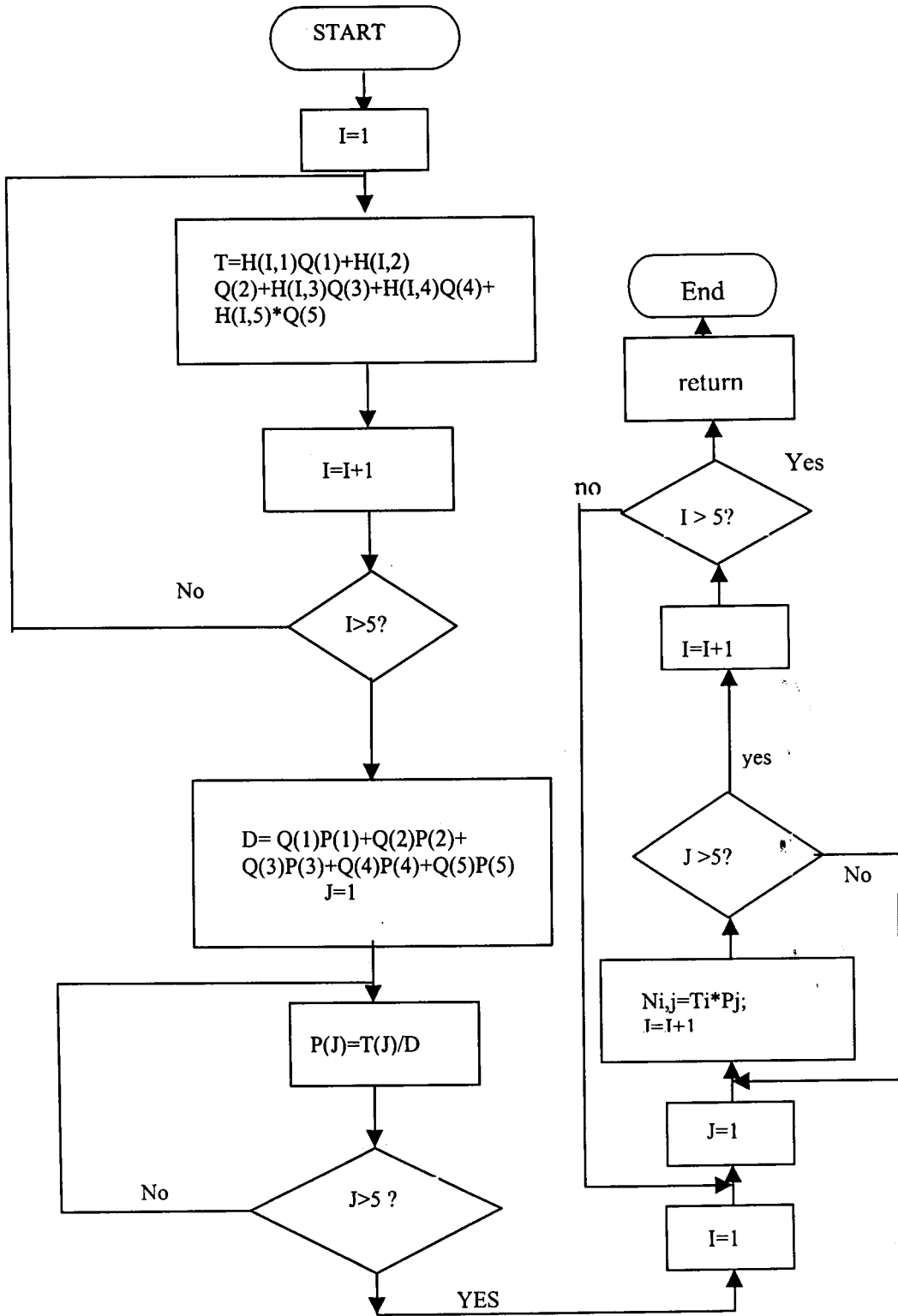




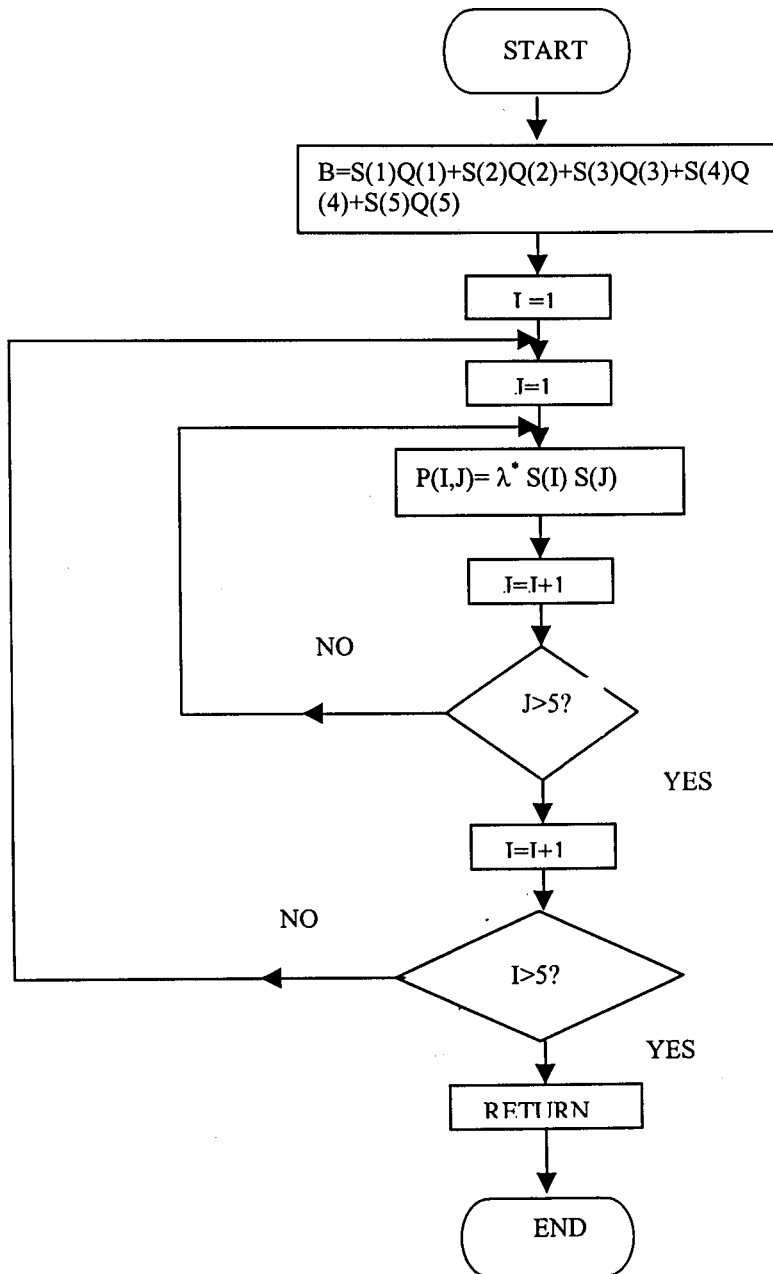
FUNCTION SUBROUTINE F(X,Y)



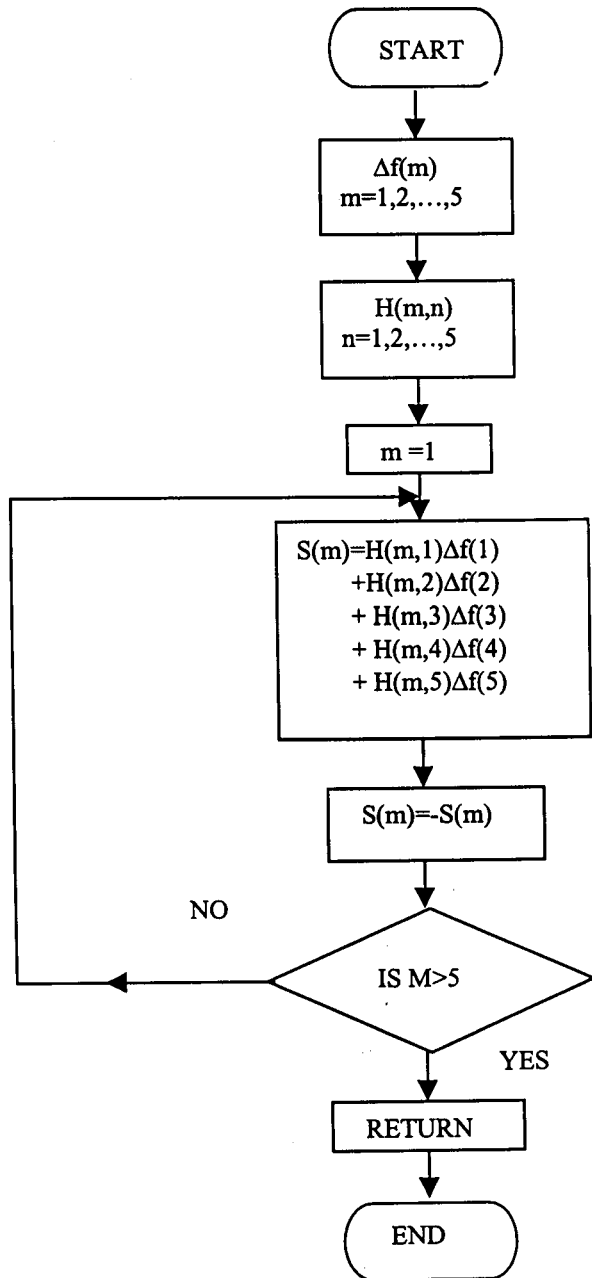
SUBROUTINE NI



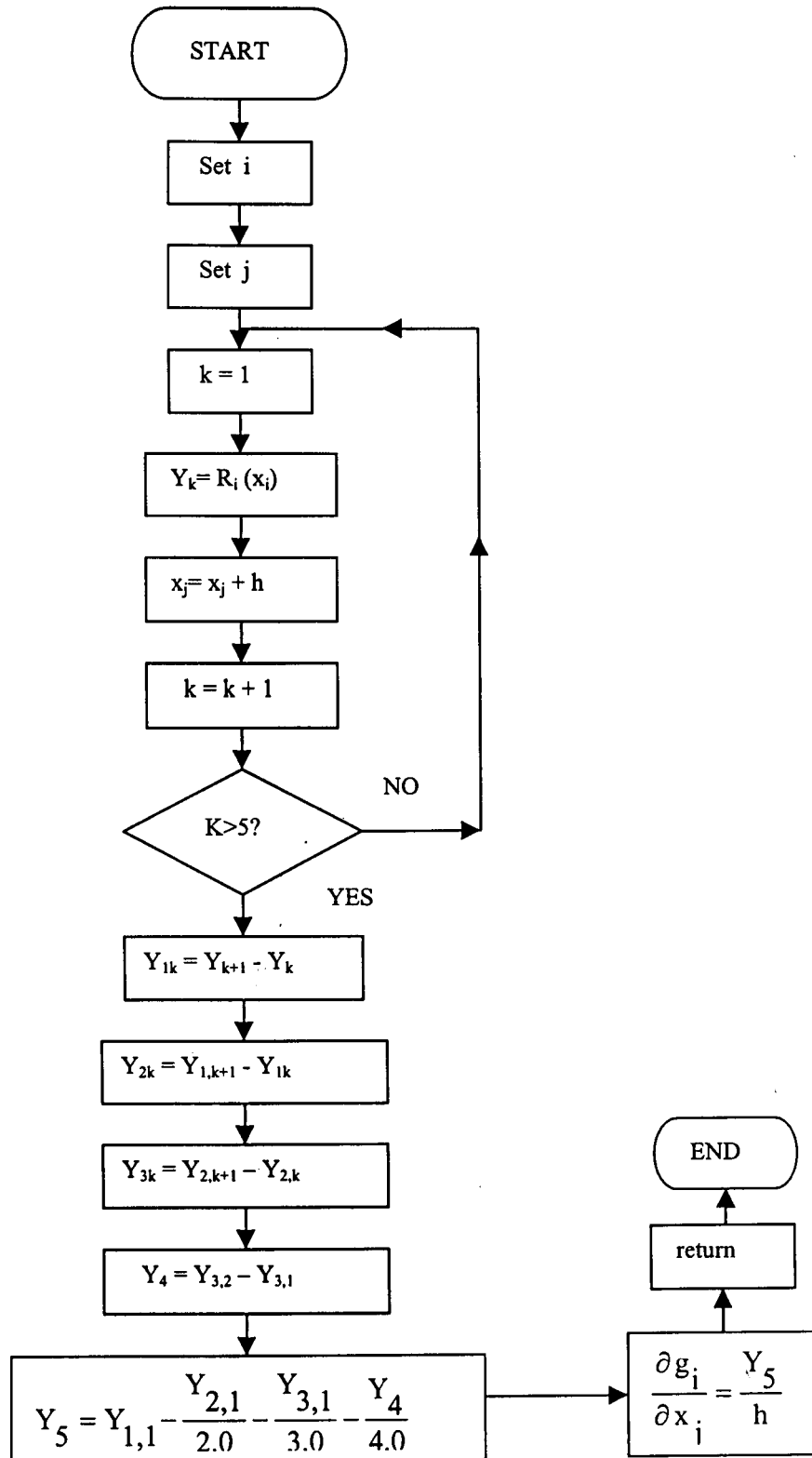
SUBROUTINE MI



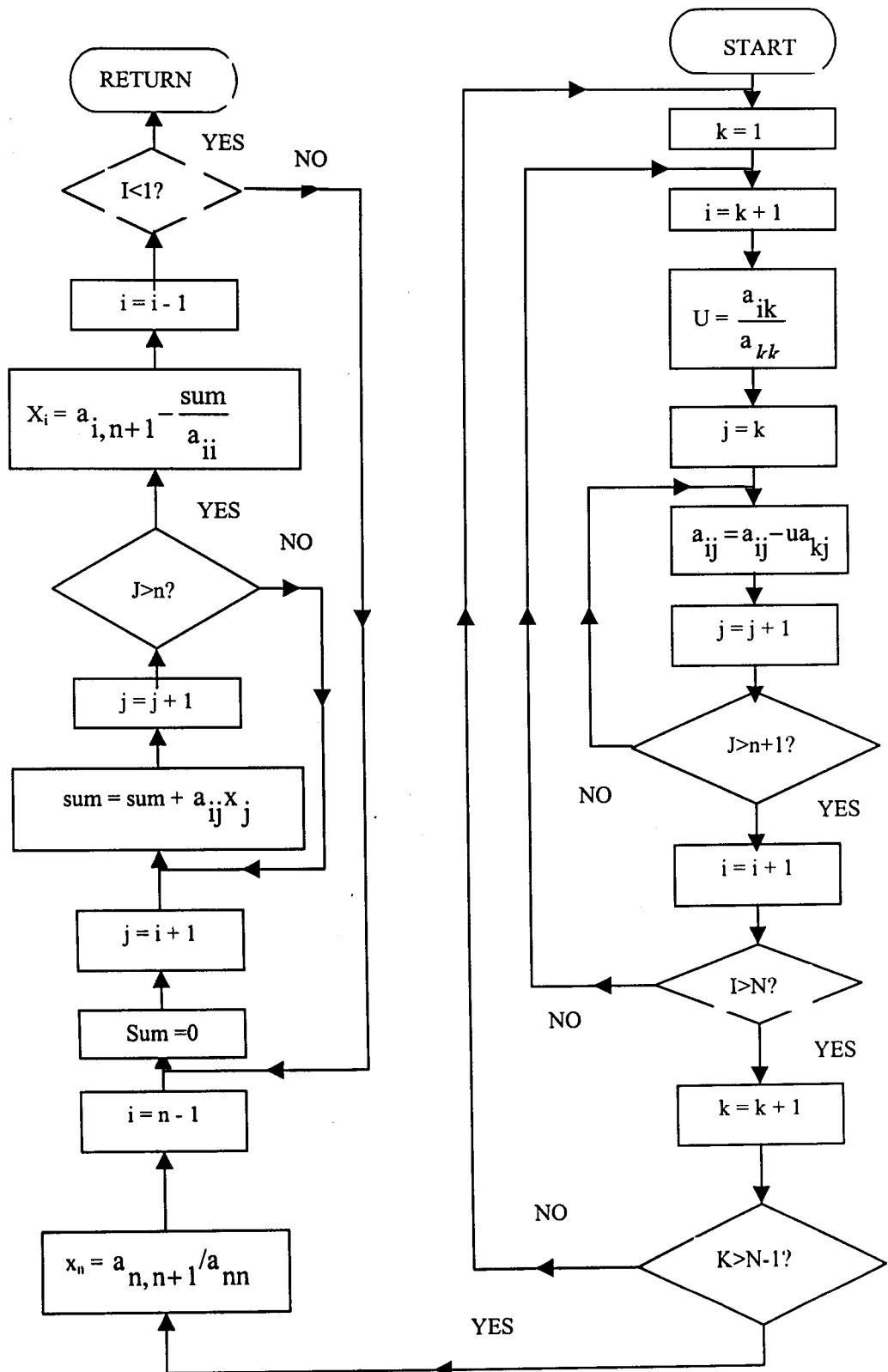
SUBROUTINE MTMN



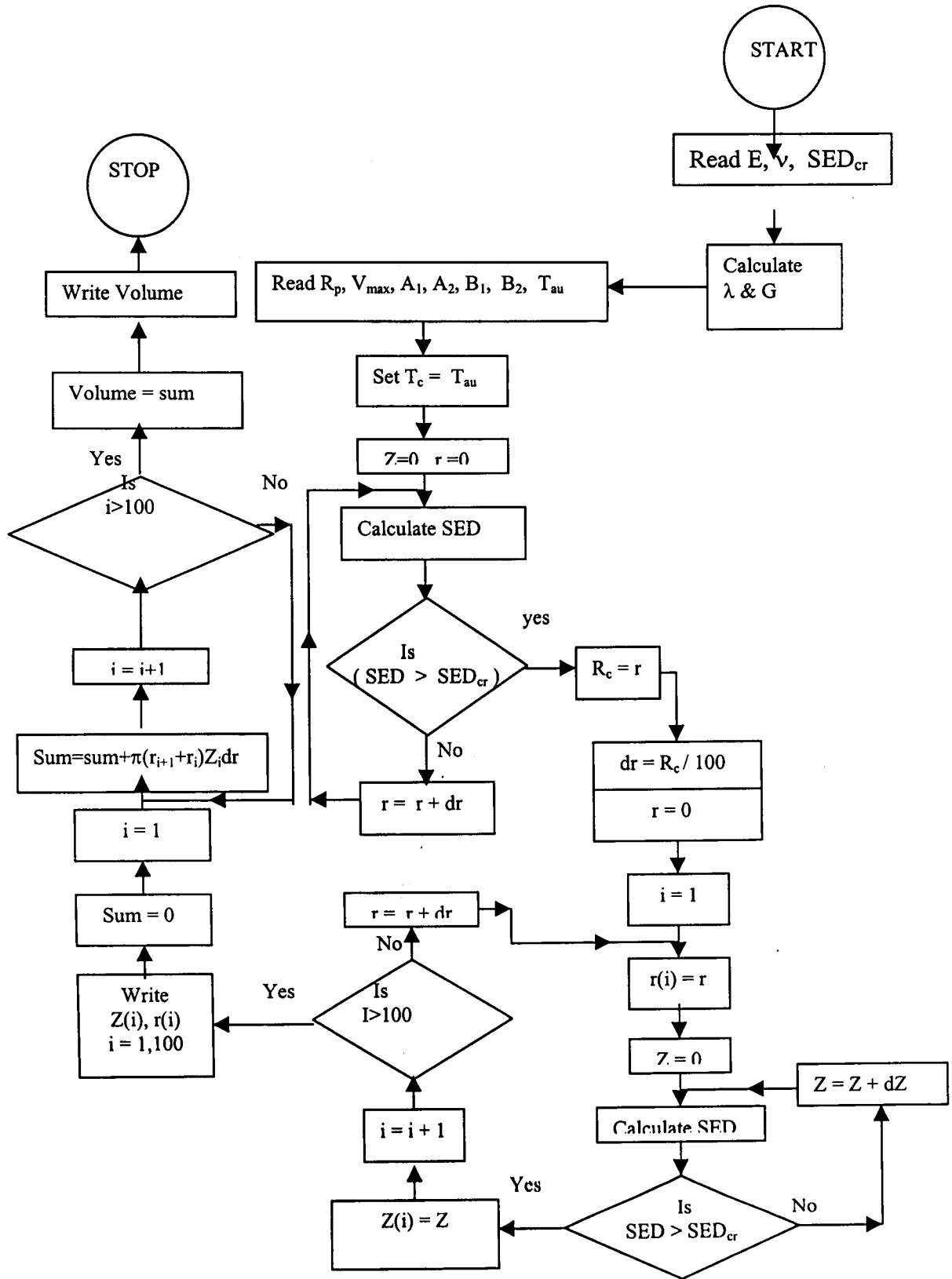
SUBROUTINE GRAD



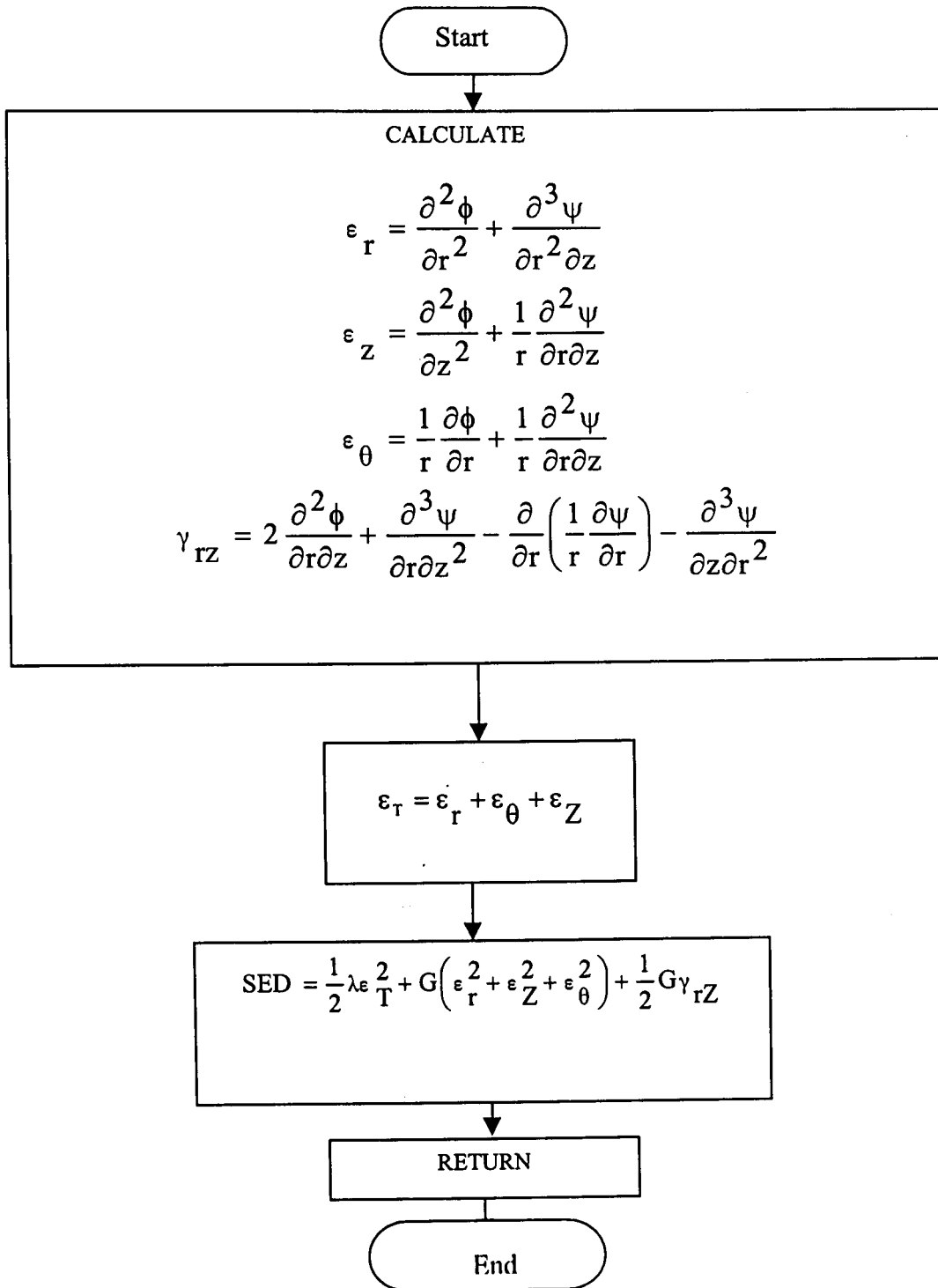
SUBROUTINE GAUSS



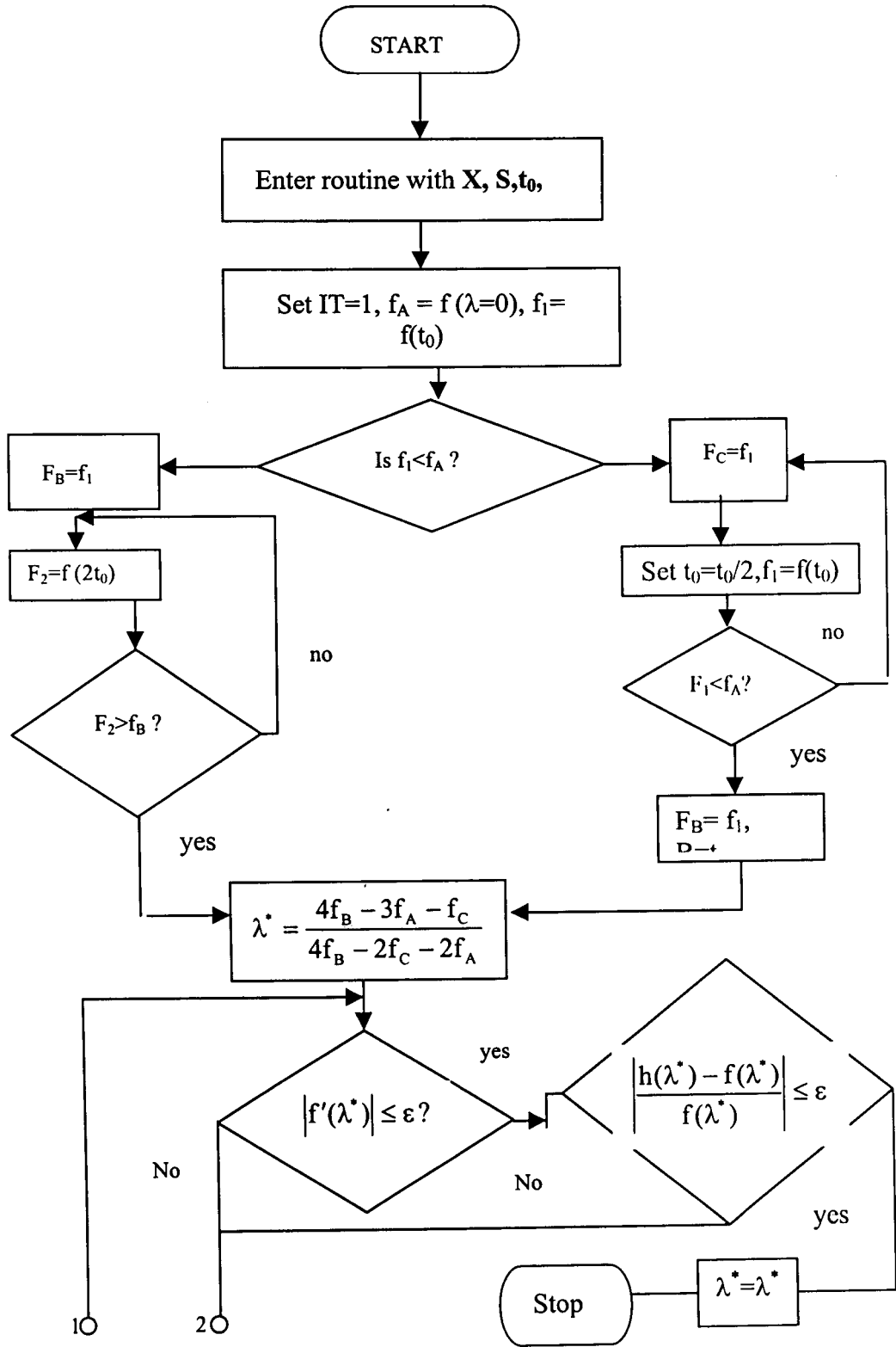
CALCULATION OF FRACTURE PROFILE & FRACTURE VOLUME

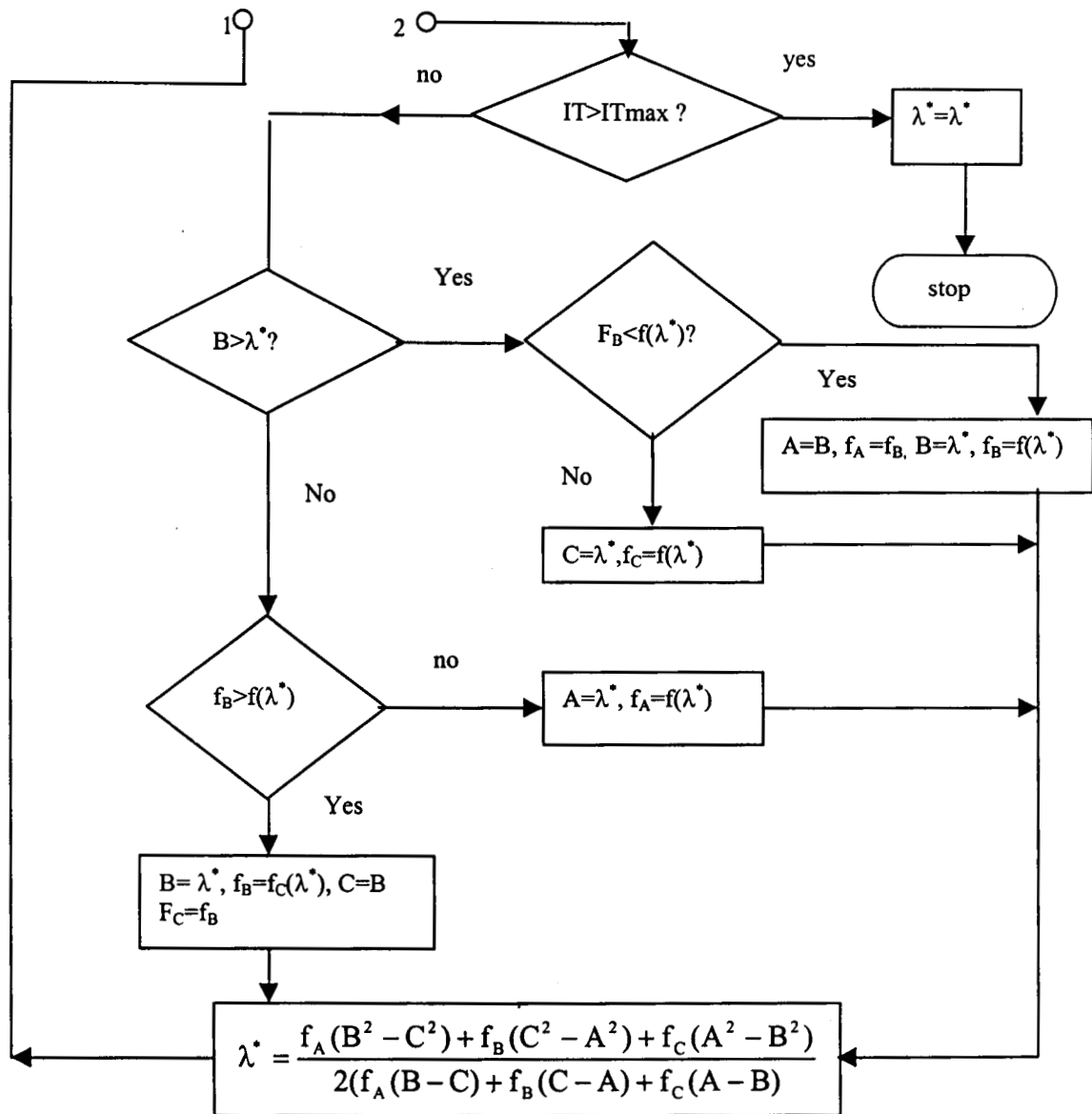


FUNCTION SUBROUTINE FOR SED



SUBROUTINE FOR STEP OPTIMISATION IN DAVIDEN FLETCHER POWELL METHOD





Appendix C

THE CRITICAL STRAIN ENERGY DENSITY

The Strain Energy Density at a point (SED) in a medium is found as the strain energy per unit volume at the point. Integration of this function over the field gives the strain energy in the medium. Thus $\int_{\Omega} (\text{SED}) d\Omega$ gives the strain energy in the field Ω .

Conversely,

$\sigma_{ij} = \frac{\partial(\text{SED})}{\partial \varepsilon_{ij}}$ and $\varepsilon_{ij} = \frac{\partial(\text{SED})}{\partial \sigma_{ij}}$. Thus to evaluate the SED, the integral $\int \sigma d\varepsilon$ is found.

In these, ε and σ are the corresponding strains and stresses.

However SED_{cr} is a property of the medium (material property) like the Young's modulus, Poisson's ratio and ultimate strength. So far, no methodology is developed to determine this property experimentally. However, the property can be calculated theoretically from the considerations given below:

The theoretical cohesive strength σ_m of materials is given by [70, 71],

$$\sigma_m = \left(\frac{\gamma E}{a_0} \right)^{\frac{1}{2}} \quad (\text{C.1})$$

where γ is the energy required to produce a unit area of fracture surface and a_0 is the equilibrium spacing of atoms. The standard properties of glass are [65, 66]: E , the Young's modulus = 0.665×10^{11} Pa, $\gamma = 3.82$ J/m² and $a_0 = 2.5 \times 10^{-10}$. Using these, the cohesive strength $\sigma_m = 0.32 \times 10^{11}$ Pa. If it is assumed that, at this stress the failure takes

place, the strain energy density SED corresponding to this stress is SED_{cr} and can be calculated as $\frac{\sigma_m^2}{2E}$ and its value is $0.764 \times 10^{10} \text{ J/m}^3$.

Similarly if the rupture strength of glass (10^8 Pa) is used in place of the cohesive strength, we get $SED_{cr} = 0.752 \times 10^5 \text{ J/m}^3$.

On the other hand, resorting to the failure theory based on the shear strength σ_s , which is approximately equal to 0.8 times the tensile strength $\sigma_t = \frac{E}{3.2\pi(1+\nu)}$ and

$$SED_{cr} = \frac{E}{(3.2\pi(1+\nu))^2} = 3.91 \times 10^8.$$

NB 3260

